1-1-2003

Connection and structural level analysis of precast hybrid frame systems

Sivakkolundu Vernu
Iowa State University

Connection and structural level analysis of precast hybrid frame systems

by

Sivakkolundu Vernu

A thesis submitted to the graduate faculty
in partial fulfillment of the requirements for the degree of
MASTER OF SCIENCE

Major: Civil Engineering (Structural Engineering)

Program of Study Committee:
Sivalingam (Sri) Sritharan (Major Professor)
Fouad Fanous
Terry Wipf
Lester W. Schmerr, Jr.

Iowa State University
Ames, Iowa
2003

Graduate College

Iowa State University

This is to certify that the master's thesis of

Sivakkolundu Vernu

has met the thesis requirements of Iowa State University

Signatures have been redacted for privacy

TABLE OF CONTENTS

LIST OF FIGURES

LIST OF TABLES

LIST OF SYMBOLS

A_{ps}	Cross-section area of post-tensined steel
A_s	Cross-section area of mild steel reinforcement
b	Width of beam cross-section
c	Neutral axis depth
C	Resultant compresion force in concrete
d	Depth of mild steel from extreme compression fibre
d_b	Diameter of mild steel reinforcement
E_c	Young's modulaus of concrete
E_{ps}	Young's modulus of post-tensioned steel reinforcement
E_s	Young's modulus of mild steel reinforcement
E_{sec}	Secant Young's modulus of concrete
E_{st}	Young's modulus of mild steel reinforcement
f'_l	Maximum effective lateral confinement stess from transverse reinforcement
f'_c	Unconfined concrete comressive strength
f_{cc}	Maximum confined confined concrete stress
f_{ps}	Stress in post-tensioned steel reinforcement
f_{psy}	Yielding stress of post-tensioned steel reinforcement
f_s	Stress in tensile mild steel reinforcement
f_{sc}	Stress in comressive mild steel reinforcement
f_{st}	Stress in tensile mild steel reinforcement
f_u	Ultimate stress of mild steel reinforcement when fracturing
f_y	Yielding stress mild steel reinforcement
h	Height of rectangular beam section
L	Length of cantilever beam
L_P	Plastic hinge length
L_{SP}	Length of strain penetration
L_u	Unbonded length of mild steel reinforcement
L_{ups}	Unbonded length of post-tensioned steel reinforcement
M	Moment resistant
M_n	Nominal moment resistant
M_p	Probable moment resistant
T_{ps}	Force in post-tensioned steel reinforcement
T_s	Force in mild steel reinforcement

Δ^{*}_{e}	Elastic component of end displacement of a cantilever beam with hybrid connection
Δ_{E}	Elastic component of end displacement
$\Delta^{\flat}_{e}$	Elastic component of end displacement a cantilever monolithic beam
$\Delta_{Monolithic}$	Total end displacement of cantilever monolithic concrete beam
Δ_{p}	Plastic displacement component of monolithic concrete beam
$\Delta_{Precast}$	Total end displacement of precast concrete beam with hybrid connection
Δ_{ps}	Elongation in the post-tensioned steel reinforcement at hybrid connection interface
Δ_{PT}	Elongation in post-tensioned steel at hybrid connection interface
Δ_{θ}	Displacement component due to interface rotation of q for a beam with hybrid connection
Δ_{S}	Elongation in tensile mild steel reinforcement at hybrid connection interface
Δ_{SC}	Elongation in comressive mild steel reinforcement at hybrid connection interface
Δ_{SP}	Elongation in post-tensioned steel at hybrid connection interface
Δ_{ST}	Elongation in tensile mild steel reinforcement at hybrid connection interface
ε_{c}	Compressive strain in concrete in extreme fiber
ε_{cc}	Strain corresponding to f_{cc}
ε_{co}	Strain corresponding to f'_{c}
ε_{e}	Elastic compontent of tensile strain in mild steel reinforcement
ε_{p}	Plastic compontent of tensile strain in mild steel reinforcement
e_{pi}	Initial prestress after losses in post-tensioned steel reinforcement
ε_{ps}	Strain in post-tensioned steel reinforcement
ε_{s}	Strain in tensile mild steel reinforcement
ε_{sh}	Strain in tensile mild steel reinforcement at the on-set of strain hardening
ε_{si}	Initial prestress after losses in post-tensioned steel reinforcement
ε_{st}	Strain in tensile mild steel reinforcement
ε_{su}	Ultimate strain in mild steel reinforcement when fracturing
ε_{u}	Ultimate strain in mild steel reinforcement when fracturing
ε_{x}	Intermidiate strain in the strain hardening region where stress is known
ε_{y}	Yield strain of mild steel reinforcement
ϕ_{e}	Elatic component of curvature
ϕ_{u}	Total or ultimate curvature
ϕ_{y}	Yielding curvature

θ	Interface rotation at hybrid connection
θ_P	Concentrated rotation at beam-column connection due to plastc hinge formation

ACKNOWLEDGEMENTS

The research presented in this thesis was partially supported by a 2001-2002 Daniel P. Jenny Research Fellowship of the Precast/Prestressed Concrete Institute (PCI), which is gratefully acknowledged.

I would like to express my sincere thanks to my major professor Dr. Sivalingam (Sri) Sritharan for providing me the opportunity to work on this research, assisting with the PCI fellowship application, and for his continuous support and guidance. Thanks are also expressed to Dr. Pampanin Stefano of the University of Canterbury for providing the required data and guidance in the component level study of the investigation.

Special thanks are due to my wife, Ranjiny, and my family for their love and support throughout my graduate study at Iowa Stare University.

CHAPTER 1

INTRODUCTION

1.1 Background

Catastrophic structural damage observed recently in major earthquakes in the United States, Japan and other countries has once again emphasized that seismic damage is largely induced by deficiencies in design concepts, detailing, and/or construction methods [1, 22]. Safety of structures in future earthquakes continues to mandate development of reliable seismic design procedures and implementation of good construction methods.

Among the various materials and concepts available for building construction, precast concrete combined with prestressing steel offers several advantages, which may be summarized as follows:

1. Utilization of high strength materials provides slender members;
2. Improves quality due to construction of components in controlled environment;
3. Makes automation possible that can result in reduced labor costs;
4. Speedy construction as a result of using prefabricated components;
5. Reduces formwork and scaffolding at the construction site;
6. Easy to introduce aesthetic architectural features.

However, exploitation of economics and other recognized advantages of precast, prestressed concrete have been limited in seismic regions. Two main reasons that may be attributed to this limitation are:

1. Poor performance of precast prestressed structures in past earthquakes [1], and

2. Lack of reliable seismic design guidelines for precast, prestressed concrete in building codes [2].

For the above reasons, building codes have typically imposed the following conditions for the construction of precast structures in seismic regions:

1. Requirement for emulating monolithic concrete [3], or
2. Confirmation of adequacy of the precast design methods by simulated testing [2].

As discussed subsequently, the use of emulation concept impedes utilization of unique properties of precast prestressed concrete in seismic design of buildings structures, and thus will not result in efficient precast systems.

1.2 Seismic Design of Precast Prestressed Buildings

1.2.1 Design Philosophy

Seismic design of structures is now based on the capacity design philosophy, which was suggested by Hollings and developed by discussion groups of the New Zealand Society for Earthquake Engineering in the 1970s [3]. This philosophy requires that structures be designed to exhibit appropriate inelastic deformation modes when they are subjected to moderate to large earthquakes. Suitable lateral load resisting systems are first selected, which are then designed for adequate ductility. Accordingly, in the case of precast, prestressed buildings with moment resisting frames as a lateral load resisting system, plastic hinge locations can be conveniently selected at precast beam ends and the connections between the columns and beams may be designed to achieve the required amount of rotational ductility corresponding to the design earthquake. At the same time, all other structural members and other possible failure mechanisms are designed with sufficient strength. This is to prevent

brittle failure of regions that are not designed for ductility and/or undesirable failure mechanisms; and to achieve enough ductility through the predetermined mechanism when experiencing the lateral deformation due to the design earthquake [4].

1.2.2 Classification of Connections

Several different beam-to-column connection types have been investigated for moment resisting ductile frames consisting of precast members [2]. These connections may be classified into several categories as shown in Figure 1.1. The first classification differentiates emulative connections from non-emulative type connections. If a precast beam-to-column connection is established to provide performance equivalent to that of a monolithic concrete connection in terms of strength and toughness, this connection is said to be an emulative connection. In contrast, non-emulative connection utilizes unique properties of precast concrete technology to ensure sufficient ductile performance for the frame systems. Non-emulative connections that have been successfully introduced to precast frame systems are the "jointed" connections [5, 6].

At the next level, connections may be divided into strong or ductile connections depending on the location where inelastic deformations are permitted to develop [7]. In frames with strong connections, precast members are designed to be weaker than the connections, forcing inelastic actions at designated locations in the precast members. On the other hand, ductile connections are detailed to be weaker than the precast elements, confining inelastic actions to the connection regions, while the precast elements remain elastic during seismic response.

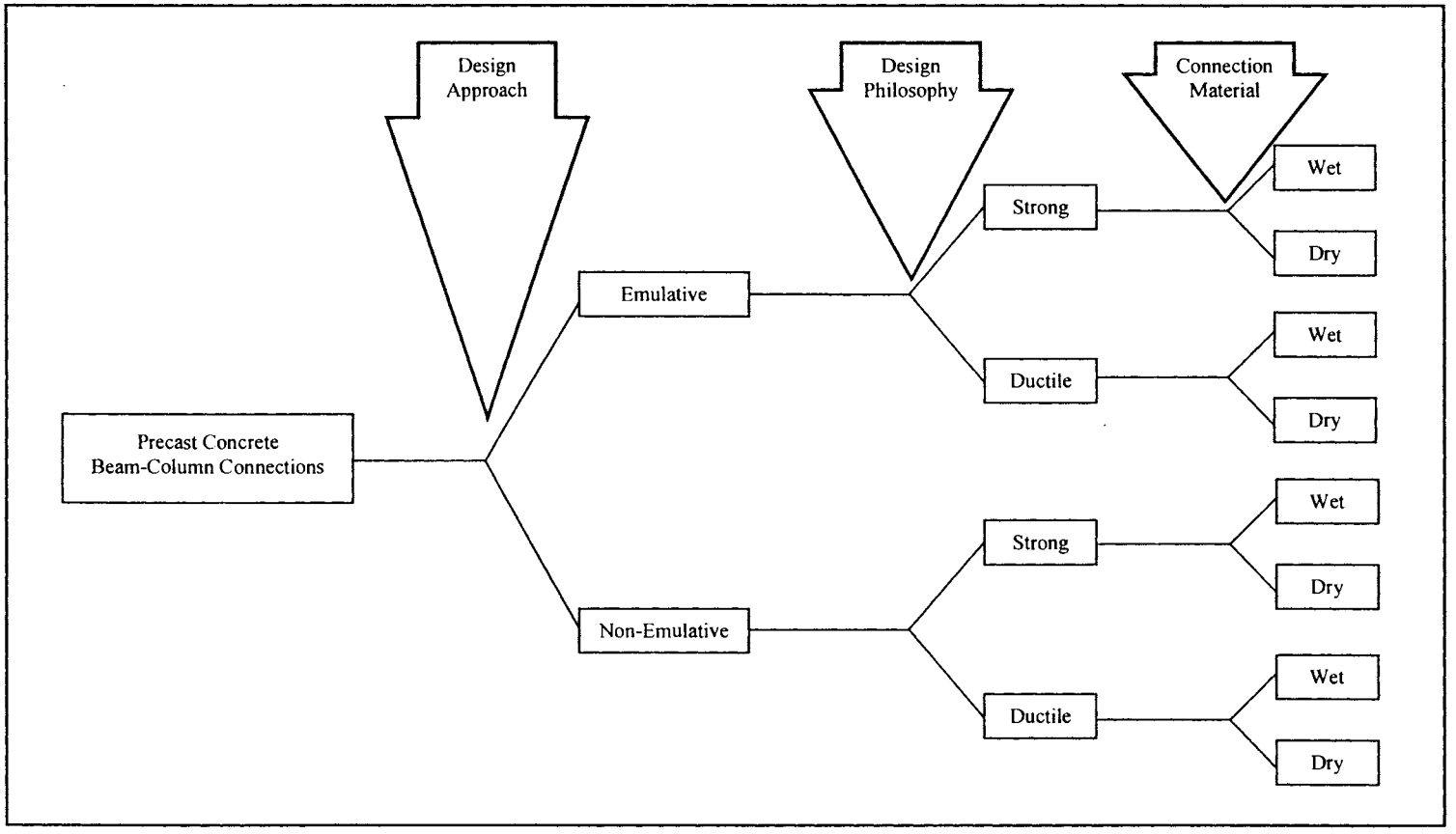

Figure 1.1 Classification of precast concrete beam-column connections based on different criteria

Finally, both strong and ductile connections may be classified into wet or dry connections. Wet connections are those that utilize concrete or grout in the field to splice reinforcement of precast members. All connections other than the wet connections are classified as dry connections [6]. Although Figure 1.1 identifies eight different connection types as discussed above, researchers have not investigated every type. A review of the connection types explored by researchers is presented in Sections 2.3 and 2.4 along with their findings.

1.2.3 Precast Frame Systems in Seismic Regions

Moment frames may develop satisfactory ductile response under lateral seismic loading through several different inelastic mechanisms involving formation of plastic hinges at beam and column ends. The two extreme mechanisms are shown in Figure 1.2. In the first mechanism as shown in Figure 1.2 (a), plastic hinges are formed at beams ends and column bases and the remaining column sections are designed to be elastic, which is referred to as the strong column-weak beam mechanism. In the second mechanism, inelastic actions are concentrated in the columns of the first floor. This mode is not generally preferable, as this will require significantly large rotational ductility demands in the plastic hinge locations, as illustrated in Figure 1.2(b). This mode of response, which is typically referred to as the soft story collapse has occurred in structures in past earthquakes due to design deficiency, causing near collapse of structures [4]. Therefore, seismic design of frames requires strong column-weak beam approach to ensure satisfactory ductile response [3].

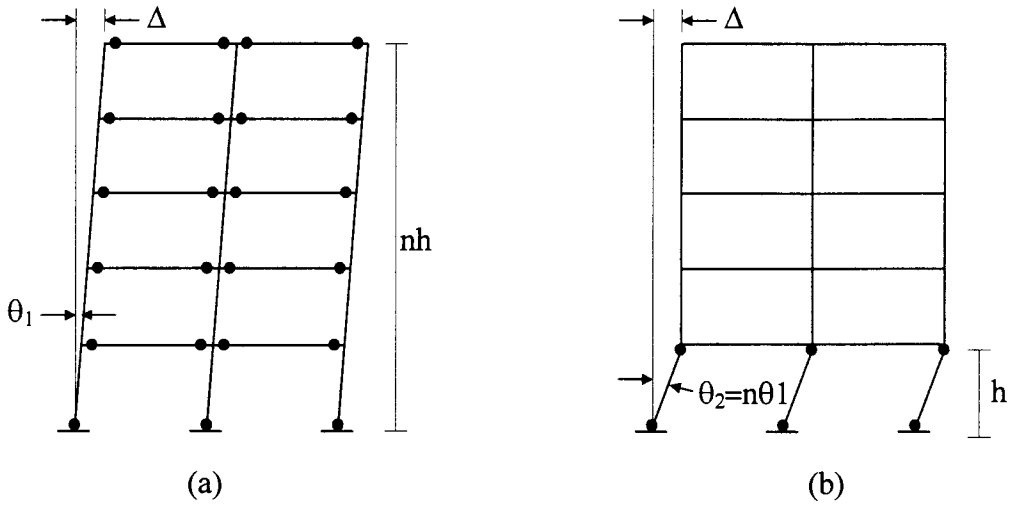

Figure 1.2 Two different failure mechanisms.

Based on the precast connection classification discussed in the previous section, either strong or ductile connections may be used with the strong column-weak beam approach. As strong connections with precast members are similar in behavior to monolithic concrete connections, they can be designed with existing code provisions. Consequently, early studies on seismic design of precast beam-to-column connections subjected to earthquake loads focused on developing emulative connections [2].

However, if precast frames are designed with ductile connections, the precast members do not require ductile details, but they need to be provided with adequate margin of strength with respect to the strength of the ductile connections. Benefits of ductile connections include cost efficiency and use of replaceable connection and members after an earthquake.

1.3 Hybrid Connection

Figure 1.3 illustrates a jointed connection known as the hybrid connection that is suitable for developing the desirable mechanism in moment resisting frames. In this concept, precast

single bay beams are connected to multi-story high precast columns using dry-ductile connections based on unbonded high strength post-tensioning (PT) steel and mild steel reinforcing bars. The PT steel is located at the mid-height of the beam and is typically designed to remain elastic during seismic loading to ensure restoring of the frame and minimize stiffness degradation. At the column-to-beam interface, shear transfer is assumed to be by a friction mechanism. Mild steel reinforcing bars are provided at the top and bottom of the beams as continuous reinforcement through the column. Strain reversals of the mild steel beyond yielding during seismic response facilitate dissipation of energy. The mild steel bars are debonded over a short distance on either side of the column to prevent premature fracture of the bars due to accumulation of inelastic strain. Both the PT and the mild steel bars contribute to the moment resistance at the connection interface.

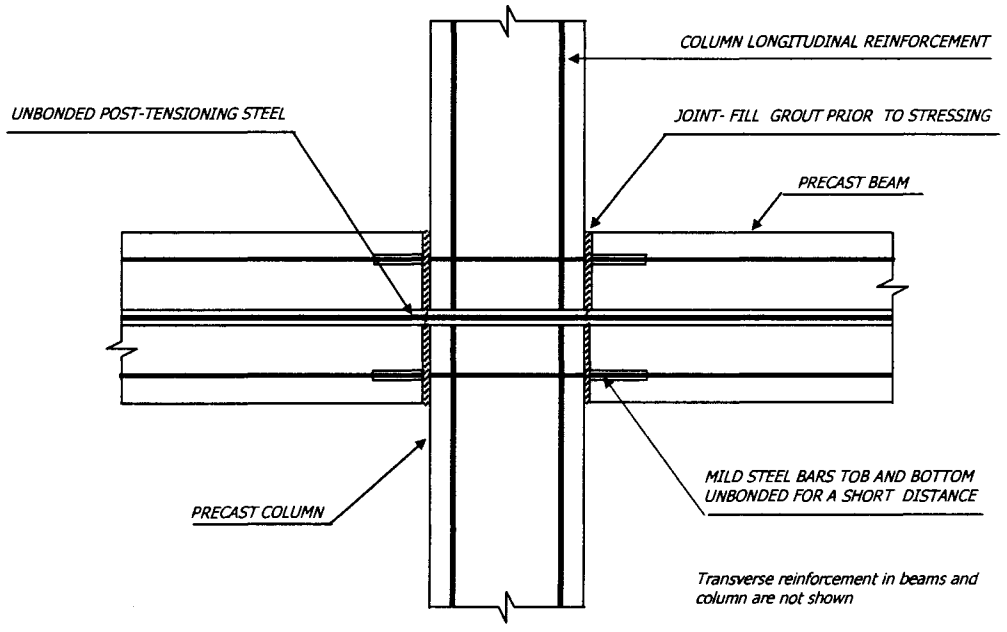

Figure 1.3 A typical hybrid precast frame connection.

The main benefit of using PT steel at the connections is that it gives the necessary restoring force to control the residual displacements, whereas the mild steel reinforcement provides energy dissipation capability to the system. Because the restoring force and energy dissipation are achieved by two different means, this dry-ductile connection is referred to as the hybrid connection. Therefore, the design of a hybrid connection relies on optimizing the following design parameters:

- The area of PT steel and the mild steel reinforcement
- The debonded length of the mild steel reinforcement
- Initial prestress in the PT steel

1.3.1 Hybrid Connection Analysis

In monolithic concrete section analysis, the condition of strain compatibility, as shown in Figure 1.4(a), establishes a relationship between strain in steel, concrete strain and neutral axis depth with the assumption that plain sections remain plain. However, strain incompatibility between concrete and unbonded steel reinforcement at a hybrid connection makes the section level analysis impossible with the conventional means. Figure 1.4(b) shows the incompatibility between strains due to the presence of unbonded reinforcing bars. An analytical procedure for the connection is needed to develop a complete moment-rotation relationship, which can be used in the design and performance assessment of moment resisting frames incorporating hybrid connections. Very little research has been done on the development of a rational connection level analysis method. The studies conducted to date have used several simplified assumptions or not provided thorough validation of the proposed methods using experimental data.

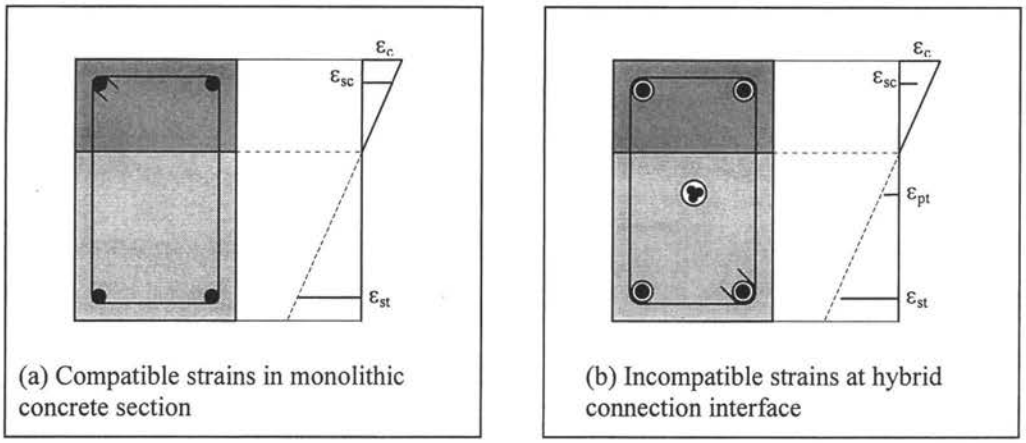

(a) Compatible strains in monolithic concrete section

(b) Incompatible strains at hybrid connection interface

Figure 1.4 Relationship between steel and concrete strain values.

1.3.2 Design Provisions

There has been little research carried out with a view to developing a design procedure for hybrid connections [10, 11]. A detailed description of the findings of these studies is presented in Section 2.4. However, no provisions are available in the building codes of the United States for hybrid connections. It is widely expected that provisions for hybrid connections will be incorporated into ACI 318-05 or International Building Code 2006 [8]. The ACI has already published a draft provision for the hybrid connection [9]. Therefore, any constructive proposal of a rational design procedure for the hybrid connection will have an impact on the industry.

1.4 Scope of Research

Considering the current state of knowledge on precast hybrid frame system, the research presented in this thesis focuses on the following areas:

1. Development of an analytical model to predict the behavior of hybrid connection as a function of rotation by adequately modeling:
    a. the stress-strain behavior of concrete, mild steel and PT steel,
    b. strain penetration of mild steel into the joint, and
    c. confinement effect of concrete
2. Development of a user-friendly computer tool that will enable the connection analysis and provide validation against test results.
3. Extend the connection level analysis to predict behavior at the member level.
4. Demonstrate the benefits of predicting the moment as a function of rotation by performing inelastic pushover and dynamic analyses of a moment resisting frame building utilizing the hybrid connections at the beam-to-column interface. Moment-rotation behavior predicted in (1) will be used to model the connection behavior in the moment resisting frame.

The procedures developed in a previous study Pampanin et al. [43] to model the hybrid connection will be refined in the first phase of this research. This involves accurately modeling of the strain penetration term of mild steel and incorporation of the stress-strain model for an accurate account of post-tensioning steel contribution. Although Pampanin at el. considered the moment contribution of the compression steel located at the connection; their publications didn't include any expressions for the strain in compression steel, however, the refined model will give a reasonable expression the train. Experimental verifications of the model will be performed using the data obtained from tests conducted at the National Institute of Science and Technology (NIST) as well as from the PRESSS test building test.

For the pushover and dynamic analysis, part of the input excitation used for the inelastic analyses were those used in the PRESSS test and several records of various percentage of design level of earthquake. Using the analysis results, the advantage of using flexible floor links, and the behavior of a hybrid building from a performance based view point will be examined. An estimate of the R factor suitable for the design of precast buildings with hybrid connections will also be studied.

1.5 Thesis Layout

This thesis contains six chapters. Following an introduction in this chapter for precast concrete design of buildings under seismic loading, Chapter 2 gives a review of performance of precast buildings in past earthquakes, experimental and analytical studies of precast beam-column connections subjected to seismic loads, and details of the seismic design provisions developed for precast concrete buildings.

Chapter 3 presents the theoretical background and development of an improved analytical model for connection level analysis of the hybrid connection. This chapter also provides comparison between analysis results and the experimental results at connection level.

Description of the model building used in the inelastic analyses and the results of the inelastic analyses are presented in Chapter 4. With a summary of the research findings, conclusions and recommendations are given in Chapter 5.

CHAPTER 2

LITERATURE REVIEW

2.1 Introduction

Application of precast concrete in seismic regions varies from the use of only architectural members (e.g., claddings) to designing the building using precast structural members such as floor systems, gravity frames, and lateral load resisting systems. Precast members have been often used in conjunction with other structural material types such as cast-in-place (CIP) concrete and steel building systems. Frame and wall are two common systems adopted to resist lateral loads in building structures. Of various applications of precast concrete, lateral load resisting moment frames are given more emphasis in this chapter, due to the research topic of this thesis.

This chapter presents literature review of precast prestressed seismic systems in four specific areas. First, a summary of reports on the performance of precast concrete buildings during the past earthquakes are presented. Next, various literatures describing experimental investigation of several types of precast prestressed concrete beam-to-column connections suitable for seismic regions are reviewed. A review of analytical studies conducted on the hybrid precast frame is then presented. Finally, a review of publications describing design methods for hybrid connections is provided.

2.2 Performance of Precast Buildings in Earthquakes

A review of reports on the performance of buildings in past earthquakes with primary emphasis on precast members and precast structural systems is presented in this section. Only

limited information was found on the performance of lateral load resisting moment frames incorporating precast concrete elements. This may be due to a limited application of precast concrete in high seismic regions. Table 2.1 shows the details of selected earthquakes, in which the performance of precast structures will be reviewed in the subsequent sections.

Table 2.1 Details of some past earthquakes

Earthquake Name	Date of Event	Local Magnitude (M_L)	Maximum Horizontal Acceleration	Duration (s)
The 1964 Alaska Earthquake [12, 14]	March 27	8.4	0.40g	>150
The 1977 Rumanian Earthquake [12, 15]	March 4	7.2	0.20g	25
The 1985 Mexican Earthquake [16]	Sept. 19 and 20	8.1, 7.5	0.17g	60
The 1988 Armenian Earthquake [1, 12]	December 7	6.9	0.25g	90
The 1989 Loma Prieta Earthquake [17]	October 17	7.1	0.64g	20
The 1994 Northridge Earthquake [12, 18]	January 17	6.8	0.94g	10
The 1995 Kobe, Japan Earthquake [19]	January 17	7.2	0.83g	20
The 1999 Kocaeli, Turkey Earthquake [20]	August 17	7.4	0.41g	15-20
The 1999 Chi-Chi, Taiwan Earthquake [21]	September 21	7.6	0.50g	20-30
The 2001 Bhuj, India Earthquake [22]	January 26	7.7	0.60g	18-21

2.2.1 The 1964 Alaskan Earthquake

This event mainly affected Anchorage, a city about 75 miles from the epicenter of the earthquake. Precast prestressed elements were used in the construction of at least 28

buildings in Anchorage. Five of these buildings experienced partial or total collapse. All collapsed structures consisted of either reinforced concrete or masonry walls as primary lateral load resisting systems with precast floor slabs, except in one structure, in which precast hammerhead frames and precast single tee beams were used to transfer gravity loads [14]. Figure 2.1 shows a partially collapsed building, which also utilized relatively thick precast nonstructural reinforced concrete cladding panels [12].

Figure 2.1 Partially collapsed building with poorly connected precast floor panels [12].

Four possible reasons were attributed to the poor performance of these structures [14]:

1. Ground accelerations several times greater than the design value
2. Failure to incorporate suitable details to ensure satisfactory inelastic behavior of several primary structural systems
3. Poor connections between diaphragms and lateral force resisting elements

2.2.2 The 1977 Rumanian Earthquake

The damage was mainly reported in the city of Bucharest, 100 miles from the epicenter [15]. In Rumania, design provisions including ductility requirements were not strictly enforced prior to this earthquake and these provisions were generally less stringent than those were in the UBC 1977 [23]. Almost all of the residential buildings in the range of ten stories and above constructed prior to and in the late 1950s and beyond utilized structural systems combining precast and cast-in-place concrete technology. They include systems with precast floors and CIP columns, precast floors with CIP walls and precast beams and columns with CIP connections. All precast concrete buildings withstood the earthquake shaking satisfactorily, except for one, in which inadequate construction procedures and inferior quality of materials were reported to be the causes of the collapse of that building [15].

2.2.3 The 1985 Mexican Earthquake

The earthquake damage was largely in the Mexico City, although the epicenter was about 250 miles away from the city [16]. It is noted that the Mexican Building Code [24] adopted provisions for lateral force requirements prior to this earthquake, but they were less stringent than those published in ACI 318-83 [25]. Precast concrete structural members in the form of slabs, beams and columns were used only in a small percentage of buildings in the Mexico City. In most structures, CIP concrete was used as toppings on precast slabs and for connecting precast beams and columns. Only five of the 265 collapsed or severely damaged buildings utilized precast structural members, but none could be attributed to the use of precast concrete members. In fact, failure modes of the buildings with precast members were found to be similar to the buildings made up of only cast-in-place concrete. Surprisingly,

three large precast concrete silos (224 ft in width, 918 ft in length and 92 ft in height) experienced the earthquake without any damage [16].

2.2.4 The 1988 Armenian Earthquake

The three major cities were affected by this earthquake and the distances to these cities from the epicenter are listed in Table 2.2. Because of the closeness of the epicenter, the damage in these cities was devastating [1].

A summary of damage to precast buildings is also included in Table 2.2. As shown in the table, large panel precast concrete structures performed very well in all three cities, while 95 percent of the precast concrete frame structures in Leninakan either collapsed or experienced damage beyond repair and none was reported to be escaped damage. On the other hand, none of the precast frame structures in Kirovakan, a city closer to the epicenter than Leninakan, was reported to be collapsed or damage beyond repair and 18 percent of the precast concrete frame structures escaped damage in that city, while the rest of the precast structure suffered only repairable damage in the city. The difference in the performance of precast concrete frame structures in these two cities was attributed to the poor soil condition in Leninakan, which was suspected to have amplified the seismic energy in the frequency range close to the fundamental periods of several buildings [1].

Table 2.2 A summary of damage of precast buildings during the 1988 Armenian Earthquake [1]

City	Epicenter distance (miles)	Large panel precast Concrete structures				Precast concrete frame structures			
		A	B	C	D	A	B	C	D
Spitak	5.6	-	-	-	1	-	-	-	-
Kirovakan	15	-	-	-	4	-	-	88	20
Leninakan	20	-	-	-	16	72	55	6	-
Total	-	-	-	-	21	72	55	94	20
Total in Armenia	-	-	-	13	65	72	57	130	77

Key: Damage to precast structures in this event was reported using four different levels:

A – Collapsed

B – Heavily damaged-beyond repair

C – Repairable damage

D – No significant damage

Figure 2.2 shows the remaining of a three-story precast-concrete-frame building, one of the 72 buildings collapsed in Leninakan. Failure of precast floor panel initiated the building collapse. A four-story precast-concrete-frame building from the same city experienced a partial collapse, as shown in Figure 2.3, due to poorly detailed connections between precast floor panels and walls. The precast building, shown in Figure 2.4 is another victim of not adequately tying precast floors to lateral load resisting systems, which also consisted of precast members [12].

Figure 2.2 Collapse of floor panels, leaving cast-in-place walls standing in a building in Leninakan [12].

Figure 2.3 Damage to a four-story building in Leninakan due to inadequate connection between precast floors and walls [12].

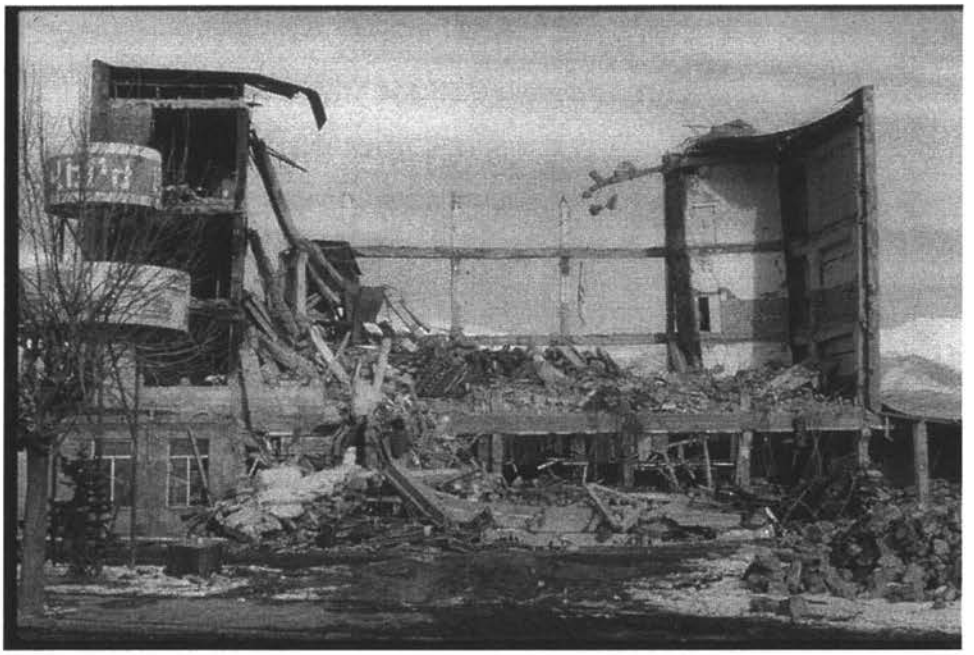

Figure 2.4 Collapse of floor panels leaving external precast frame standing in a building in Spitak [12].

2.2.5 The 1989 Loma Prieta Earthquake

The epicenter of the earthquake was located near Santa Cruz in the southeastern part of San Francisco. Several parking structures constructed with topped double-tee diaphragms and cast-in-place concrete shear walls or frames experienced the earthquake in this event. No severe damage to precast structures was reported. However, it has been reported that some cracks caused by the earthquake were visible in some structures, which were suspected to be due to poor design. Parking structures in Oakland, Emeryville and Berkeley areas performed satisfactorily [17].

2.2.6 The 1994 Northridge Earthquake

The epicenter was located in Northridge, California, where precast concrete members were commonly used in parking structures. The precast concrete was also found in residential

buildings in Northridge, but it was generally limited to architectural components [18]. Seismic performance of parking structures constructed with precast components was studied and compared with performance of other types of parking structures in reference [18]. Of the 30 parking structures located within 20 miles radius of the epicenter, 15 of them utilized precast concrete gravity columns, while 10 of them used precast double-tee slabs. Most of these structure used cast-in-place shear walls and/or moment resisting frames as lateral-load resisting systems with precast columns in the gravity frames.

Precast lateral-load resisting systems were found in one parking structure located in California State University, Northridge. This system included precast exterior frames with precast interior beams and precast interior columns. The exterior frames were designed as a special lateral-load moment frames. Haunches in the exterior frame and the interior columns supported the interior beams.

The earthquake damage to precast and non-precast parking structures in Northridge is summarized in Table 2.3. As seen in this table, five structures incorporating precast concrete gravity columns with cast-in-place lateral-load resisting systems experienced no damage, while four such structures exhibited minor cracks. However, four similar structures and the structure with precast exterior moment resisting fames experienced partial collapse. In comparison, only two of the 15 structures, which had no precast components, partially collapsed, while damage to the rest of the structures was localized and generally limited to some structural members [18].

Table 2.3 Degree of damage to precast parking structures during the 1994 Northridge Earthquake

Parking Structures	Quantity	Collapsed		Damage to structural members	Minor damage	No damage
		Extensive	Partial			
Precast exterior frames and precast gravity columns	1	-	1	-	-	-
Precast gravity columns	14	1	4	-	4	5
No precast elements	15	-	2	13	-	-
Total	30	1	7	13	4	5

A view showing the collapsed portion of the parking structure at California State University, Northridge is shown in Figure 2.5. Failure of interior columns due to overloading in the vertical direction appeared to have initiated the collapse, as this failure resulted in interior beams being dropped from the haunches of failed interior columns and the interior beams being rotated vertically downward. This in turn caused the sagging of slabs and pulling of the exterior frame inwards in the out-of-plane direction. Figure 2.5 shows the separated exterior frames at a corner, as the frames in the orthogonal direction were not connected to one another. A second view of the parking structure on the campus of California State University is shown in Figure 2.6.

Figure 2.5 Collapse of center columns, floors and external moment frame of a parking structure at Northridge [2].

The followings were reported to be the common shortcomings in the design of the parking structures presented in Table 2.3 [18]:

1. Inability of gravity load frames to deform laterally with lateral-load resisting systems;
2. Presence of insufficient number of lateral-load resisting systems in the plan of the structure
3. Improper transfer of horizontal forces by intermediate elements, referred to as collector elements, before transferring the horizontal forces to lateral load resisting systems; and
4. Brittle behavior of gravity load elements when overloaded in the vertical direction.

Figure 2.6 Another view of the collapsed parking structure at Northridge [12].

2.2.7 The 1995 Kobe Earthquake

The epicenter was located about 12 miles southwest from downtown Kobe, Japan. In the region where damage to structures was mainly reported, there were 11 buildings that utilized precast concrete members, while non-structural precast components were found in another 49 buildings. Buildings with precast structural members were relatively new and regular in shape with uniform distribution of mass and stiffness. Most of these structures performed remarkably well except for a few buildings, in which some structural damage was evident. Typical damage included the followings [19]:

1. Failure of cast-in-place concrete columns prior to yielding of prestressed beams connected to the columns;

2. Unseating of roof panels from peripheral beams due to the failure of steel bolts connecting the panels to the beams; and
3. Failure of cast-in-place concrete columns causing precast roof panels to unseat.

2.2.8 The 1999 Kocaeli Earthquake

In Turkey, precast frame buildings have been widely used for single-story warehouses [20]. The lateral load resisting frames used in these structures were designed by modifying the connection details of gravity load resisting frames that are typically used in Western Europe. Performance of the precast structures in the epicentral regions was reported to be unsatisfactory due to inadequate detail at the base of the columns to allow formation of flexural hinges to meet the ductility demand imposed during this event. Another reason attributed to the poor performance of these structures is pounding of precast elements at the roof level [20].

2.2.9 The 1999 Chi-Chi Earthquake

Most of the mid-rise buildings were constructed with reinforced concrete and high-rise buildings with structural steel. Although a number building failure was reported, information specific to precast buildings was not reported in the literature [21].

2.2.10 The 2001 Bhuj Earthquake

This was an intra-plate earthquake and compared to event of the 1811 and 1812 New Madrid earthquakes [26]. The application of precast concrete was limited to some single-story school buildings in the region where this event caused damage. The single-story

structures consisted of large precast concrete panels as roof and walls and precast concrete columns. It was reported that about one-third of such buildings experienced roof collapse due to the following reasons [22]:

1. Poor connections between roof panels; and
2. Inadequate seating of roof panels that were supported on walls and beams.

2.3 Experimental studies

2.3.1 Background

Over the past three decades, there has been significant number of experimental studies that have investigated framing aspects of precast members for seismic resistance. These investigations were motivated by:

- potential benefits of precast concrete technology
- absence of design provisions to establish reliable precast systems for seismic applications
- requirement of hysteretic energy dissipation in seismic design
- poor performance of precast systems in past earthquakes

A review of various experimental studies is presented below for both emulative and non-emulative type precast frame systems based on their connection types.

2.3.2 Emulative Connections

2.3.2.1 Ductile-Wet Connections

Research on ductile-wet emulative connection for precast systems suitable for seismic design has been conducted in New Zealand, United States and Canada. As previously noted, this connection type emulates performance of equivalent monolithic systems in terms of strength, stiffness, ductility, story-drift and energy dissipation capacity. Inelastic actions and energy dissipation mechanisms are concentrated within the connections.

Blakeley and Park (New Zealand, 1971) [27]

Four full-scale precast subassemblies were tested. Amount of transverse confining steel in the beam-to-column connection region and the position of the plastic hinge were varied between test units. Reinforcement details of Unit 1, one of the specimens tested, is shown in Figure 2.7. Columns and beams of the specimens were pretensioned and mortar was used at the precast joint interface to ensure continuity between members. Figure 2.8 shows cyclic loading history used in the tests.

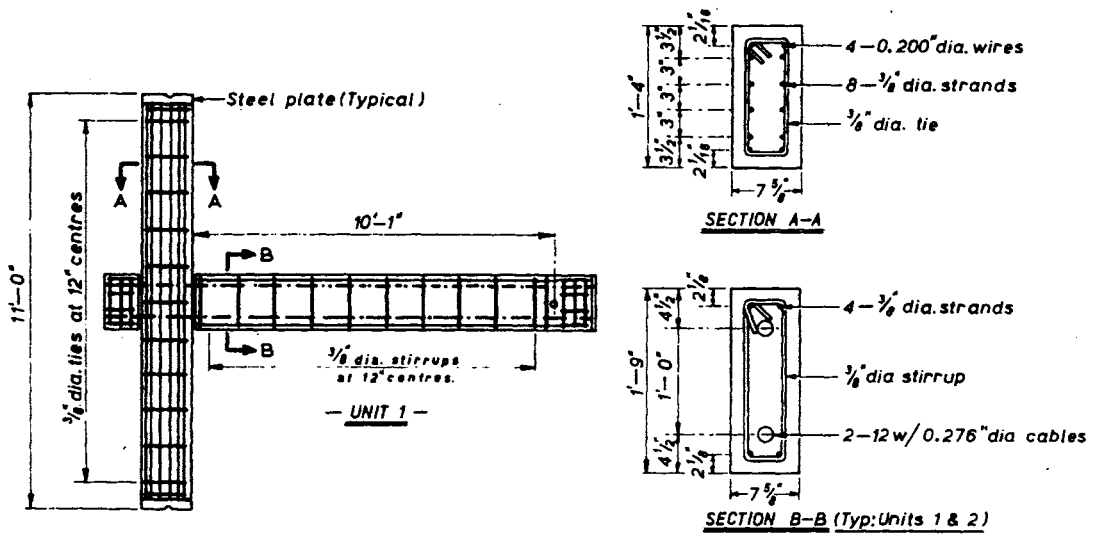

Figure 2.7 Details of Unit 1 [27].

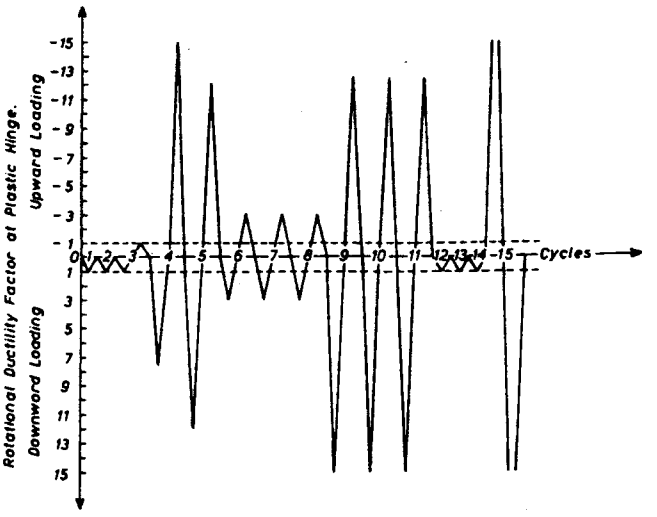

Figure 2.8 Cyclic load sequence used by Blakeley and Park [27].

Variation of curvature along the beam and columns, as shown in Figure 2.9 for Unit 1, shows that the connection accommodated large post-elastic deformation and behaved similar to an equivalent monolithic connection. However, as a result of stiffness degradation and bond failure at extremely large loading, the connections used between precast members were concluded to be adequate for moderate level of earthquakes and would cause structural damage in severe earthquakes. Transverse reinforcements in all specimens were remained elastic and it was reported that no significant advantage would be gained by increasing the transverse reinforcement content. Further study was suggested for improving energy dissipating capacity at large displacements.

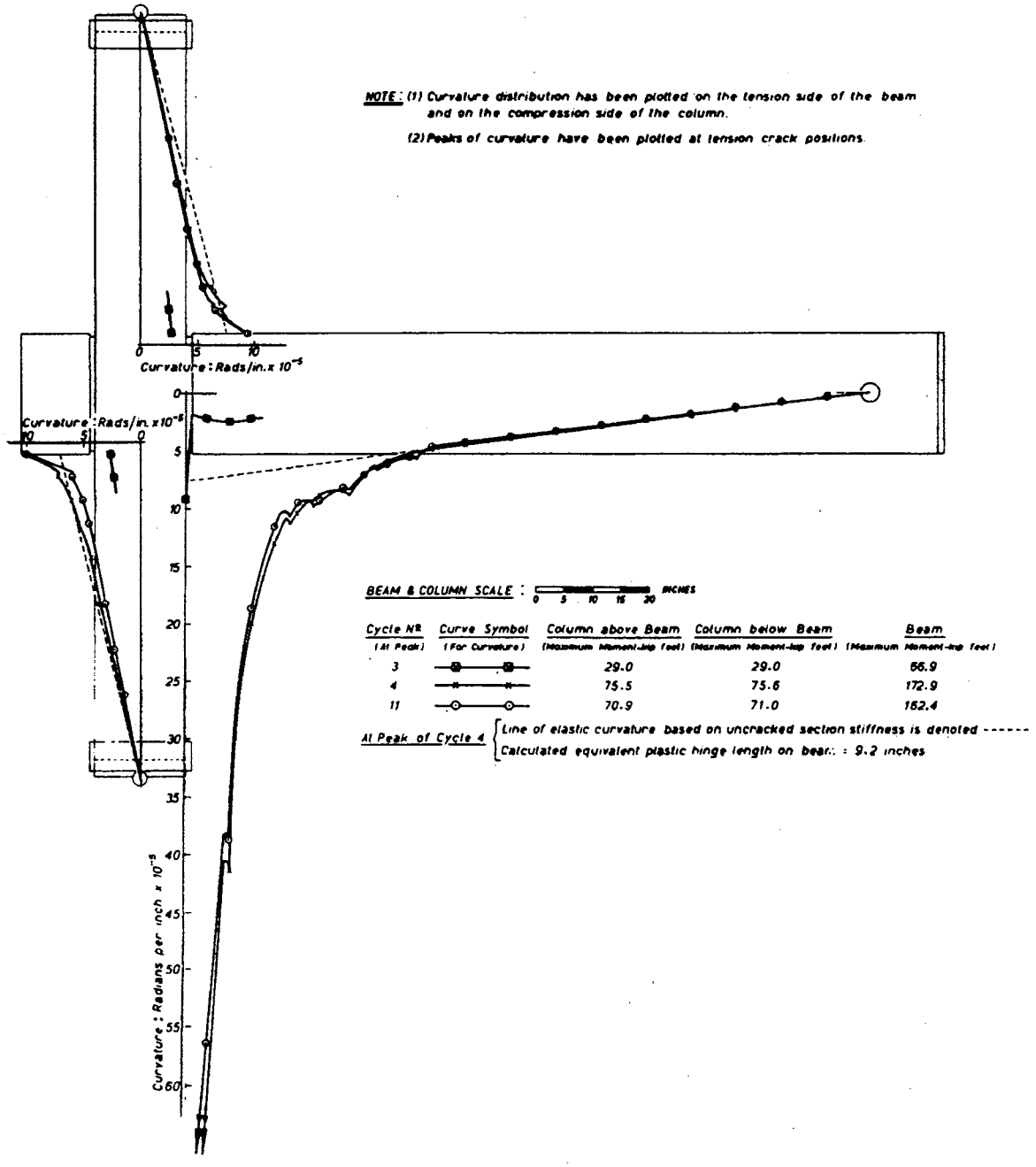

Figure 2.9 Curvature distribution along members of Unit 1 [27].

Pillai and Kirk (Canada, 1981) [28]

Nine precast concrete and two monolithic concrete beam-column connections were tested. A typical precast concrete beam-to-column connection detail is shown in Figure 2.10. This connection was made by welding top beam longitudinal reinforcement to short U-bars anchored into the column and by welding plates embedded in the beam.

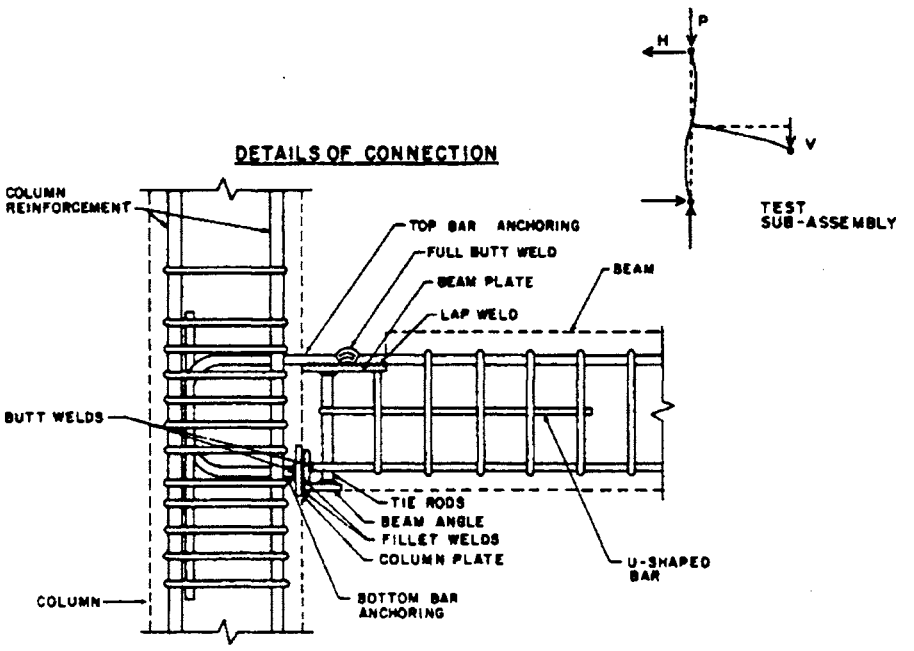

Figure 2.10 Details of connection [28].

These precast and monolithic beam-column systems were subjected to cyclic loading sequence shown in Figure 2.11(a). It was observed that the number of cycles that all precast systems sustained equal or greater number of load reversals than the monolithic frame systems. Rotation at the beam end was measured over a distance of 400 mm as shown in Figure 2.11(b), which resulted in rotational ductility values in the range of 5 to 13 for precast specimens.

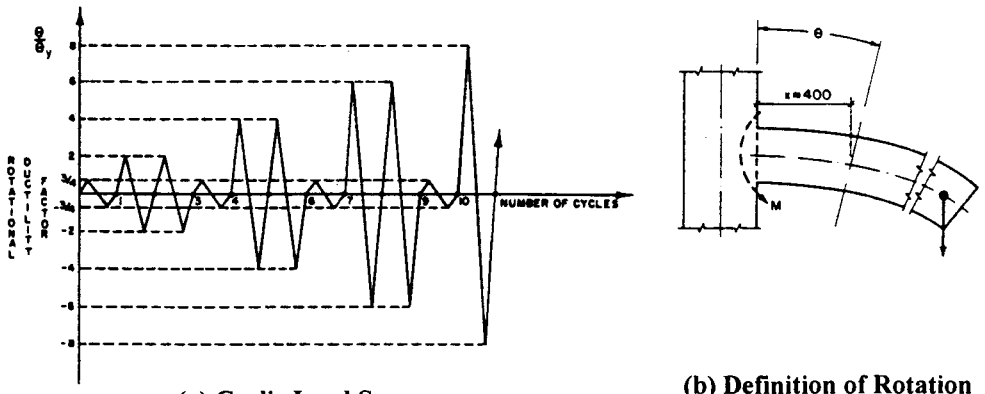

(a) Cyclic Load Sequence

(b) Definition of Rotation

Figure 2.11 Loading Criteria [28].

Even though no sufficient stiffness degradation was observed, residual rotations were seen at the end of the loading cycles. It was reported that all precast systems had behavior comparable to the monolithic systems in terms of strength, stiffness, energy-absorption capacity and ductility.

French, Hafner, and Jayashankar (USA, 1989) [29]

Seven connection details suitable for precast beam-to-column frames were tested. These connections utilized:

- bonded post-tensioning in 1 specimen
- threaded reinforcing bars in 3 specimens
- cast-in-place concrete topping with post-tensioning in 1 specimen
- cast-in-place concrete topping with bolted details in 1 specimen
- cast-in-place concrete topping with welded details in 1 specimen

The first and the last connections were detailed to be strong connections, forcing hinging to develop in precast beams away from the connection interface, while the rest of them were designed as ductile connections. Figure 2.12 shows a longitudinal cross section of the post-tensioned framing concept. All of the specimens were tested with cyclic loading by controlling beam end displacement and the cyclic load history, as shown in Figure 2.13 was used in the tests.

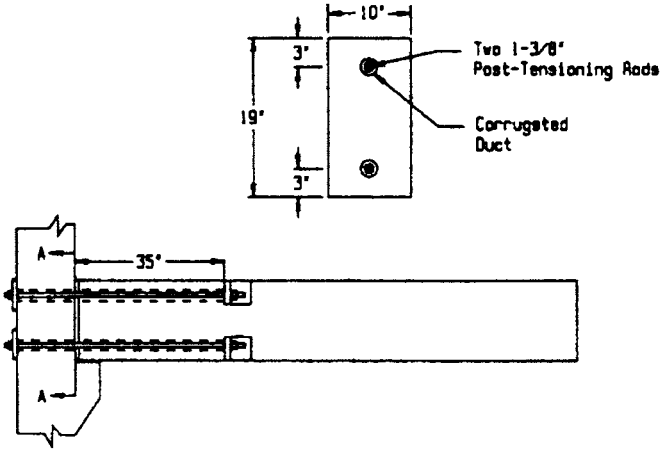

Figure 2.12 Detail of bonded post-tensioned connection [29].

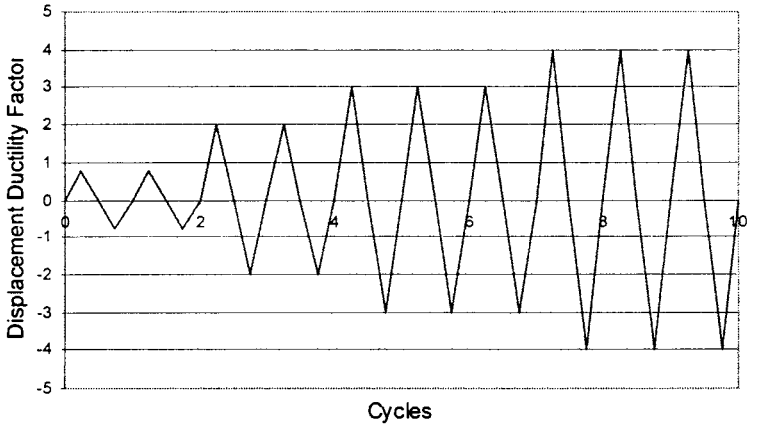

Figure 2.13 Cyclic load history used by French et al. [29]

All the connections performed well providing satisfactory strength, ductility, and energy dissipation, except for specimens with strong connections, which exhibited limited ductile behavior. In general, the specimen that utilized threaded bars with tapered-threaded splices exhibited more promising performance suitable for use in seismic regions.

Seckin and Fu (Canada, 1990) [30]

Three precast and one monolithic beam-column connections were tested. Connections between precast beam and column members were made by welding two sets of embedded beam plates to two sets of embedded column plates as shown in Figure 2.14. One set of horizontal plates connected the top and bottom of the beam to the column to provide moment connection, while the other set of plates was used to transfer shearing forces.

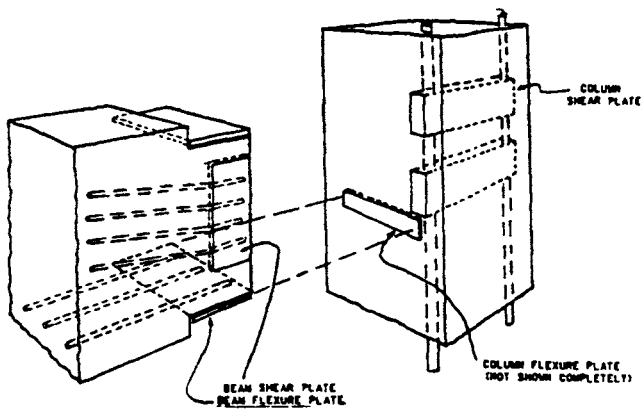

Figure 2.14 Precast framing concept using flexural and shear plates [30].

It was reported that the precast beam-column connections with the simple and economic flexural and shear plates performed in a manner comparable to their performance of the

monolithic counterpart. However, authors suggested further research prior to formalizing design recommendations.

Restrepo, Park, and Buchanan (New Zealand, 1995) [31]

Six subassemblages with varying connection details that could be used in precast reinforced concrete perimeter frames were tested. These perimeter frames were designed for mid-rise buildings located in seismic regions and were assumed to take the lateral design forces. Figure 2.15 shows dimensions and reinforcement details, one of the test units, while cyclic load sequence applied to the test specimens is shown in Figure 2.16.

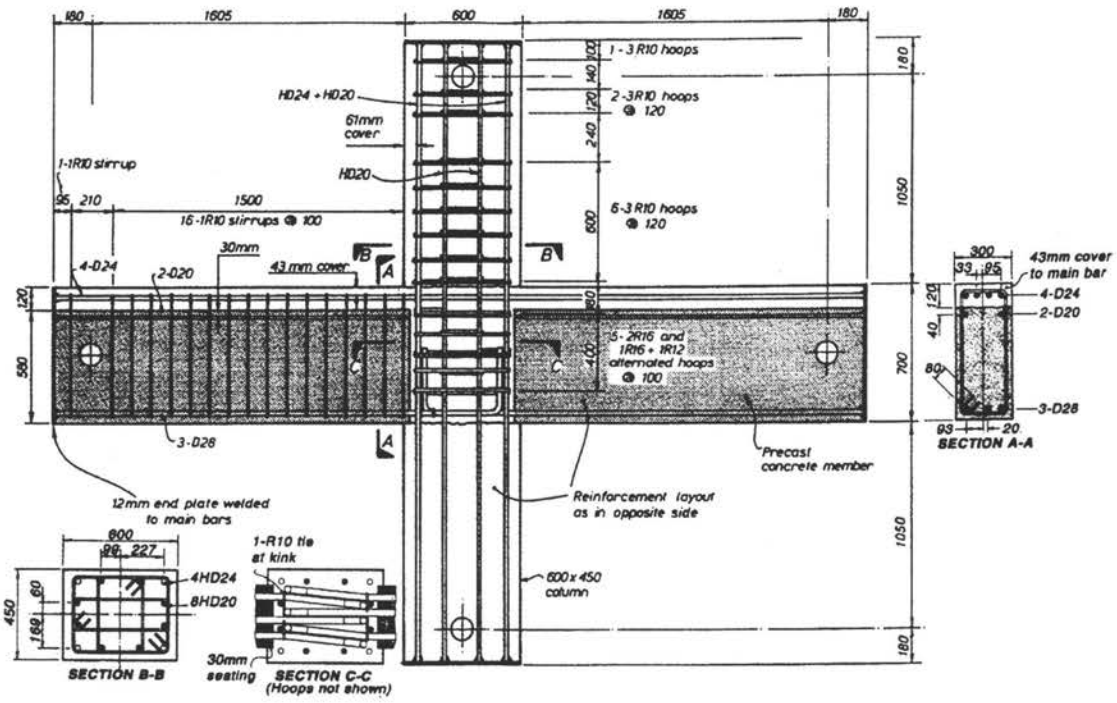

Figure 2.15 Reinforcing details of Unit 5 tested by Restrepo et. al. [31].

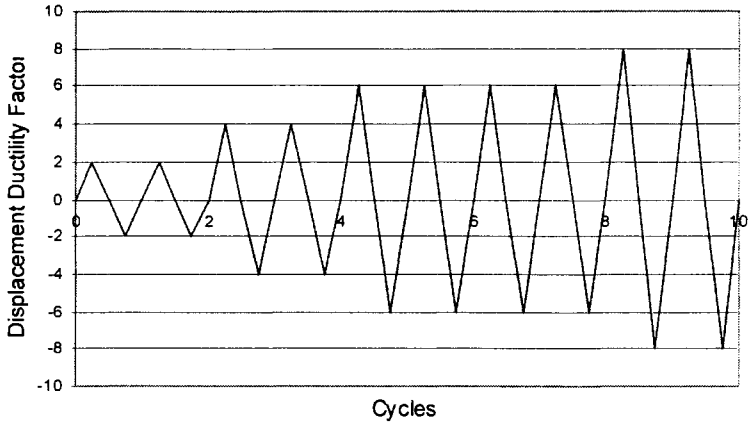

Figure 2.16 Cyclic load sequence used in the tests by Restrepo et al. [31].

A summary of the test observations are as follows:

- All test units, except Unit 4, exhibited displacement ductility factor of at least 6.0 and inter-story drift of at least 2.4 percent during the tests, while resisting at least 80 percent of the all units, except for Unit 5, were within the requirement of the local code.
- In Unit 5, cast-in-place concrete placed to form a tee-joint between the column and the two beams showed excessive bleeding and plastic settlement during casting appeared to be poor quality. Consequently, bond failure of the top beam bars anchored in the cast-in-place concrete joint core was observed, causing a larger inter-story drift than that observed for the other units, despite the excellent performance in terms of ductility.
- Performance of mid-span connections between precast beam elements was excellent.
- The construction joint of a unit, which consisted of a continuous precast beam passing through the column and grouting of the column bars in vertical corrugated ducts in the joint region performed very well.

- The New Zealand concrete code requires that the compressive strength of grout in precast connection to be larger than the compressive strength of precast concrete elements. In the test units, the grout strength was at least 1.45 ksi greater than the average compressive strength in precast elements, which was found to be satisfactory.

Alcocer at el. (Mexico, 2002) [32]

Two full-scale subassemblies consisting of precast beams and columns were tested. These framing of the systems established using cast-in-place concrete joint core and cast-in-place concrete topping on the beams. The precast column was discontinuous through the joint and was made continuous using the cast-in-place concrete in the joint region and for a column region above the joint, as shown in Figure 2.17. the cyclic load sequence used for this test series is given in Figure 2.18.

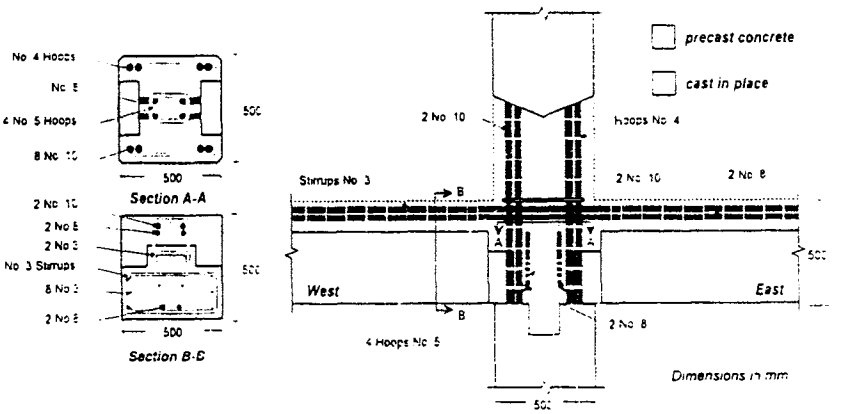

Figure 2.17 Connection detail of precast beams with column [32].

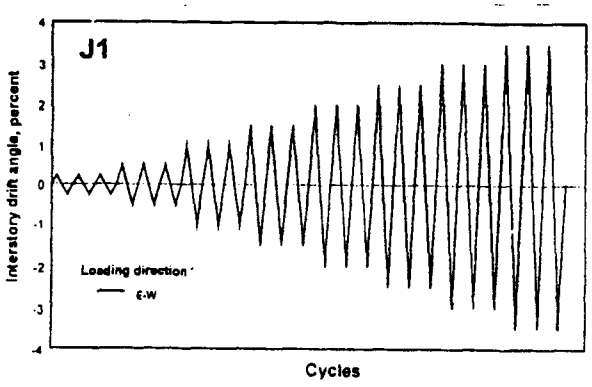

Figure 2.18 Displacement-controlled cyclic load sequence adopted by Alcocer et. al. [32]

All test specimens exhibited ductile behavior and no significant reduction in the lateral load resistance was seen up to an inter-story drift of 3.5 percent. The test specimens also attained shear strength values at least 80 percent, of the expected values from equivalent monolithic systems. It was concluded that, even though the connections did not fully emulate monolithic systems, the tested precast concept would be appropriate for use in seismic regions.

2.3.2.2 Strong-Wet Connections

Limited studies have been conducted on emulative type strong-wet connections. This method of connection generally requires the connections to be designed for over strength [7] and precast elements to form plastic hinges at preselected locations. Two specimens were tested by French et. al. [29] as part of an investigation summarized in Section 2.3.2.1. The first author with two others carried out another experiment on strong-wet connections. The detail of that study is presented below.

French, Amu, and Tarzikham (USA, 1989) [33]

Four different types of specimens were tested, which are:

- one connection with post-tensioned tendon;
- one connection with threaded bars;
- one connection with post-tensioned steel and cast-in-place concrete toppings; and
- one connection with welded plates.

The connections and the precast elements were designed to relocate the plastic hinge at 35 inches away from the beam-column connection interface. The detail of the specimen connection with welded plate connection is shown in Figure 2.19. The cyclic load history used for these tests was the same as that is shown earlier in Figure 2.13.

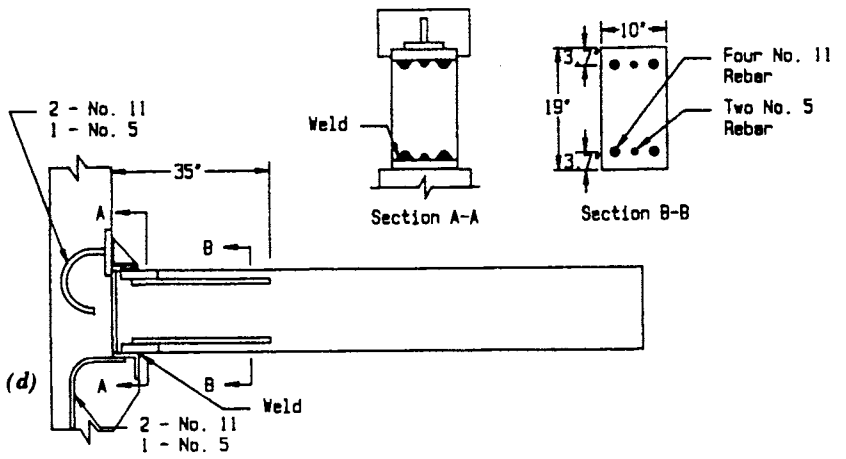

Figure 2.19 Cross-section details of the frame system with welded plate connection used by French et. al. [33].

The two specimens with connections using the threaded bars and post-tensioned tendons combined with cast-in-place concrete failed to attain the calculated flexural capacities and exhibited limited energy dissipation, despite the fact that the latter was expected to show

more energy dissipation due to the presence of reinforcement bars at the top of the beam. All units demonstrated good ductility capacities and inter-story drifts. This study concluded that these strong-wet connections experimented in this study could be designed effectively for adequate strength, ductility, stiffness, and energy dissipation capacity to resist earthquake loading.

2.3.2.3 Ductile-Dry Connections

Dry joints exploit intrinsic features of precast concrete technology and promote speedy construction practice. However, establishing suitable strong or ductile connections has been a challenge. An experimental study investigating development of ductile connection behavior is discussed below.

Nakaki, Englekirk, and Plaehn (California, 1994) [34]

An embedded ductile link was used to connect precast beams and precast columns by bolting the beams to the column faces. The prime element in this connection is the ductile rod, which is made of high quality steel with well-defined strength characteristics and high elongation capacity. Components used in the connection are shown in Figure 2.20 and a plan view of a connection is shown in Figure 2.21.

During the tests, even though the connection rod was subjected to several repeated stress reversals, no horizontal cracking was appeared in the joint. However, more diagonal cracking was apparent in the connection with precast elements than an equivalent monolithic connection. It is reported that this system achieves the inherent attributes of precast concrete systems in seismic regions without increasing the erection costs much.

A significant number of joint diagonal cracks were visible on the test units, which appeared to more severe than that expected in equivalent monolithic frames. The authors concluded that the proposed system utilized the inherent attributes of precast concrete systems to provide a satisfactory framing concept for the application in seismic regions without significant increasing the erection costs.

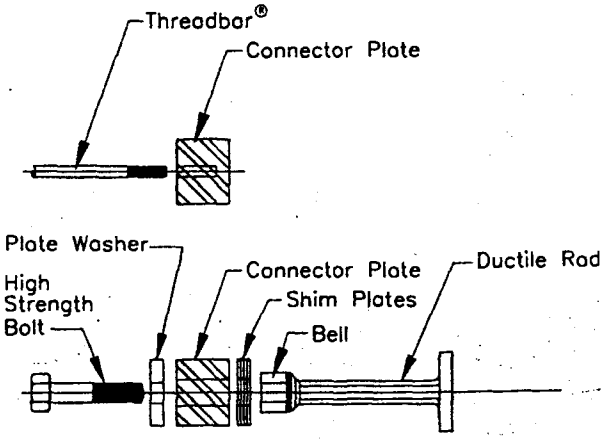

Figure 2.20 Ductile connector components [34].

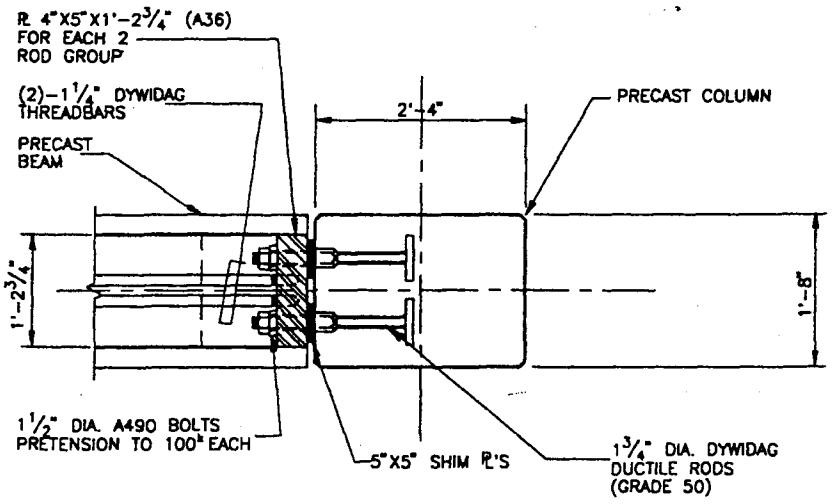

Figure 2.21 Ductile connection detail in plan [34].

2.3.2.4 Strong-Dry Connections

There are two logical approaches to establish a strong-dry connection based on the definition of this framing concept given in Section 1.2.2. In the first approach, One way is to joint precast beams and column brackets at the places away from the column face in a manner to form plastic hinges at the joint while the interface of the beam and column, generally cast, is designed to be stronger than the precast elements. In the second approach, precast beams, which are designed to form plastic hinges at selected intermediate locations away from beam ends, are connected to precast columns such that moment resistance of the connections are greater the selected plastic hinges [7]. The following is a summary of experiments that investigated the two possible strong-dry connections.

Ersoy and Tankut (Turkey, 1993) [35]

Five precast units simulating two different connection types and two monolithic connections were tested to qualify the use of the dry connections in four-story precast concrete buildings to be built by FEGA-GAMA Construction Company. Two different precast connections, as shown in Figure 2.22, were investigated with Type I in two specimens and Type II in three specimens.

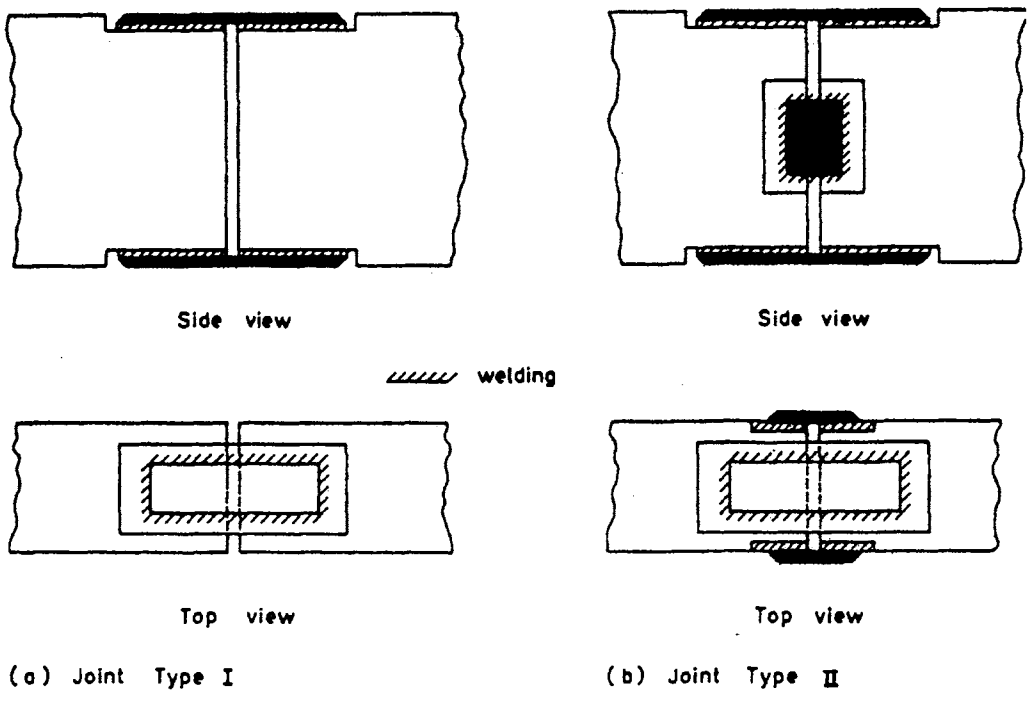

Figure 2.22 Two types of joints investigated by Ersoy and Tankut [35].

The precast members were connected at 30 inches away from the column face by two steel plates, one at the top and the other at the bottom, welded to the anchored steel plates in the column bracket and the beam. Additional site plates and the joint width were the test variables.

Figure 2.23 shows a typical specimen, support and loading arrangements, where the central block represents the column and loading sequence used in the tests is given in Figure 2.24 The precast members were connected at 30 inches away from the column face by two steel plates, one at the top and other at the bottom, and welded to the anchored steel plates in the column bracket and the beam. Additional site plates and the joint width were the test variables.

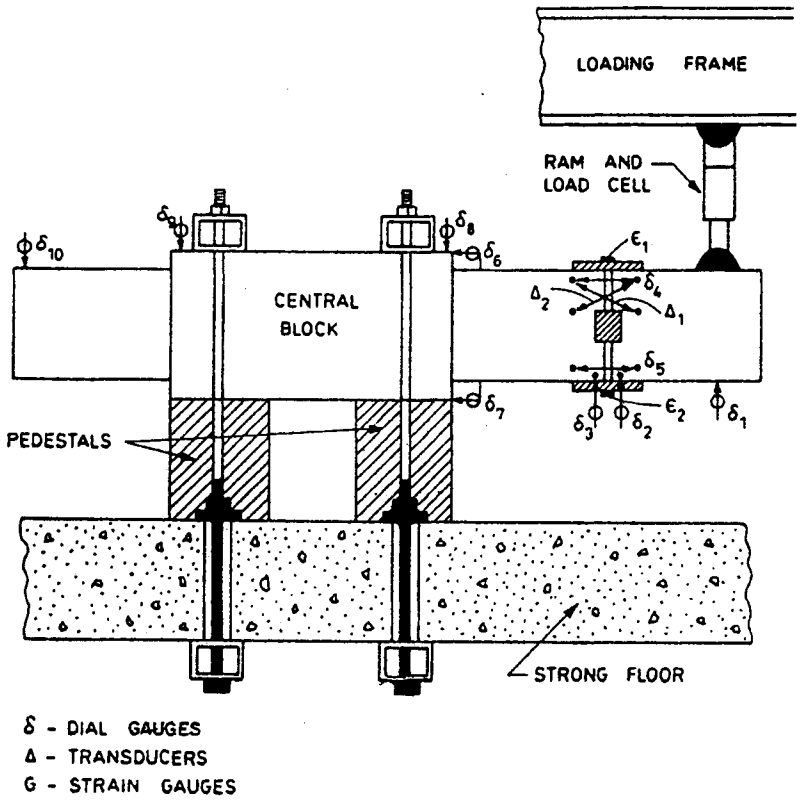

Figure 2.23 Test unit arrangement [35].

Three specimens (one with Type I and two with Type II) were redesigned, as a result of premature failure observed due to the poor reinforcement detailing at the beam end, which is connected to the column bracket.

During the tests, it was found that the use of the side plates reduced the deformations and increased the load carrying capacity. The joint width was found to be an important factor when the member is subjected to cyclic loadings and needed careful attention in the design stage. The strength, stiffness and energy dissipating capacity of the dry joints were comparable to those of monolithic connections. It was reported that the improved design connection details tested in the study were used in all the dormitory building constructed by FEGA-GAMA Construction Company.

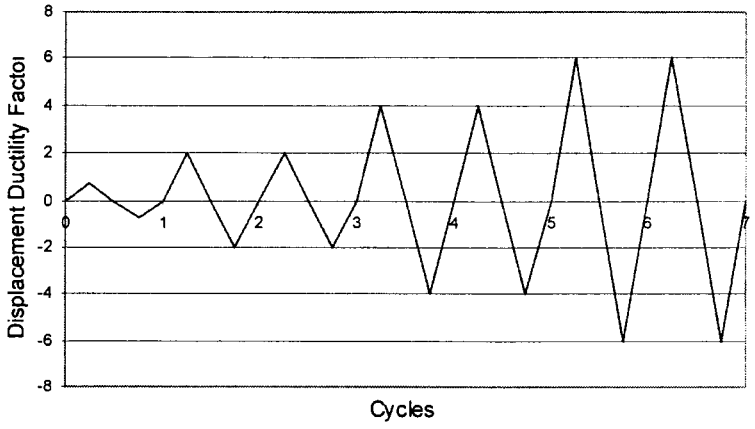

Figure 2.24 Cyclic loading sequence.

Ochs and Ehsani (USA, 1993) [36]

Two subassemblages of precast elements with plastic hinges at the column face, two subassemblages of precast elements with relocated plastic hinges, and one monolithic concrete frame were tested. The relocated plastic hinges were designed to be one beam depth away from the column face. The precast connections were made by welding a fabricated steel tee-section embedded in the column to a steel angle embedded in the beam. The welded connection applied at the top and bottom of the beam as shown in Figure 2.25.

The test confirmed that the plastic hinges can be successfully relocated with intermediate layers of tension and compression longitudinal reinforcement. The connection regions in both precast and monolithic units, which had the same amount of confinement reinforcement, exhibited comparable behaviors in terms of strength and ductility. Therefore, researchers concluded that the confinement requirement for monolithic concrete is also adequate for precast frames.

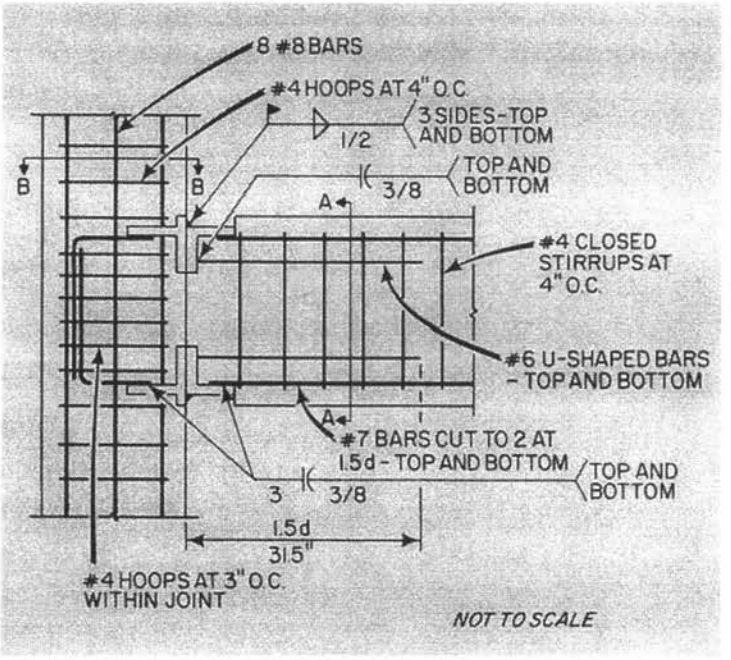

Figure 2.25 Typical connection details adopted by Ochs and ehsani [36].

2.3.3 Non - Emulative Connections

A non-emulative design approach exploits the intrinsic features of precast, prestressed concrete technology, which enable efficient construction techniques. A series experiments on non-emulative type ductile-dry connections, often referred to as jointed connections, was carried out at NIST. Similar connection details were also tested as a part of the PRESSS research program. A review of published information on ductile-dry connections is presented below.

Cheok and Lew (NIST, 1991) [37]

An extensive experimental investigation was conducted at NIST on precast frame sub-assemblages with the objective of developing rational design procedures for precast frame connections for seismic regions. The tests were done in three phases on one-third scale monolithic and precast beam-column connections subjected to cyclic loading. Phase I was an exploratory stage where the performance of precast connections were compared with that of monolithic counterparts. Three units of precast connections with post-tensioned steel were planned to be tested in Phase II. Factors such as hysteretic behavior, strength and ductility were investigated in phase III, which was intended to be coordinated with the PRESSS program.

Four monolithic and two precast specimens were tested in Phase I. The monolithic connections were designed in accordance with UBC 1985, with two specimens suitable for Zone 4 and two other for Zone 2. The precast specimens, which used grouted post-tensioning, were similar in dimensions to the monolithic specimens designed for Zone 4. The gap between precast beams and columns were filled with fiber-reinforced grout.

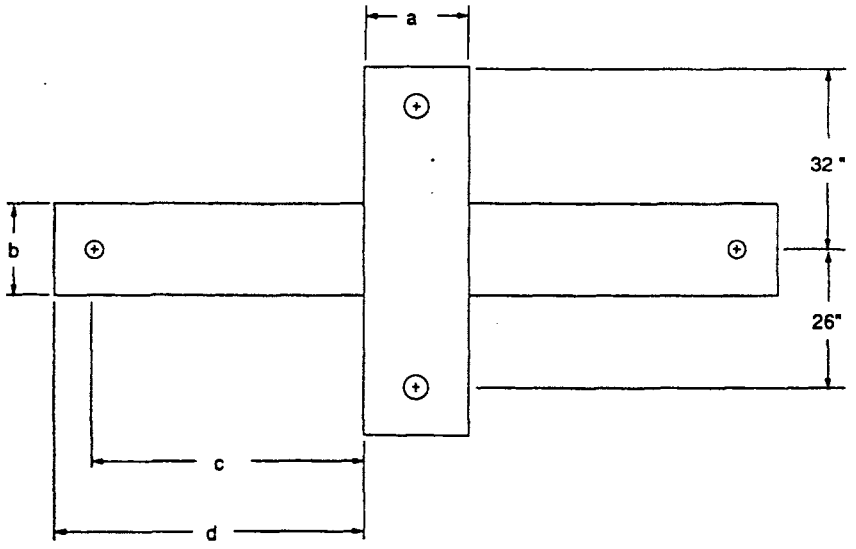

(a) Schematic diagram of a typical specimen

	ZONE 2	ZONE 4	
	A-M-Z2 & B-M-Z2	A-M-Z4 & B-M-Z4	A-P-Z4 & B-P-Z4
a	10"	18"	18"
b	10	16	16
c	40	41-3/4	37
d	46	47-3/4	43

(b) Specimen dimensions

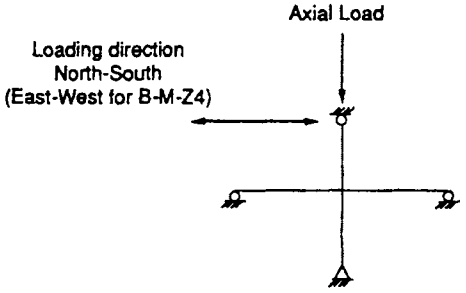

(c) Support conditions

Figure 2.26 Details of specimens [37].

Details of specimens tested during the Phase I are shown in Figure 2.26. They were denoted by three alphabets followed by a numeral. The middle alphabet is either M or P corresponding to monolithic or precast, respectively, and the last two letters are either Z2 or Z4 representing Zone 2 or Zone 4, respectively. For example, B-M-Z4 means monolithic type B designed for Zone 4.

These specimens were subjected to a cyclic load sequence, which is shown in Figure 2.27. The precast specimens generally, exhibited the behavior in a manner at least equivalent to the behavior of monolithic specimens in terms of strength, ductility and drift level. However, the energy dissipation capacity of precast concrete specimens needed improvements. Figure 2.28 shows load-displacement behavior of one set of monolithic and precast specimens.

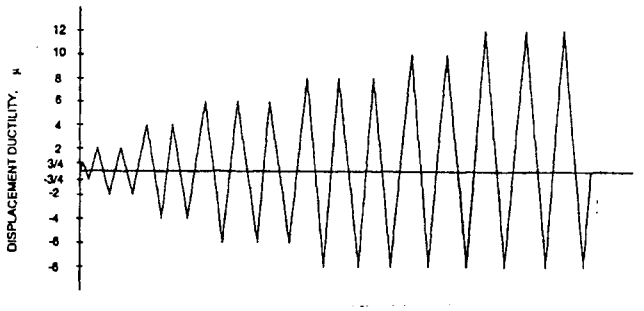

Figure 2.27 Loading sequence [37].

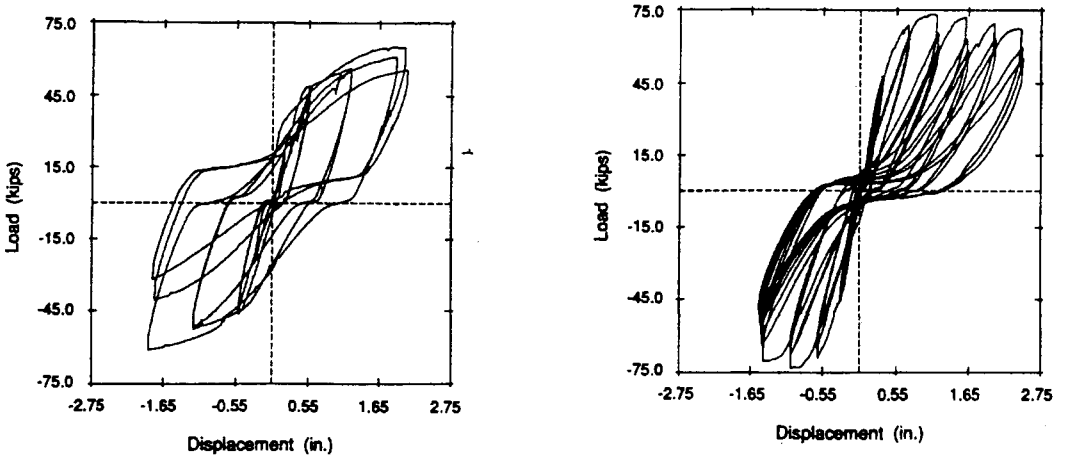

(a) Specimen dimensions (A-M-Z4)

(b) Support conditions (A-P-Z4)

Figure 2.28 Load-displacement hysteresis [37].

In comparison with the monolithic specimen, the precast concrete connections designed for zone 4 exhibited only 30 percent of the energy dissipation per load cycle. In order to enhance the energy dissipation capacity per cycle, locating the prestress bars closer to the mid-height of the beam and debonding the prestressing strands were suggested for consideration in Phase II and Phase III, respectively.

Cheok and Lew (NIST, 1993) [38]

The test program described above was expanded to Phase IV. In Phase II, six precast specimens, two for Zone 2 and four for Zone 4, were tested. Two specimens with partially debonded specimens were tested in Phase III. In addition to changing the location of prestressing steel, the effect of using prestressing strands instead of post-tensioning bars was investigated in Phase II.

In Phase III, the strands were left unbonded in the connection region to avoid a zero slope of the hysteresis loops upon load reversal that was observed during Phases I and II. The previous tests, the inelastic response of the strands was considered to be the main contributor to the observed hysteresis response. The concept of partially bonded post-tensioning steel used in these tests was suggested by Priestley and Tao [16/42].

Considering the results from Phase II, the connection strength, ductility and drift levels of precast connections tested in Phase III were superior to those of monolithic counterparts tested in Phase I. Even though the precast specimens designed for Zone 4 displayed accumulated energy dissipation more monolithic specimens, energy dissipation in precast systems was about 60 percent of monolithic ones when determined for a particular loading cycle. It was also reported that the opening at the beam-column interface was increased, as

the post-tensioning bars was moved closer to the beam centroid. However, the increased interface opening did not significantly affect the connection strength.

As shown in Figure 2.29, the specimens tested in Phase III with partially bonded post-tensioning did not result in zero stiffness upon load reversal as experienced in Phase I, despite the fact that partially bonded specimens produced narrower hysteresis loops compared to bonded specimens. This implied that lower energy was dissipated due to elastic behavior of post-tensioning steel. Examining the advantage of adding mild steel reinforcement, as a means of energy dissipating elements, was suggested for consideration in Phase IV.

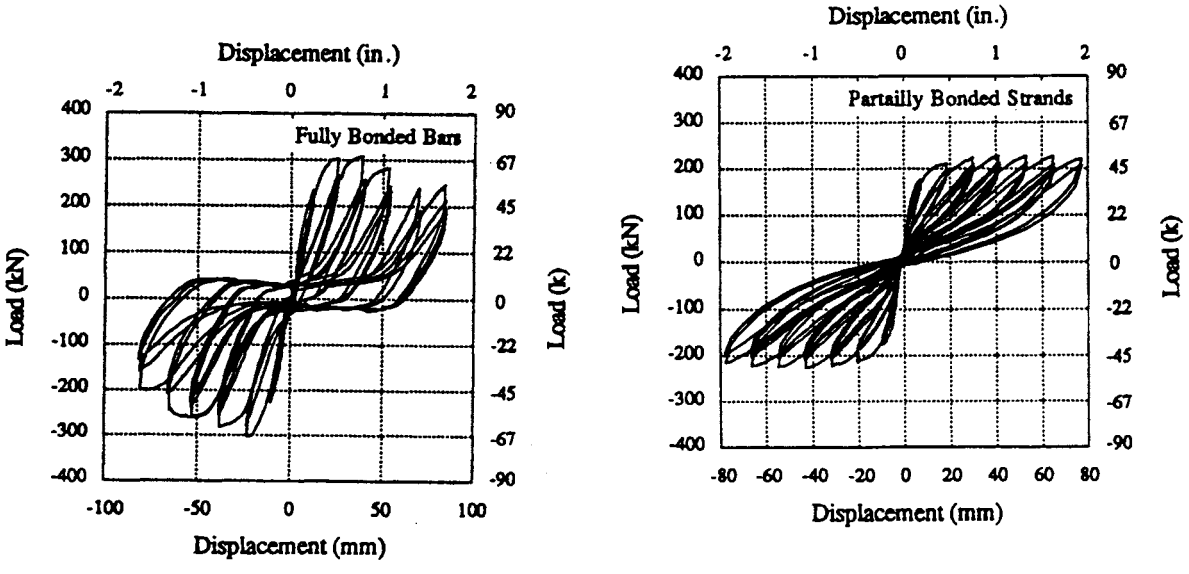

(a) F-P-Z4 (Fully bonded strand)

(b) F-P-Z4 (Partially bonded strand)

Figure 2.29 Load-displacement behavior for connections with fully and partially bonded stands [38].

Stone, Cheok and Stanton (NIST, 1995) [39, 48]

In Phase IV of the series on experimental studies at NIST, ten hybrid connections consisting of unbonded post-tensioning and mild steel reinforcement were tested in two sub-phases, namely Phase IV-A and B. Phase IV-A involved testing of six specimens with three different design specifications. There were two connections with fully bonded mild steel at the top and bottom of the beam and the post-tensioning steel located at mid-height of the beam, one connection was designed with fully bonded mild steel and unbonded post-tensioning steel, both located at the top and bottom of the beam. Three other connections were designed with unbonded mild and post-tensioning steels. Variables in the test of Phase IV-A were the location of the post-tensioning steel, amount and type of energy dissipation steel.

Phase IV-A results were used as guidance to detail connections for Phase IV-B. From the results of Phase IV-A, it was found that placing the post-tensioning steel at the mid-height was appropriate to provide adequate shear resistance at the precast connection interface. It was also felt appropriate to debond the mild steel in beam on either side of the precast interface to prevent accumulation of inelastic strains and thus premature fracture, as observed in tests of Phase IV-A.

Four hybrid connections, M-P-Z4 through P-P-Z4, were tested in Phase IV-B and the dimensions and test configuration of the specimens are shown in Figure 2.30. The specimens were provided with three ½ in. Grade 270 prestressing strands located at the beam mid-height of the beam. The strands were prestressed to 118.8 ksi. The main test variables were the amount and type of mild steel reinforcement at the precast connection. Two No. 3 and three No. 3 mild steel reinforcing bars at the top and bottom of the beam were used in specimens

M-P-Z4 and O-P-Z4, respectively. Two 0.31- inch and three 0.31 - inch diameter stainless steel bars at the top and bottom of the beam were used in specimens N-P-Z4 and P-P-Z4, respectively. All reinforcing steel placed at the top and bottom of the beam were debonded over an inch length on either side of the column, except in P-P-Z4. Fully bonded reinforcement was provided in P-P-Z4 to avoid bond failure observed in the test of N-P-Z4.

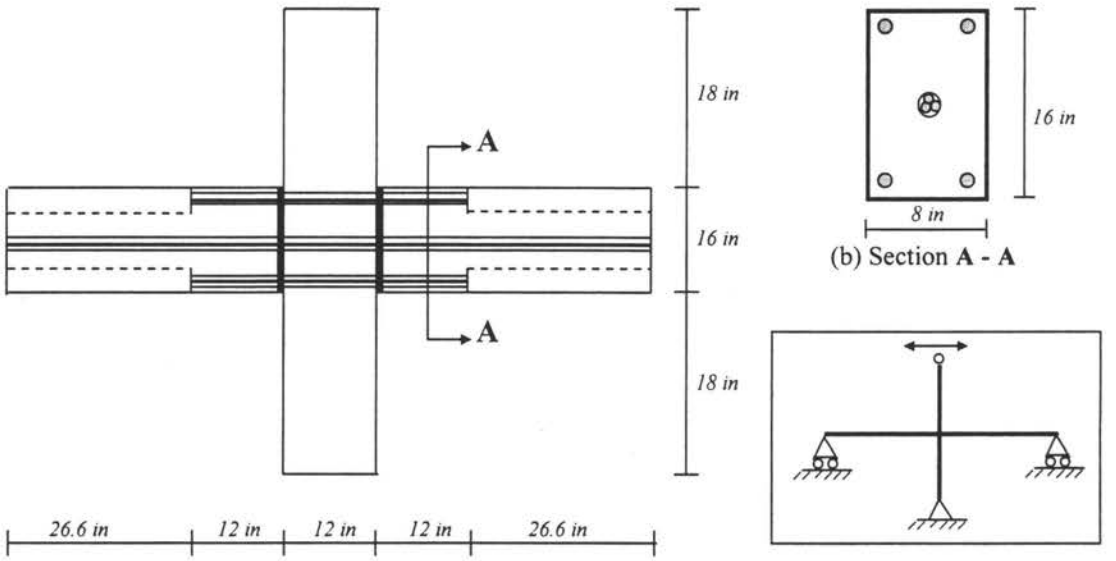

(a) Schematic of the test specimens

(b) Section **A - A**

(c) Support conditions of the specimens

Figure 2.30 Precast subassembly with hybrid connection tested in Phase IV-B by Stone al el. [39].

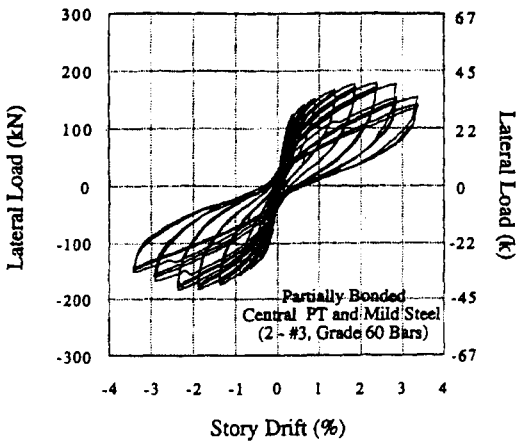

(a) For M-P-Z4

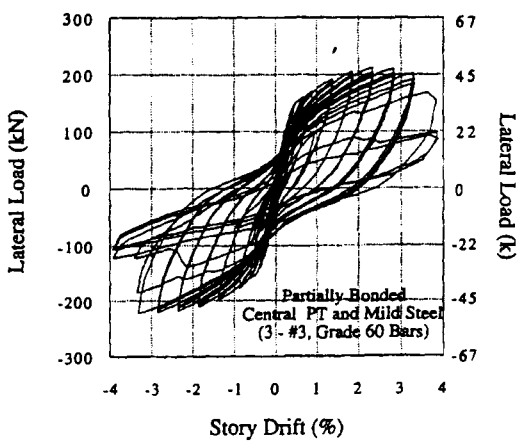

(a) For O-P-Z4

Figure 2.31 Hysteresis curves obtained for hybrid connections by Stone al el. [39].

Fracture of mild steel bars at a column drift level greater than 3.5 percent initiated the failure of the specimens M-P-Z4 and O-P-Z4. In the case of N-P-Z4, bond failure of stainless steel resulted in premature failure of the specimen. Post-tensioning steel remained elastic through out the test in all specimens with the average peak stress recorded in the post-tensioning steel being less than 90 percent of the ultimate strength. The loss in the initial prestressing force due to testing was reported to be negligible.

The followings conclusions were drawn from the observations:

- No strength degradation was observed prier to fracturing of mild steel reinforcing bars.
- At drift levels of ± 6 percent, it was found that systems provided 55 percent of the maximum strength while yielding zero residual drifts.

- Up to drifts 1.5 percent, hybrid systems dissipated more energy per load cycle than the equivalent monolithic systems. At larger drifts, energy dissipated by hybrid system was 75 percent of energy dissipated by equivalent monolithic systems.
- The level of damage in hybrid systems was negligible compared to equivalent monolithic systems.
- The transverse reinforcement remained elastic and no shear cracks was visible upon removal of the load. In contrast, shear cracks were observed in the case of equivalent monolithic connections.

Priestley and MacRae (UCSD, 1996) [40]

An exterior and interior precast beam-column connection subassemblages with partially bonded tendons were tested. The specimens were designed based on the results obtained from the theoretical analysis of similar connections by Priestley and Tao [42].

Details of a specimen for interior connection are shown in Figure 2.32. Prestressing tendons, which were placed at about $0.25h_b$ and $0.75h_b$ distance from the beam top surface, where h_b is the beam depth, were unbonded in the connection region on either side of the column to avoid development of inelastic strains and loss of prestress when subjected to lateral loads. The specimens were tested under cyclic loading using the load history shown in Figure 2.33.

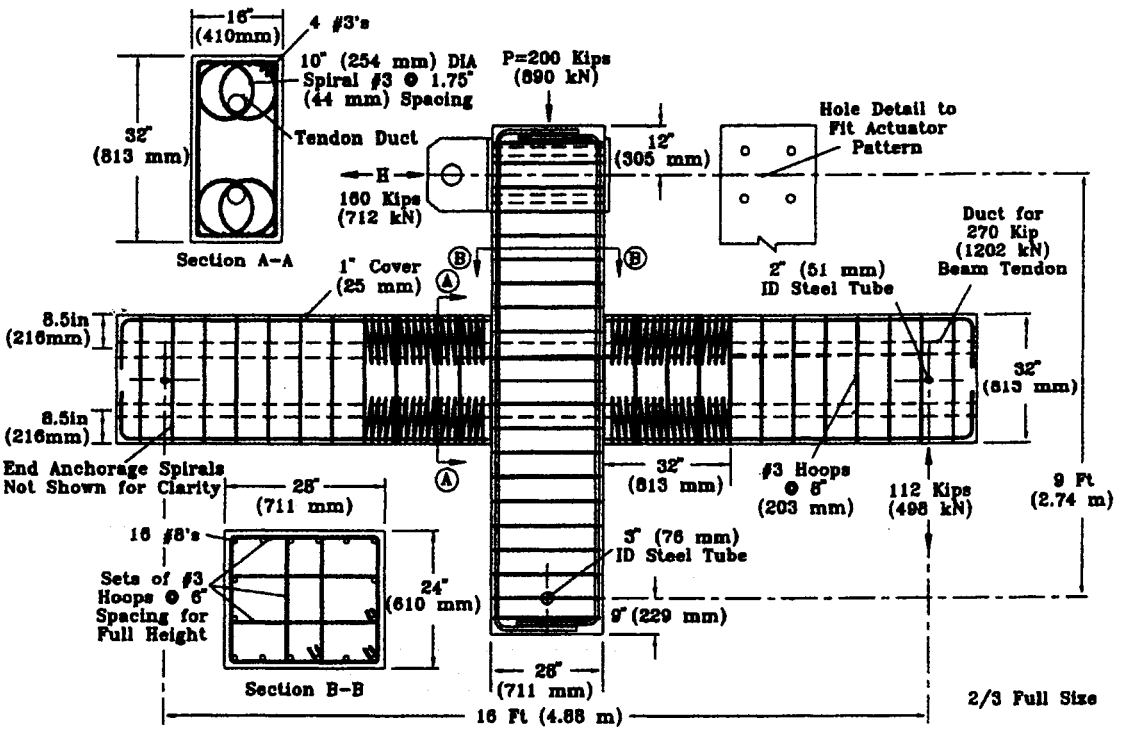

Figure 2.32 Subassembly of interior beam connection tested by Priestley and MacRae [40].

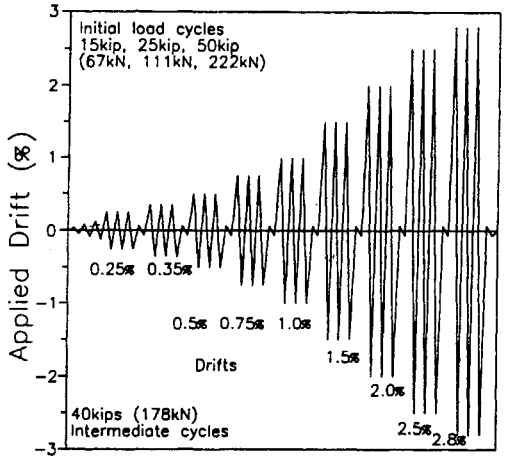

Figure 2.33 The cyclic loading history used by Priestley and MacRae [40].

The unbonded precast frame system exhibited inter-story drifts of 2.8 and 4.0 for the interior and exterior connections, respectively, without significant degradation. Compared to equivalent monolithic systems, neither significant beam damage nor residual drift was observed. Due to the elastic behavior of the tendons, the precast systems exhibited very low hysteretic energy dissipation, which can be seen in Figure 2.34. Additional research was recommended for the optimum design of connections with partially bonded tendons.

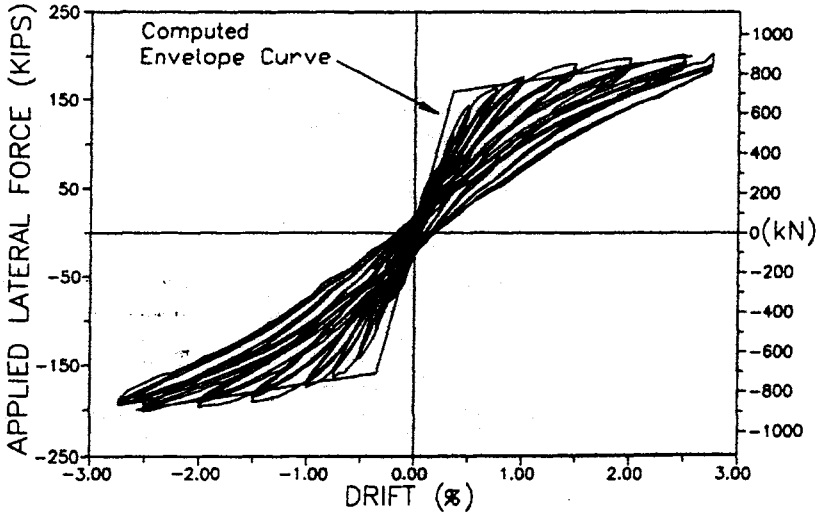

Figure 2.34 Force-drift behavior of interior beam connection tested by Priestley and MacRae [40].

2.4 Analytical Studies for Hybrid Connection

2.4.1 Introduction

As indicated in Section 1.3.1, examining seismic behavior of hybrid frame buildings using conventional frame analysis methods requires development of a relationship between moment and rotation at the connection level. Although such a relationship can be readily established for monolithic frame systems, strain incompatibility that exists between concrete and unbonded mild steel and prestressing reinforcement makes the connection level analysis of hybrid connection system complicated. Analytical investigation that may be applicable to characterize hybrid frame systems at connection level has been limited and a summary of available research findings is provided in the following sections.

2.4.2 Englekirk (1989) [41]

In order to assess performance of precast concrete ductile earthquake resistant frames, the concept of ductility was used. Component ductility and system ductility concepts were introduced to evaluate displacements associated with ultimate load or ultimate strain level for individual members and beam-column subassemblages, respectively. For the cantilever beam shown in Figure 2.35, ultimate displacement was given by:

$$\Delta_u = \left[l - l_p/2\right] l_p \Phi_u + \Delta_y \qquad (2.1)$$

where, l is length of beam, l_p is plastic hinge length, Φ_u is plastic curvature and Δ_y is beam end displacement at yielding.

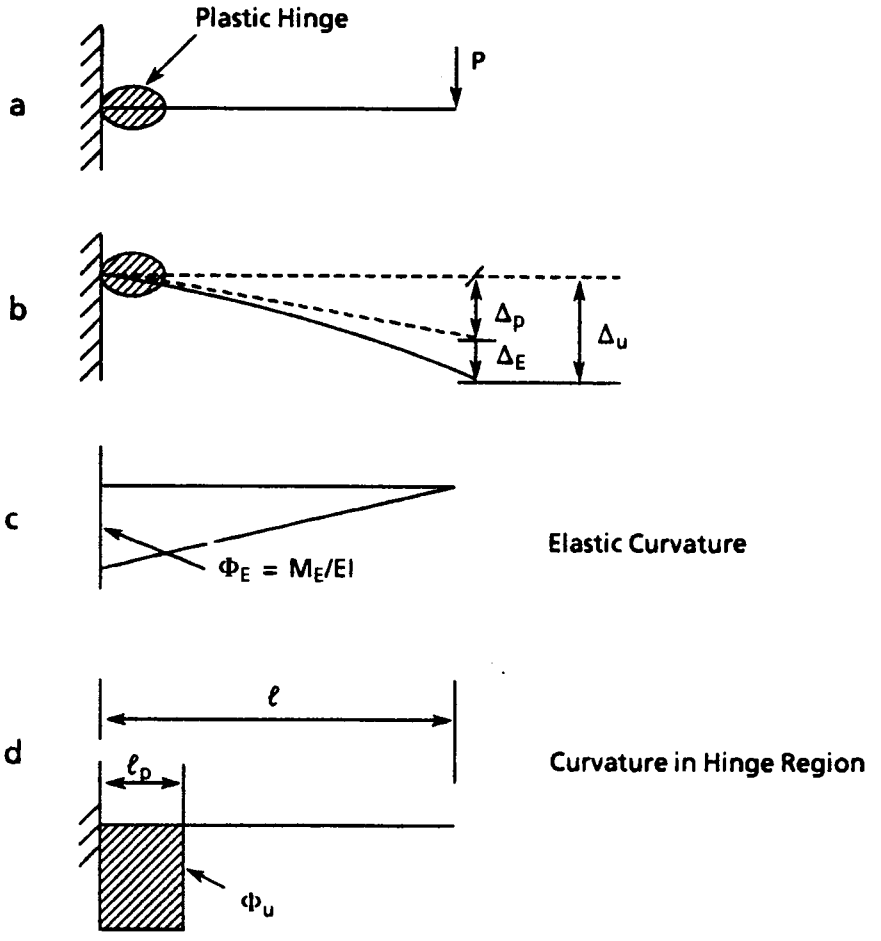

Figure 2.35 Curvature and displacement distribution for cantilever beam [41].

System ductility concept identifies three components for the ultimate displacement of a subassembly shown in Figure 2.36. These components include column flexure, beam flexure and plastic rotation of beam. Using the parameters shown in Figure 2.36, the ultimate displacement components can be expressed as follows:

$$\text{Due to column flexibility, } \delta_c = \frac{2}{3}\frac{M_p}{h}\left(\frac{l}{l_p}\right)\frac{l_c^3}{EI} \qquad (2.2)$$

$$\text{Due to beam flexibility, } \delta_b = \frac{2}{3}\frac{M_p l_b^2}{EI}\frac{h}{l} \tag{2.3}$$

Due to plastic rotation at the connection,

$$\delta_p = l_p \Phi_u \left(l_p - \frac{l_p}{2} \right) \left(\frac{2h}{l} \right) \tag{2.4}$$

$$\text{Therefore, total end displacement, } \Delta_u = \delta_c + \delta_b + \delta_p \tag{2.5}$$

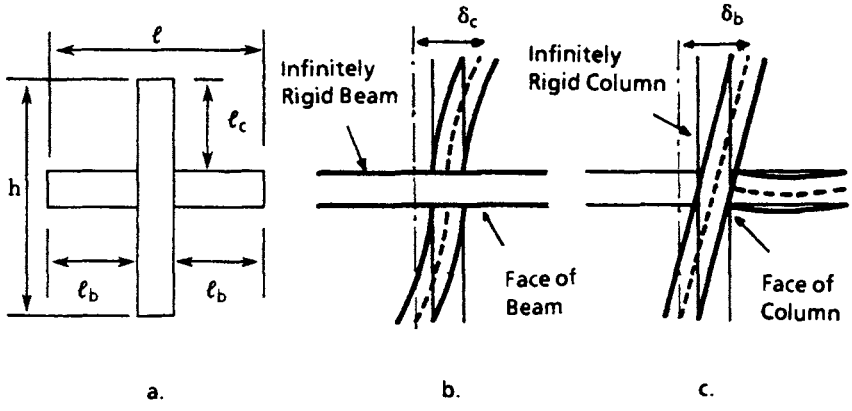

Figure 2.36 Displacement components for beam-column subassembly [41].

The proposed method is applicable to precast systems at member and structural levels for approximate analysis. However, the analysis method was not meant for section level analysis to quantify strains at beam-to-column precast connection interface.

2.4.3 Priestley and Tao (UCSD, 1993) [42]

An analysis technique was investigated for precast beam-column subassemblages with partially debonded tendons and no mild steel reinforcement. The tendons were designed to

remain elastic to avoid the loss of prestressing during seismic response as discussed in Section 2.3.3.

The authors were able to predict a tri-linearly idealized force-deflection profile of the subassemblages using three control points, as shown in Figure 2.37. Point 1 is called decompression point. It corresponds to the condition where precompression stress in the extreme fiber reaches zero and a flexural crack is assumed to develop at the interface, propagating from the extreme tension fiber.

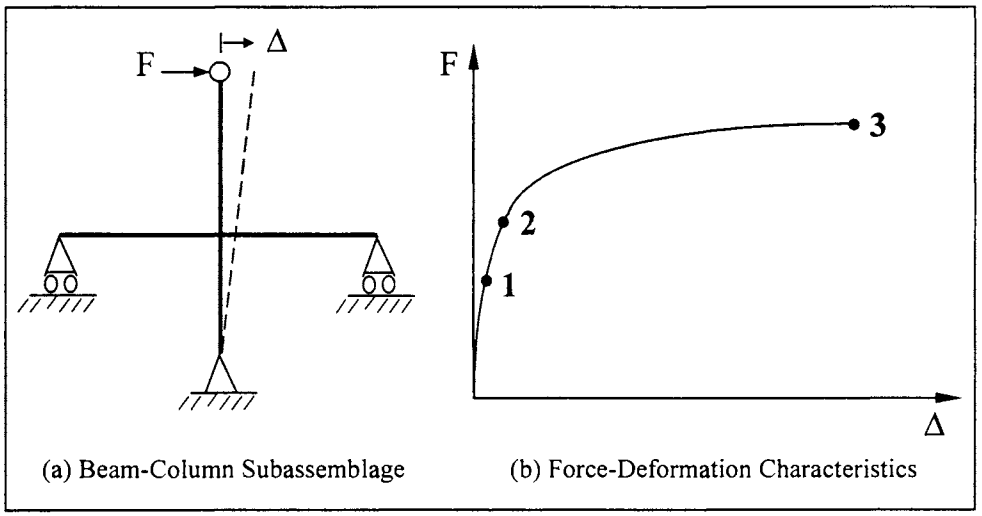

Figure 2.37 Force-deformation response idealized for a beam-column subassembly by Priestley and Tao [42].

At Point 2, it is assumed that the interface crack has propagated to the centroidal axis of the section. Point 3 corresponds to the limit of proportionality on the stress-strain curve of prestressing steel. At this stage, it is assumed that concrete strain reaches the ultimate value.

Even though the linear variation assumed for the force-deflection between Point 1 and Point 2 is difficult to be predicted between the last two points.

The moments corresponding to Point 1 and Point 2 were evaluated using a linear compressive stress distribution at the connection with the predetermined neutral axis depth. The moment at Point 3 was determined using the concept of equivalent rectangular compression stress block without considering the confinement effect. As a result, section level analysis at Point 3 was not sensitive to the strains at the critical section.

The authors performed series of dynamic inelastic analyses using linear elastic, bi-linear elastic, bi-linear elastoplastic and bi-linear degrading force-deformation characteristics based on the theoretical response envelope developed above. A range of earthquake accelerograms was used in the analyses. The study showed that the partially debonded tendons in the connection region maintained prestressing even after larger displacements, as well as provided improved shear performance and reduced residual displacements. The dynamic analyses showed that the presence of partially debonded tendons resulted in lower ductility demand compared to bonded prestressing. However, the need for experimental studies was emphasized to confirm the actual behavior of force-deformation characteristics.

2.4.4 Cheok, Stone and Nakaki (NIST, 1996) [10]

Guidelines given by the authors for designing hybrid connections may be used for analyzing the connections at two different states. The first state that defines the nominal moment capacity assumes that the strain in the mild steel tension reinforcement is equal to strain at the onset of hardening. The second state determines the probable moment capacity assuming that the tensile steel has reached the ultimate value.

To determine both moments, an iterative procedure was suggested, in which the neutral axis depth is determined using the force equilibrium condition at the connection interface. In the this procedure, the following assumptions are made:

- Equivalent rectangular compression (Whitney) stress block is used to approximate confined concrete stress distribution.
- Compression steel contribution is neglected.
- A constant value of additional length of $5.5d_b$ is added to account for growth in unbonded length of mild steel reinforcing due to cyclic strain, where d_b is mild steel reinforcing bar diameter.

The different steps involved in the calculation of the two moments are described below:

(a) For nominal moment capacity, M_n, assuming tensile steel strain,

Assume, $$\varepsilon_s = \varepsilon_{sh} \quad (2.6)$$

Therefore stress in tensile steel,

$$f_s = f_y \quad (2.7)$$

As shown in Figure 2.38, elongation in tensile reinforcement is given by:

$$\Delta_s = \varepsilon_s L_u \quad (2.8)$$

where L_u is unbonded length of mild steel reinforcement. The additional term for the growth in the unbonded mild steel reinforcement is not included, as no significant inelastic strains has been developed at this stage.

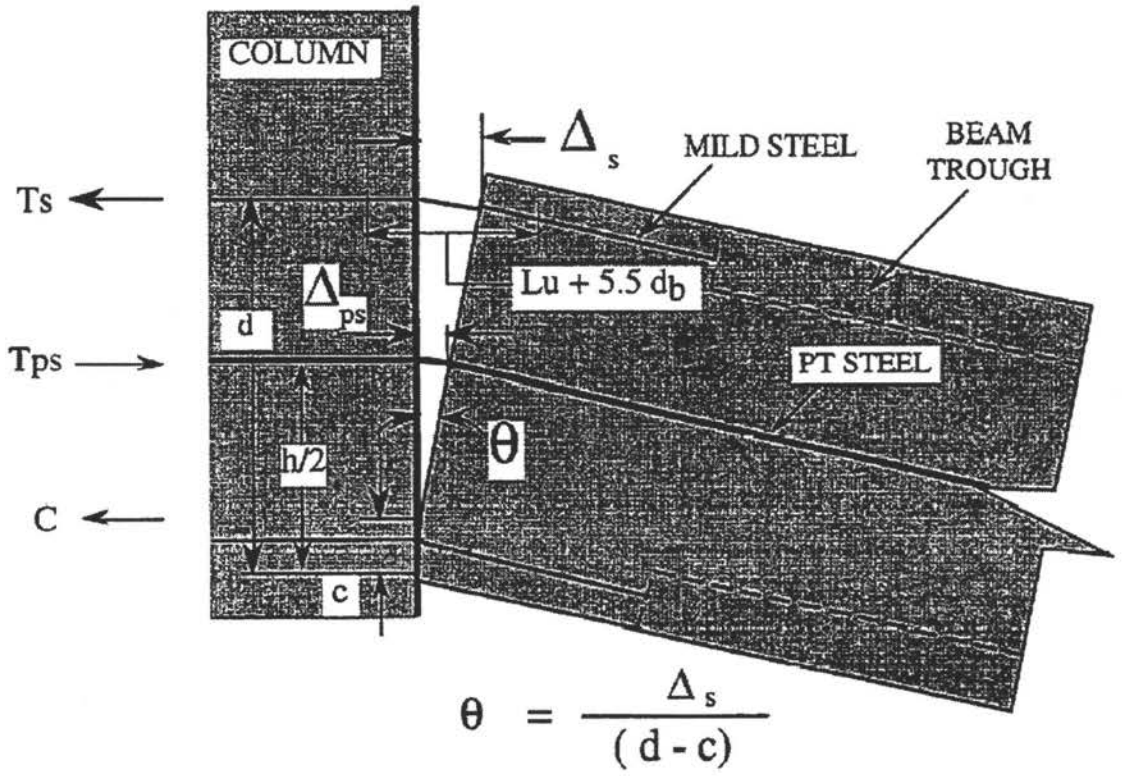

Figure 2.38 Forces and displacements at hybrid connection interface [10].

Assuming a neutral axis depth, c, elongation in the tendon as shown in Figure 2.38 can be expressed as:

$$\Delta_{ps} = \left[\frac{h/2 - c}{d - c}\right]\Delta s \qquad 2.9$$

where h is the beam height. For an unbonded length of L_{ups} and initial prestressing of ε_{si}, strain in the prestressing tendon is given by:

$$\varepsilon_{ps} = \left[\frac{\Delta_{ps}}{L_{ups}}\right]\varepsilon_{si} \qquad 2.10$$

Using Alan Mattock's stress-strain model suggested for Grade 270 strands, stress in the tendon can be expressed as:

$$f_{ps} = \varepsilon_{ps} E_{ps} \left[0.02 + \frac{0.98}{\left[1 + \left[\varepsilon_{ps} E_{ps} / 1.04 f_{psy} \right]^{8.36} \right]^{0.1196}} \right] \qquad 2.11$$

where, E_{ps} is Young's modulus of the tendon.

With a tendon cross section of A_{ps}, force in the tendon,

$$T_{ps} = A_{ps} f_{ps} \qquad 2.12$$

Tensile force in mild steel is given by

$$T_s = A_s f_s \qquad 2.13$$

where, A_s is the mild steel cross-section area. Using equilibrium equation, concrete compression force, C, is the summation of the tensile forces.

$$C = T_s + T_{ps} \qquad 2.14$$

Using the concept of equivalent rectangular compression stress block, the required neutral axis depth to satisfy the equilibrium condition of Eq. 2.14 is determined from

$$c = \frac{C}{0.85 f_c' b \beta_1} \qquad 2.15$$

The procedure is repeated until the assumed neutral axis depth, c converges to the calculated value in Eq. 2.15. Once the neutral axis depth is determined, forces in mild and post-tensioning steels are known, thus the nominal moment is obtained from the following expression:

$$M = T_{ps}\left[\frac{h}{2} - \frac{\beta_1 c}{2}\right] + T_s\left[d - \frac{\beta_1 c}{2}\right] \qquad 2.16$$

Corresponding to the nominal moment, drift capacity is given by:

$$\theta = \frac{\Delta_s}{d - c} \qquad 2.17$$

(b) Probable moment capacity, M_p,

Assuming $\varepsilon_s = \varepsilon_u$ 2.18

Therefore, $f_s = f_u$ 2.19

Using the assumed increased unbonded length, elongation in the mild steel tensile reinforcement is obtained as

$$\Delta_s = \varepsilon_s\left[L_u + 5.5 d_b\right] \qquad 2.20$$

However, it was reported that further research was required for a reasonable estimate of growth in the unbonded length of the mild steel reinforcement.

Assuming a neutral axis depth, c, Eq. 2.9 through Eq. 2.17 are followed to determine the probable moment and the corresponding beam end rotation.

2.4.5 Pampanin, Priestley and Sritharan (2000) [43]

The authors proposed an analytical model to predict a continuous moment-rotation envelope for jointed precast frame systems under monotonic loading. This model, which uses an analogy of equivalent monolithic system, makes the connection level analysis possible by assuming identical global displacement for the members with jointed and monolithic

connections, as illustrated in Figure 2.8. This concept, referred to it by authors as the monolithic beam analogy, enables relationships between neutral axis depth, concrete strain, and steel strains to be established [43]. Establishing these relationships are not possible through conventional means due to the strain compatibility by the presence of unbonded reinforcing bars and prestressing tendon at the connection.

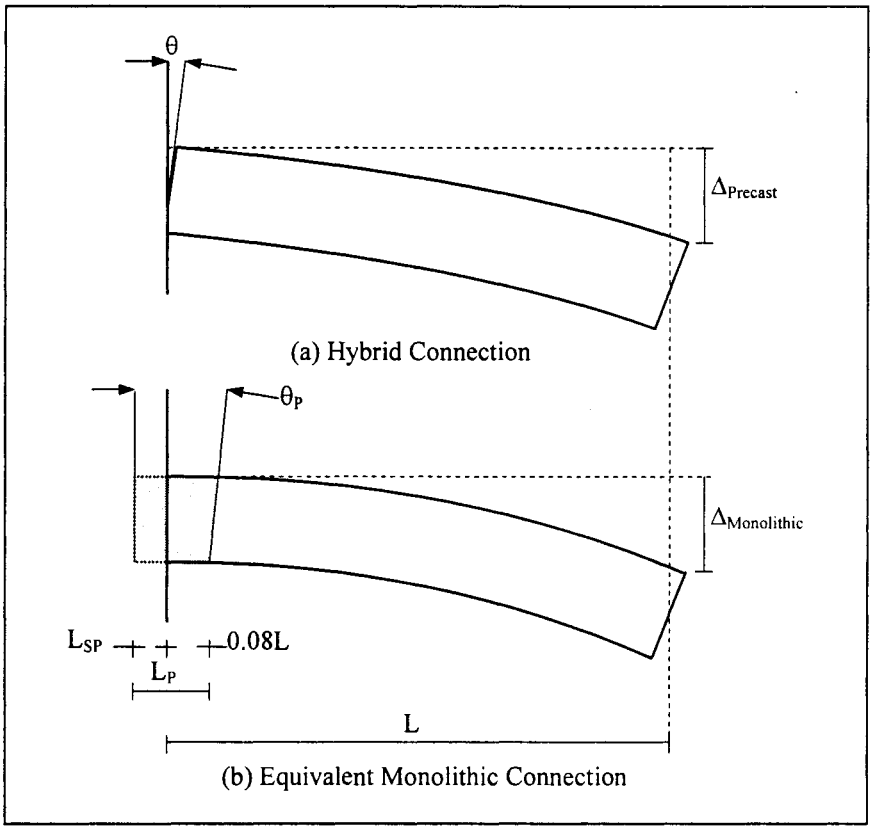

Figure 2.39 Equivalent monolithic beam analogy [43].

2.4.5.1 Concrete Strain

The monolithic beam analogy uses the distance between the connection interface and the contra-flexure point in derivation of equations at the connection level

Using the equal displacement assumption, as shown in Figure 2.39,

$$\Delta_{Precast} = \Delta_{Monolithic} \quad 2.21$$

In the jointed system, the precast beam element is designed to behave elastically, while the beam rotation is concentrated at the connection interface which results in opening of a gap rather than distribution of cracks along the beam. Therefore, displacement due to elastic curvature along the precast beam, Δ_e, and displacement due to concentrated rotation at the connection, Δ_θ are the components of the total displacement at the beam end with a jointed connection.

$$\Delta_{Precast} = \Delta_e + \Delta_\theta \text{, and} \quad 2.22$$

$$\Delta_\theta = L\theta \quad 2.23$$

where L is the length of the beam and θ is the concentrated rotation at the connection interface, which includes the elastic and inelastic components.

The equivalent monolithic beam exhibits plastic behavior in the critical moment region adjacent to the beam-column interface and in the beam-to-column joint due to strain penetration effects, identified by a shaded area in Figure 2.39. In addition, the elastic behavior along the beam and the corresponding strain penetration term should be included. Various elastic and plastic components constitute the total beam end displacement in the equivalent monolithic beam as discussed in details by Paulay and Priestley [20].

Therefore, for the beam in Figure 2.39(b),

$$\Delta_{Monolithic} = \Delta_e + \Delta_p \qquad 2.24$$

where,

$$\Delta_p = \left[L - \frac{L_p}{2}\right]\theta_p \qquad 2.25$$

$$\theta_p = L_p\left[\phi_u - \phi_y\right] \qquad 2.26$$

where L_p is the length over which plastic rotation is assumed to occur. the Substituting Eq. 2.22-2.26 in Eq. 2.21,

$$\Delta_e + L\theta = \Delta_e + L_p\left[L - \frac{L_p}{2}\right]\left[\phi_u - \phi_y\right] \qquad 2.27$$

$$\left[\phi_u - \phi_y\right] = \frac{L\theta}{L_p\left[L - L_p/2\right]} \qquad 2.28$$

$$\phi_u = \frac{\varepsilon_c}{c} \qquad 2.29$$

$$\varepsilon_c = \left[\frac{L\theta}{L_p\left[L - L_p/2\right]} + \phi_y\right]c \qquad 2.30$$

Eq. 2.30 is suggested for estimating extreme fiber concrete strain for a given neutral axis depth at any rotation θ, imposed at the connection interface. However, it was reported that ε_c in Eq. 2.30 can be further approximated by

$$L \approx \left[L - L_p/2\right] \qquad 2.31$$

$$\text{Hence,} \quad \varepsilon_c = \left[\frac{\theta}{L_p} + \phi_y\right] c \qquad 2.32$$

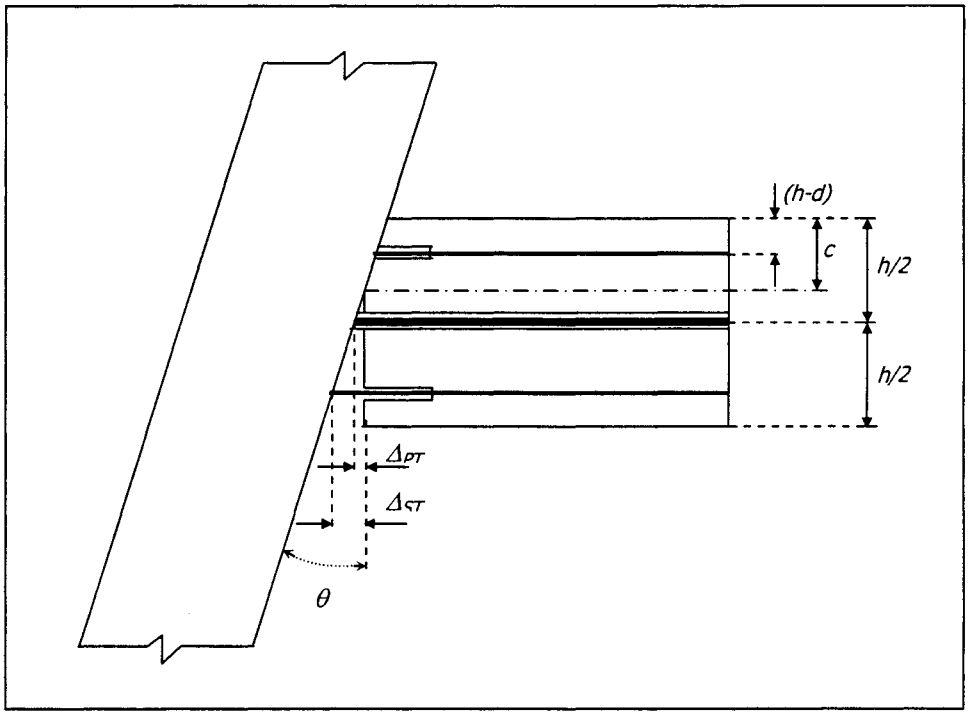

Figure 2.40 A hybrid connection with imposed interface rotation of θ.

2.4.5.2 Strain in Mild Steel

Based on the gap opening mechanism at the hybrid connection, as shown in Figure 2.40, an expression for strain in mild steel tensile reinforcement was established as a function of θ for an assumed value of neutral axis depth, c.

$$\varepsilon_{st} = \frac{\Delta_{st} - 2\Delta_{sp}}{L_{ub}} \qquad 2.33$$

$$\text{From geometry, } \Delta_{st} = [d - c]\theta \qquad 2.34$$

$$\text{but, } \varepsilon_{st} = \varepsilon_e + \varepsilon_p \qquad 2.35$$

Expressing the strain penetration term, $\Delta_{sp,}$ as suggested by Sritharan [44],

$$\Delta_{st} = L_{sp}\varepsilon_p + \frac{2}{3}L_{sp}\varepsilon_e \qquad 2.36$$

Substituting Eq. 2.30 in Eq. 2.31,

$$\Delta_{sp} = L_{sp}[\varepsilon_{st} - \varepsilon_e] + \frac{2}{3}L_{sp}\varepsilon_e \qquad 2.37(a)$$

$$\Delta_{sp} = L_{sp}\varepsilon_{st} - \frac{1}{3}L_{sp}\varepsilon_e \qquad 2.37(b)$$

$$\varepsilon_e = \frac{f_{st}}{E_{st}} \qquad 2.38$$

Substituting Eq. 2.34, 2.37(b) and 2.38 in Equation 2.33,

$$\varepsilon_{st} = \frac{\left[[d - c]\theta + \frac{2}{3}L_{sp}\frac{f_{st}}{E_{sp}}\right]}{[L_{ub} + 2L_{sp}]} \qquad 2.39$$

2.4.5.3 Strain in Post-Tensioned Steel

$$\varepsilon_{pt} = \frac{\Delta_{pt}}{L_{up}} + \varepsilon_{pi} \qquad 2.40$$

where,

$$\Delta_{pt} = [h/2 - c]\theta \qquad 2.41$$

$$\varepsilon_{ps} = \frac{[h/2 - c]\theta}{L_{ups}} + \varepsilon_{pi} \qquad 2.42$$

2.4.5.4 Moment-Rotation Response

At a given rotation θ, Eq. 2.30 or 2.32, 2.39 and 2.42 are used to evaluate strains in concrete, tensile mild steel and post-tensioned steel, respectively, for an assumed value of neutral axis depth. From the strain values, using appropriate stress-strain profile for the materials, stresses and forces can be determined. The neutral axis depth is refined iteratively, using the force equilibrium conditions. By repeating the procedure for different rotations, a continuous moment-rotation envelope is established that can describe monotonic response of hybrid connection.

2.5 Design Provisions

2.5.1 Recommended Design Procedures

There have been only a few studies that has found on developing design procedures for precast hybrid frame connections. A summary of design procedures recommended by Cheok et al. [10] and by ACI Innovative Task Group [9] is presented in this section.

2.5.1.1 Cheok, Stone, and Nakaki (1996) [10]

The authors recommended a design procedure for hybrid frame connection based on many simplified assumptions, which are listed in Section 2.4.4. The recommended design steps are summarized below.

- **Design parameters**

  The following design parameters are assumed at the beginning of design:

  a) Steel areas: A_{ps}, A_s

  b) Beam section details: h, b, d

  c) Unbonded lengths: L_{ups}, L_{ub}

- **Minimum area of mild steel reinforcement**

  If shear demands at the connection interface due to dead and live loads, are V_D and V_L, respectively, and M_{p1} and M_{p2} are probable moment capacities of hybrid connections on the ends of the single-bay beam section, then, the total shear demand at the connection interface is

$$V_u \leq 1.4V_D + 1.7V_L + (M_{p1} + M_{p2})/L \tag{2.43}$$

Vertical shear resistance at the connection interface is provided by friction created by compression force in concrete. This compression force has two components: a portion due to force in prestressing steel, F_p and the other portion C, due to gravity, live and seismic moment couple. Therefore, shear resistance can be expressed as:

$$V_n = \mu(F_p + C) \tag{2.44}$$

where μ is the friction coefficient and a value of 1.0 was recommended for use in accordance with UBC 94, Section 19911.7.4.3.

For satisfactory performance at the connection, it should be ensured that

$$\Phi V_n \geq V_u \tag{2.45}$$

where Φ is shear resistant factor.

To resist gravity load in case of strand failure, a minimum mild steel area is suggested using Eq. 34-35.

$$A_s \geq (V_D + V_L)/f_y \tag{2.46}$$

- **Minimum Force in Strand**

From Eq. 2.43-2.46, the minimum required clamping force could be deduced as,

$$F_p \geq (1.4V_D + 1.7V_L)/\Phi\mu \tag{2.47}$$

- **Moment Design**

If moments due to dead load, live load and earthquake load are M_D, M_L, M_E, respectively, nominal moment should satisfy the following:

$$\Phi M_n \geq 1.4M_D + 1.7M_L \tag{2.48}$$

$$\Phi M_n \geq 1.4(M_D + M_L + M_E) \tag{2.49}$$

$$\Phi M_n \geq 0.9M_D + 1.4M_L \tag{2.50}$$

where ϕ_f is strength reduction factor for flexure.

Nominal moment capacity is calculated using the procedure described in Section 2.4.4.

- **Flexural Strength Ratio**

The moment contribution of the mild steel reinforcement should be checked and that this contribution does not exceed 50 percent of the total moment capacity of the connection.

- **Vertical Shear Design**

By determining probable moment capacities from Eq. 2.43 and compressing forces from Eq. 2.44 using the procedure described in Section 2.4.4, Eq. 2.45 has to be satisfied to ensure sufficient vertical shear resistance at the connection interface.

- **Maximum Drift**

The requirements in UBC 1994 [13] are recommended to determine the maximum drift demand. Drift capacity at the probable moment can be determined using the procedure described in Section 2.4.4 and it should be less the demand suggested in the building code.

2.5.1.2 ACI Innovative Task Group [9]

The American Society of Concrete (ACI) appointed a group of experts, namely, ACI Innovative Task Group 1, to investigate and document a proposed design procedure for precast hybrid frame connections. The procedure that was recommended by the group was similar to that was recommended by Cheok et al. [10] (See Section 2.5.1.1) except for the following changes:

- **Shear Demand**

  In the calculation of shear demand, a factor of 0.75 was used for gravity load component in Eq. 2.43.

$$V_u \leq 0.75(1.4V_D + 1.7V_L) + (M_{p1} + M_{p2})/L \tag{2.51}$$

- **Moment Contribution of Compression Steel**

  For the calculation of probable moment, the contribution of compression mild steel reinforcement is taken into account assuming a stress of $1.25f_y$.

CHAPTER 3

CONNECTION LEVEL ANALYSIS

3.1 Overview

Two conditions that are typically used in a section level analysis of reinforced concrete members are the equilibrium of forces and compatibility of strains between concrete and steel reinforcement. The latter condition is only possible because of the assumption that there is perfect bond exists between the concrete and steel reinforcement. The presence of unbonded prestressing bars and mild steel reinforcement at the hybrid connection creates strain incompatibility between the concrete and steel reinforcement at the critical section, making the section analysis difficult at the beam-column interface as well as along the beam.

The concept of "monolithic beam analogy", introduced by Pampanin et al. [43], as summarized in Section 2.4.5, may be used to overcome the strain incompatibility issue and to estimate concrete and steel strains at the critical section. In this concept, the use of global displacement condition makes the section level analysis possible. Together with the stresses obtained from material constitutive relations and equilibrium conditions, the section level analysis may be performed at hybrid connections. Pampanin at el. examined the accuracy of this methodology by comparing the analytical moment-rotation behavior with experimental results of specimens M-P-Z4 and O-P-Z4 tested by Stone at el. at NIST [39, 48]. In both cases good agreement between the experimental and analytical moment-rotation envelope was reported. Furthermore, application of this concept was used to quantify the response of the PRESSS test building subjected to different segments of earthquake conditions.

Satisfactory comparison was generally found, but some of the response peaks were underestimated.

Although the monolithic beam analogy was found to be satisfactory in predicting the moment-rotation response and the response of the PRESSS test building, it was not clear as to how the predicted stresses are appropriate for use in the design. This is because the monolithic beam analogy assumes that the theoretical plastic hinge length for the jointed system is the same as the discussed for monolithic frame systems. Furthermore, Pampanin et al. found that the moment-rotation analysis of the jointed system insensitive to the estimated concrete strain from the monolithic beam analogy concept.

Motivated by the fact that estimation of accurate strains at the critical section is vital for introducing the monolithic beam analogy in the design of the hybrid connection, this study investigates the ability of the monolithic beam analogy in predicting the critical strains at the section level. Such an investigation was not conducted in previous study [43]. It was found possible to improve the quantification of strains suggested by Pampanin et al by considering the followings:

- Account for the contribution of compression steel in the equilibrium equation and in the calculation of bending moment at the hybrid connection interface
- Accurately modeling the strain penetration and elastic component strain hardening of the mild steel tension reinforcement at the connection.
- Using Mattock's model to represent the stress-strain relation of the tendon

3.2 Assumptions

The following assumptions are made in the development of a modified set of expressions using the monolithic beam analogy for hybrid frame connections:

- The plane section at the column-beam interface remains plane for all rotations. The compressive strain in concrete is zero at the center of rotation at the connection and varies linearly within the contact region between beam and column.
- The steel in the unbonded region is assumed to be perfectly unbonded.
- The beam segment outside the unbonded length of the mild steel reinforcement is assumed to remain elastic for all rotations at the precast interface.
- The prestressing force used in the analysis account for losses due to time dependent effects, such as creep and shrinkage.
- Stress-strain relations for concrete, mild steel and prestressing steel are accurately represented by the constitutive relations presented in Section 3.3.

3.3 Quantifying Strains

3.3.1 Concrete Strain

In establishing a relation between concrete strain and neutral axis depth using the monolithic beam analogy, components of the end displacements of beams with hybrid and monolithic connections, as shown in Figure 2.40, are examined with some modifications over that proposed by Pampanin et al.

Considering the strain penetration term in the monolithic connection, the total displacement at the beam end is

$$\Delta_{Monolithic} = \Delta_e + \Delta_p \tag{3.1}$$

where using geometry,

$$\Delta_p = L\theta_p \tag{3.2}$$

$$\theta_p = L_p[\phi_u - \phi_e] \tag{3.3}$$

It is noted that Pampanin et al. used ϕ_y instead of ϕ_e, due to the difficulty in estimating the above expression to simplify ϕ_e. (See Equation 2.30.) In the enhanced approach, ϕ_e is estimated using the previous value from the previous θ and then iterated to refine the appropriate ϕ_e for the current θ.

Accounting for the strain penetration contribution to Δ_e as suggested by Sritharan [44], Δ_e may be expressed as

$$\Delta_e = \frac{1}{3}\phi_e L^2 + \left[\frac{2}{3}\phi_e L_{sp}\right]L \tag{3.4}$$

Substituting equations 3.2 – 3.4 in Equation 3.1,

$$\Delta_{Monolithic} = \Delta_e' + L_p[\phi_u - \phi_e]L + \left[\frac{2}{3}\phi_e L_{sp}\right]L \tag{3.5}$$

where, member elastic deformation, $\Delta_e' = \frac{1}{3}\phi_e L^2$ 3.6

For the hybrid beam the total displacement at the beam end is

$$\Delta_{Precast} = \Delta_e^* + \Delta_\theta \tag{3.7}$$

where, Δ_e^* is beam end displacement due to the elastic curvature along the beam and

$$\Delta_\theta = L\theta \tag{3.8}$$

Based on the monolithic beam analogy (See Eq. 2.21.),

$$\Delta_{Precast} = \Delta_{Monolithic} \tag{3.9}$$

Therefore,
$$\Delta_e^{'} + L_p[\phi_u - \phi_e]L + \left[\frac{2}{3}\phi_e L_{sp}\right]L = \Delta_e^{*} + L\theta \tag{3.10}$$

Assuming $\Delta_e^{'} \approx \Delta_e^{*}$ and simplifying Eq. 3.10,

$$L_p[\phi_u] = \theta + \left[L_p - \frac{2}{3}L_{sp}\right]\phi_e \tag{3.11}$$

But,
$$\phi_u = \frac{\varepsilon_c}{c} \tag{3.12}$$

Combining Equations 3.11 and 3.12, the prediction of concrete strain based on the enhanced model is,

$$\varepsilon_c = \left[\theta + \phi_e\left[L_p - \frac{2}{3}L_{sp}\right]\right]\frac{c}{L_p} \tag{3.13}$$

For a given rotation at the column-beam interface, Eq. 3.13 gives a relationship between concrete strain and neutral axis depth. This expression with the equilibrium equation at the interface can be used to solve for the steel and concrete strains, forces and bending moment for a given interface rotation.

3.3.2 Strains in Steel

- **Compressive Mild Steel Reinforcement**

Pampanin at el. did not provide an expression for estimating strain in the compression steel. Recognizing that the compression bar is also debonded over L_{ub} as in Figure 2.9, and assuming that the steel strain at the critical section is same as that in concrete at the same level, Eq. 3.14 is suggested for estimating the strain in the compression steel reinforcement. This expression averages strains obtained at the critical section and at a distance of L_{ub} from the critical section. At the latter section, the strain is assumed to be a value based on a condition that compressive steel yields at the ultimate moment.

$$\varepsilon_{SC} = \frac{1}{2}\left[\frac{(c-d')}{c}\varepsilon_c + \varepsilon_y \frac{M}{M_y}\right] \qquad 3.14$$

- **Tensile Mild Steel Reinforcement**

The expression from Equation 2.39, suggested by Pampanin at el. is used.

$$\varepsilon_{st} = \frac{\left[[d-c]\theta + \frac{2}{3}L_{sp}\frac{f_{st}}{E_{sp}}\right]}{\left[L_{ub}+2L_{sp}\right]} \qquad 3.15$$

- **Prestressing Steel**

Equation 2.42 derived by Pampanin at el is used and given below.

$$\varepsilon_{ps} = \frac{[h/2-c]\theta}{L_{ups}} + \varepsilon_{pi} \qquad 3.16$$

3.4 Moment-Rotation Envelope

Since strain values in concrete and steel are function of rotation and neutral axis depth, as expressed in Eq. 13 through Eq. 16, for a given level of rotation at the hybrid connection interface, an iteration procedure is used to find the neutral axis depth so that the equilibrium equation can be satisfied. A continuous moment-rotation plot for a hybrid connection can be produced by repeating the above procedure for a range of θ. The iteration procedure is described in Figure 3.9 by means of a flow chart. The following is a brief description of the flow chart.

STEP 1: Quantifying Strains

For a given level of rotation and assumed neutral axis depth, strains are evaluated using the expressions given in Eq. 13 through Eq. 16.

SPEP 2: Quantifying Stresses

Following the estimation of strains at the critical section, stresses in concrete, mild steel and prestressing bars are determined using appropriate stress-strain models.

- **Confined Concrete**

A confined concrete model proposed by Mander et al. [45] is used for estimating the concrete stresses. According to this model, the stress-strain profile obtained from the following equations:

$$f_c = \frac{f'_{cc}\, xr}{r-1+x^r} \tag{3.17}$$

Where, $$f_{cc} = f'_c\left[2.254\sqrt{1+\frac{7.94 f'_l}{f'_c}} - \frac{2f'_l}{f'_c} - 1.254\right] \tag{3.19}$$

$$x = \frac{\varepsilon_c}{\varepsilon_{cc}} \qquad 3.20$$

$$r = \frac{E_c}{E_c - E_{sec}} \qquad 3.21$$

$$E_{sec} = \frac{f'_{cc}}{\varepsilon_{cc}} \qquad 3.22$$

$$\varepsilon_{cc} = \varepsilon_{co}\left[1 + 5\left[\frac{f'_{cc}}{f'_c} - 1\right]\right] \qquad 3.23$$

- **Mild Steel**

A stress-strain profile suggested by Dodd and Restrepo [46] for mild steel reinforcement is used for the analysis, which is by the following equations:

$$f_s = E_s\varepsilon_s \quad \text{for} \quad \varepsilon_s \le \varepsilon_y \qquad 3.24$$

$$f_s = f_y \quad \text{for} \quad \varepsilon_y \le \varepsilon_s \le \varepsilon_{sh} \qquad 3.25$$

$$f_s = f_{su} + (f_y - f_u)\left(\frac{\varepsilon_{su} - \varepsilon_s}{\varepsilon_{su} - \varepsilon_{sh}}\right)^p \quad \text{for} \quad \varepsilon_{sh} \le \varepsilon_s \le \varepsilon_u \qquad 3.26$$

$$\text{Where,} \quad p = \log\left[\frac{f_{su} - f_x}{f_{su} - f_y}\right] \Big/ \log\left[\frac{\varepsilon_{su} - \varepsilon_x}{\varepsilon_{su} - \varepsilon_{sh}}\right] \qquad 3.27$$

- **Prestressing Steel**

The following relation recommended by Alan Mattock [47] for Grade 270 strands is used to determine the stress in the prestressing tendons for a given level of strain.

$$f_{ps} = \varepsilon_{ps}E_{ps}\left[0.02 + \frac{0.98}{\left[1 + \left[\varepsilon_{ps}E_{ps}/1.04f_{psy}\right]^{8.36}\right]^{0.1196}}\right] \qquad 3.28$$

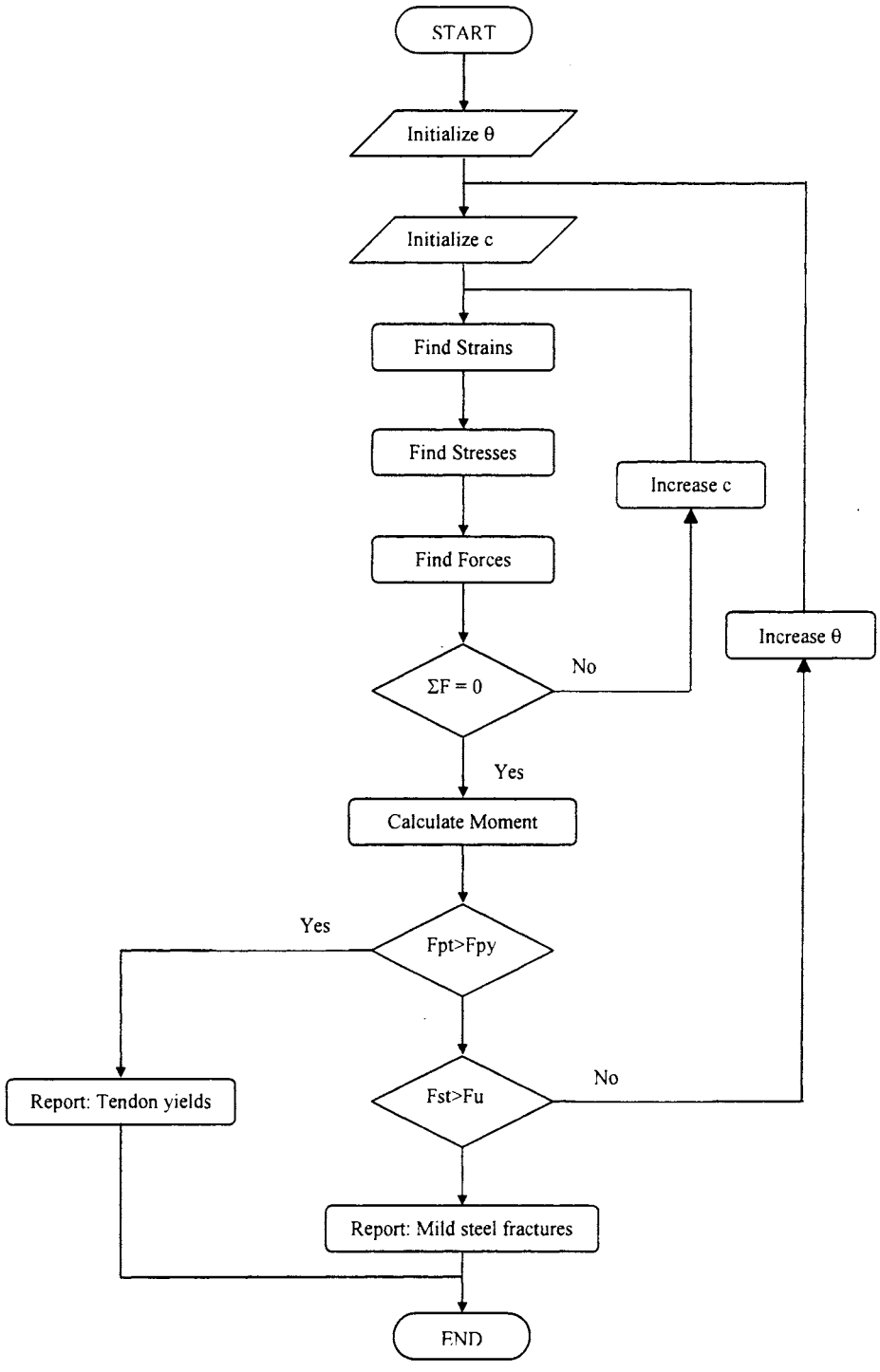

Figure 3.1 Iteration procedure adopted in the connection level analysis of a hybrid frame system.

STEP 3: Find Forces

For the mild steel reinforcement and post-tensioning steel the forces were calculated using their corresponding cross sectional areas. For concrete, the compressive region was divided into finite number of strips and forces for the individual strips were calculated assuming a linear distribution of strain. The resultant of the forces established with the strips determined the location and magnitude of the compression force at the section

At the next step, the equilibrium condition is checked. If the condition is not satisfied, the neutral axis depth is improved and Steps 1, 2 and 3 are repeated until the equilibrium condition is satisfied. This procedure is repeated for range of θ values. Incorporating this analysis procedure, a computer program, hereafter referred to as HYBRID, was developed in Visual C++, which was used to perform various analysis reported in the reminder of this thesis.

3.5 Experimental Validation

In order to assess accuracy of the improved set equations developed for the monolithic beam analogy concept that were derived in Section 3.3, experimental data obtained from two tests at NIST and the PRESSS test building are compared with the analysis results obtained using the computer program HYBRID. Section details of three hybrid frame connections are given in Figure 3.2. Specimens M-P-Z4 and O-P-Z4 were tested at NIST in Phase IV-B [39, 48], as described in Section 2.3.3. The PRESSS section details shown in Figure 3.2 is the connection detail used in the first floor of the hybrid frame in the PRESSS test building [10, 49].

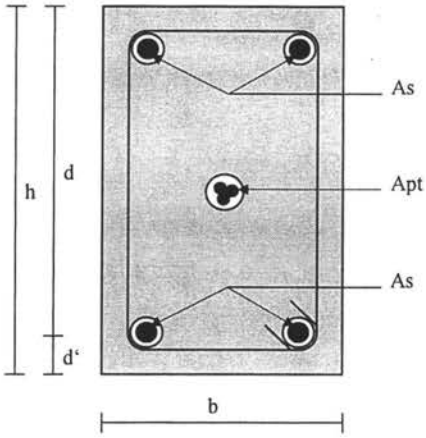

Parameter	M-P-Z4	O-P-Z4	PRESSS
h (in)	16.0	16.0	23.0
b (in)	8.0	8.0	14.0
d (in)	11.0	11.0	20.25
d' (in)	1.0	1.0	2.25
As (in^2)	0.22	0.33	0.4
Apt (in^2)	0.459	0.459	1.459

Figure 3.2 Section details of hybrid specimens.

3.5.1 Moment-Drift Envelopes

Following moment-rotation analysis at the critical connection using HYBRID, moment-drift envelopes for the NIST specimens were obtained by theoretical calculations to enable comparison of results with experimental data. Typical configuration and support conditions of these specimens are shown in Figure 3.3. Dimensions of this subassembly are found in Figure 2.31. As these subassemblages were determinate structures, the displacements at the top of the column corresponding to monotonically increasing lateral force applied at the top of the column were calculated using elastic properties of beams and columns and inelastic properties of rotations springs representing the hybrid connections.

Comparison of analytical and experimental beam moment vs. column drifts is shown in Figure 3.3 and Figure 3.4 for the specimens M-P-Z4 and O-P-Z4, respectively, which indicates that the analytical model with modified equations satisfactorily predicts response envelope obtained for the test specimens. Similar predictions were also made with the original equations obtained from the monolithic beam analogy by Pampanin et al. [43].

However, the improved equations produce better estimation of the elastic stiffness and yield strength.

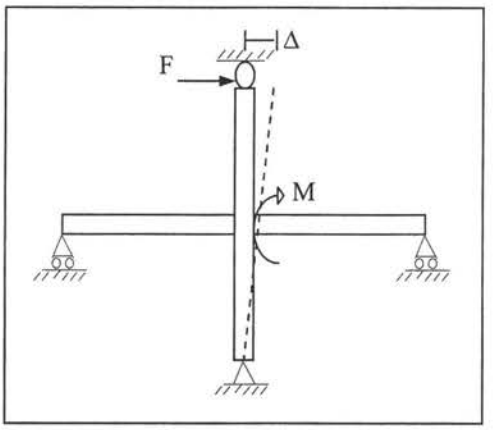

Figure 3.3 Specimens M-P-Z4 and O-P-Z4 tested at NIST [39, 48]

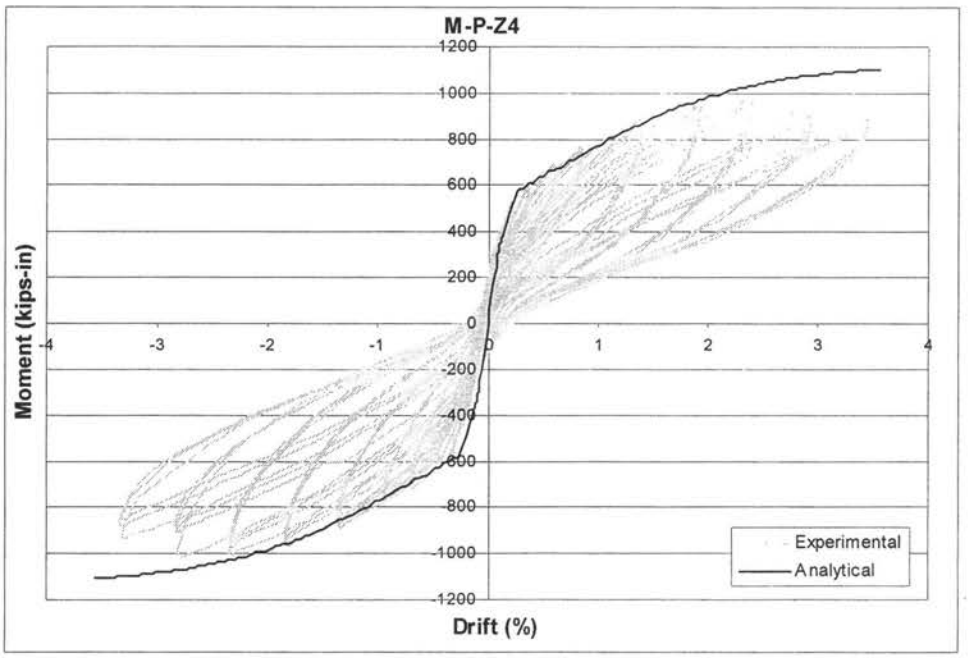

Figure 3.4 Moment vs. drift obtained for M-P-Z4

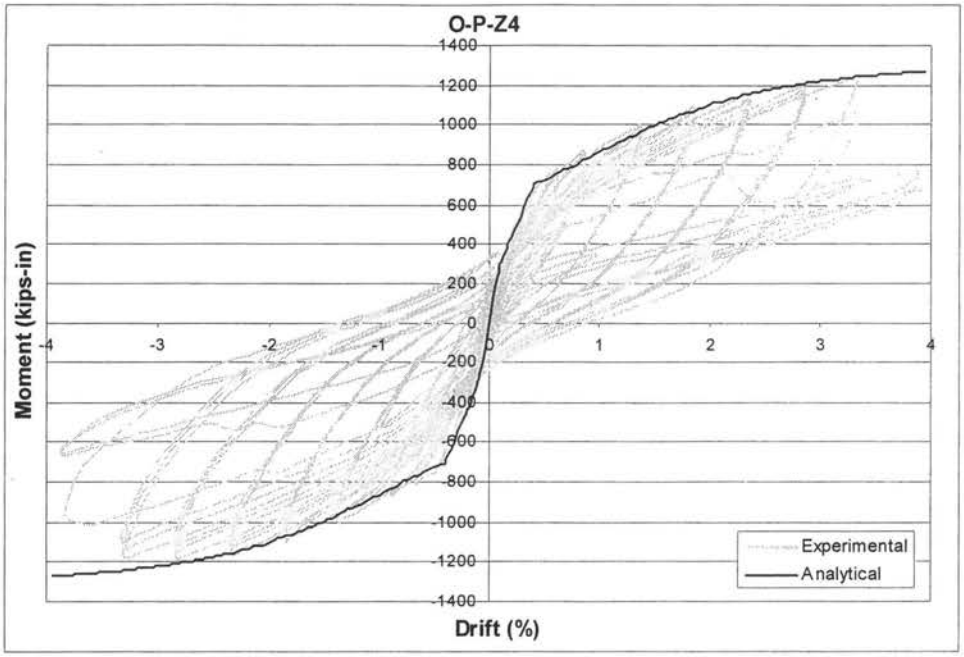

Figure 3.5 Moment vs. drift obtained for O-P-Z4

3.5.2 Neutral Axis Depth

The PRESSS test building was instrumented with displacement transducers at the interior column interface of the first floor of the hybrid frame. Figure 3.6 shows the locations of the displacement transducers, identified with labels A, B and C. As shown in the figure, let a, b and c be the readings of the micrometers A, B and C, respectively, and h_1, h_2 and h_3 define the location of the micrometers A, B and C respectively, then using the features of triangle shown in the figure, neutral axis depth, c, and corresponding rotation, θ, may be determined in terms of a, b, c, h_1, h_2, h_3, and h, where h is the height of the beam.

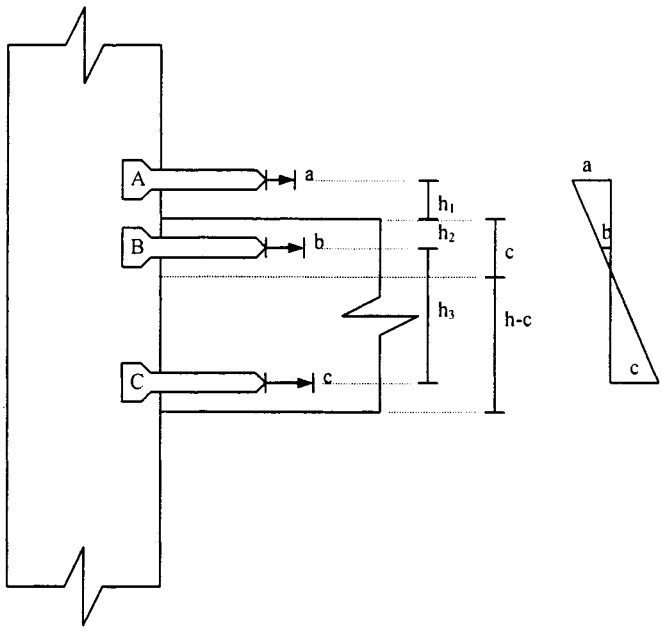

Figure 3.6 Arrangements of displacement transducers at the first floor hybrid connections in the PRESSS test building

The first floor hybrid connection of the PRESSS test building was analyzed using HYBRID and the neutral axis depth from the estimated the extreme compression fiber is plotted as a function of beam rotation at the interface, as shown in Figure 3.7 along with the experimental results. The prediction of the neutral axis depths was also performed using the analytical procedure described by Cheok, Stone and Nakaki [11] (See Section 2.4.4) at nominal and probable moments and are also included in Figure 3.7. The analytical prediction obtained from HYBRID correlates satisfactorily captures envelope of the experimental values. However, the comparison based on the procedure recommended by Cheok, Stone and Nakaki is unsatisfactory and shows increase in neutral axis depth with increasing rotation. This trend, which should be expected due to the equivalent rectangular stress block to quantify forces, contradicts the actual behavior expected at the connection.

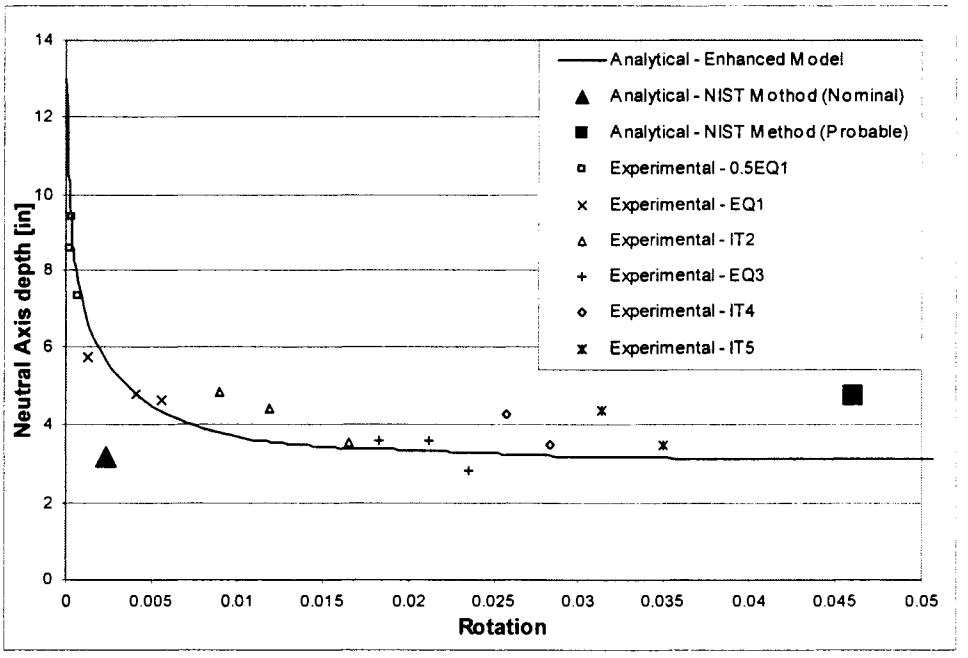

Figure 3.7 Validation of neutral axis depth

3.5.3 Elongation of PT steel vs. Rotation

Experimental values of the elongation of post-tensioned steel in the first floor hybrid connections of the PRESSS test building were compared with the analytical values based on the strain in the post-tensioned steel estimated by analyzing the first floor hybrid connection using HYBRID. The comparison is shown in Figure 3.8. The post-tensioned steel was unbonded throughout the beam, and therefore, the elongation was calculated by assuming that the strain is uniform over the unbonded length. Predicted values of the tendon elongation using the NIST analytical procedure [10], as explained in Section 2.4.4 are also shown in Figure 3.9. A good correlation between the predicted and experimental elongation-rotation behavior reveals that the analytical model incorporating the modified expressions can be

satisfactorily used for connection level analysis in estimating strain in post-tensioning tendon.

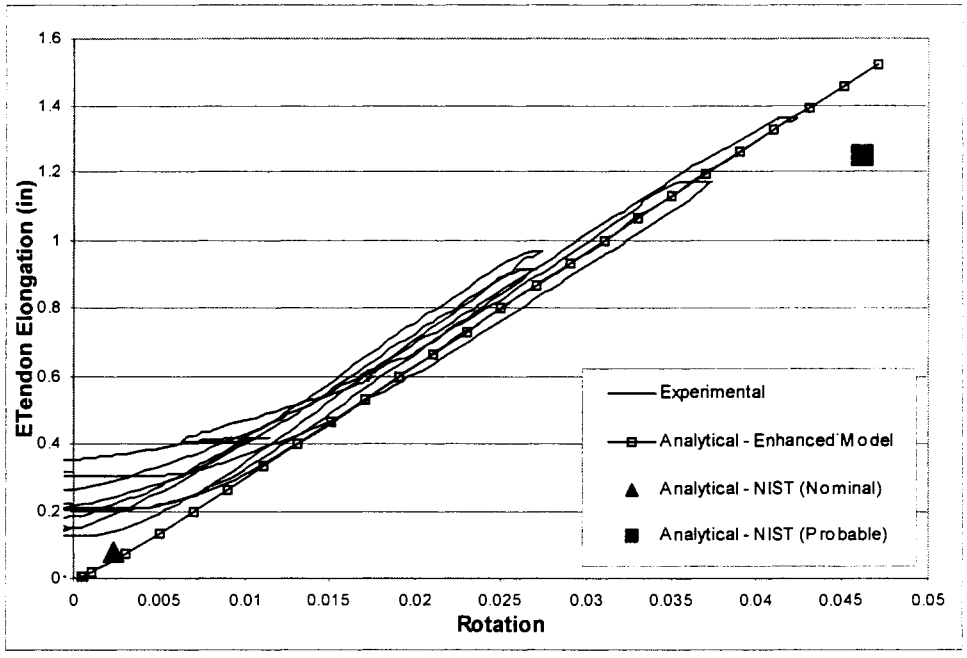

Figure 3.8 Comparison of predicted stand elongation with experimental values.

CHAPTER 4

ANALYSIS OF A HYBRID FRAME BUILDING

4.1 Introduction

Response behavior of building systems may be evaluated by performing static and/or dynamic analysis on suitable analytical model representing the building systems with appropriate loading conditions. This chapter presents description of models used and results obtained in a series of pushover and dynamic nonlinear analyses of a hybrid frame building. Theses analyses were carried out using a finite element computer program "RAUAMOKO" [58], which incorporates many element types and hysterisis rules to represent post-elastic behavior of structural members.

The goal of theses analyses was to predict structural level response behavior of a hybrid frame building using the connection level analytical model developed in Section 3.4. The modeling technique adopted was verified by performing structure level-dynamic analysis on a five-story precast hybrid building and these results were compared with test data. In the next step, a series of dynamic analyses were carried out on the five-story precast concrete building with the view to investigating the followings:

1. Effect of using flexible floor links
2. Behavior of the building from a performance-based view point
3. An appropriate performance reduction (R) factor that may be used in force-based seismic design

4.2 Modeling

Although a rapid development of the finite element technique and increasing availability of powerful micro-computers made analysis of structures with desired level of refinement possible, a reliable prediction of dynamic and inelastic behavior of structures depends on the accuracy of the mathematical models in representing the actual behavior of structural members. This section describes analytical modeling of the hybrid frame connection.

4.2.1 Hybrid Connection

As described in Section 1.3, the hybrid connection is a ductile connection with inelastic rotations concentrated at the connection interface through opening of a single crack. Therefore, as shown in Figure 4.1, hybrid connections can be modeled using zero-length rotational spring elements with defined elastic and post-elastic behavior.

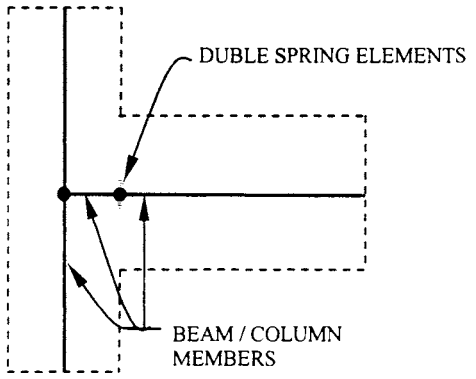

Figure 4.1 Finite element model for a hybrid connection

Following the approach suggested by Pampanin et al. [43], contributions to bending moment at a hybrid connection interface were investigated to suitably model the connection behavior using hysterisis models available in RAUMOKO. Bending moment at hybrid

connection has two components. These contributions are from mild steel and prestressing steel reinforcement, as illustrated in Figure 4.2, which presents the results of the hybrid connection used in the first floor of the PRESSS [50] test building.

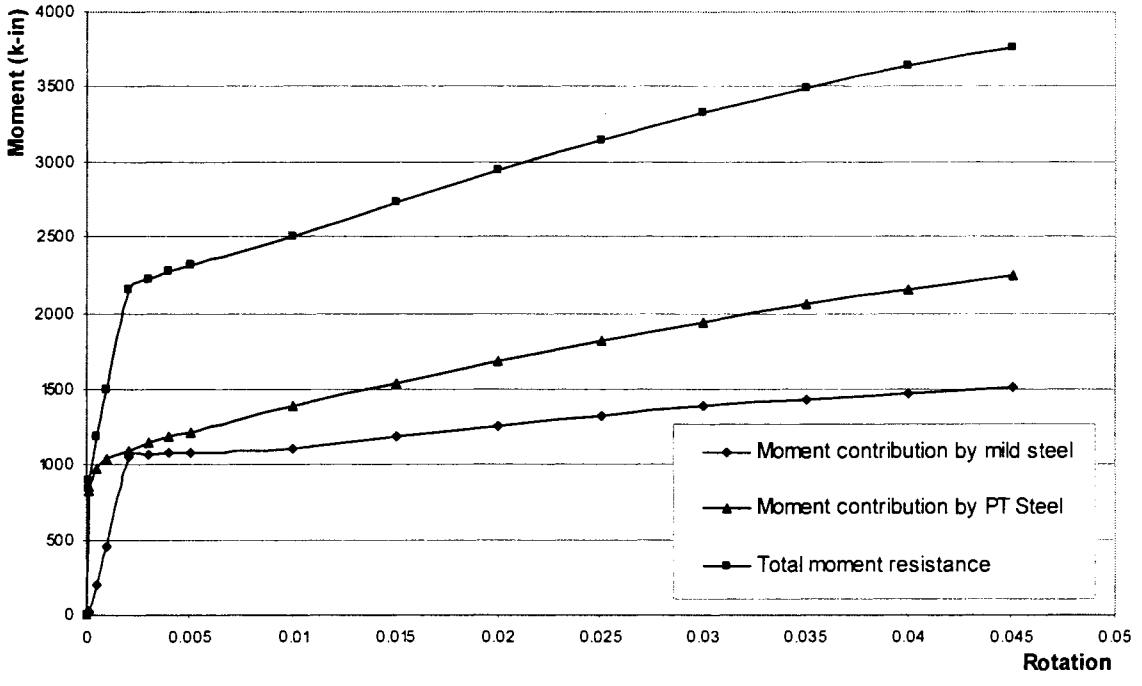

Figure 4.2 Components of bending moment resistance of a hybrid frame connection.

Hybrid connection concept allows mild steel to go into plastic region, while prestressing steel is expected to remain elastic. Therefore, Pampanin et al. [43] suitably modeled the hybrid connection by two separate rotational springs based on mild steel and prestressing steel moment contributions. In finite element analysis using RAUAMOKO, Takeda model [58] was used to characterize the moment-rotation behavior of mild steel component, as it accommodates energy dissipation due to post-elastic behavior. For moment-rotation behavior of prestressing component, bi-linear elastic spring was used. Figure 4.3 through Figure 4.5

show the comparison of moment-rotation behavior of these springs obtained by connection level pushover analysis with hybrid connection behavior obtained from the analytical model using RAUAMOKO.

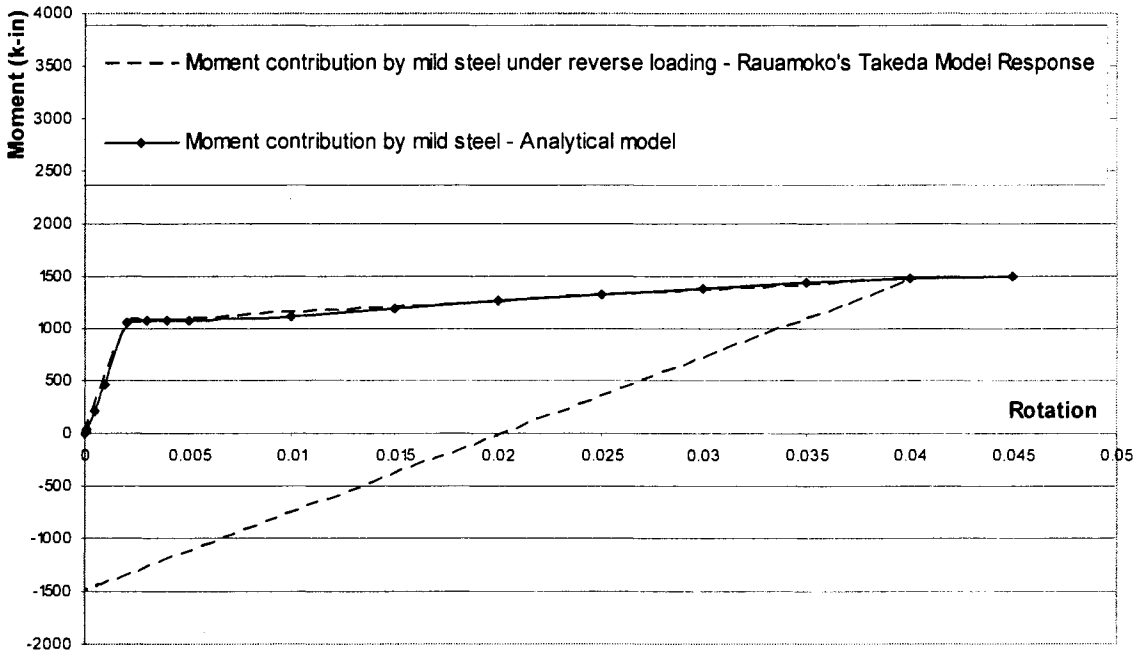

Figure 4.3 Moment contribution by the mild steel reinforcement.

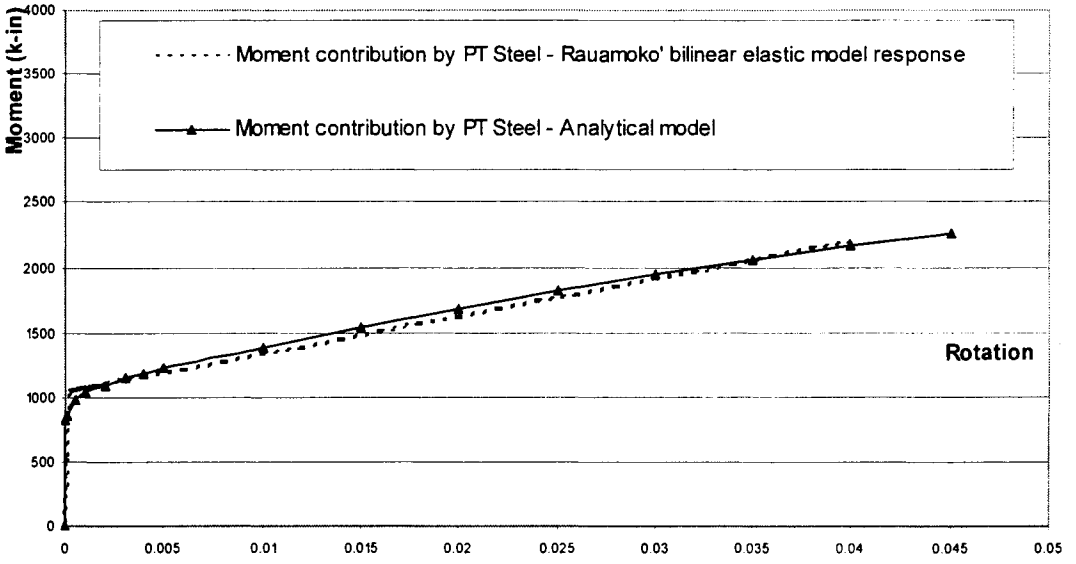

Figure 4.4 Bilinear elastic model represents the prestressing steel moment contribution

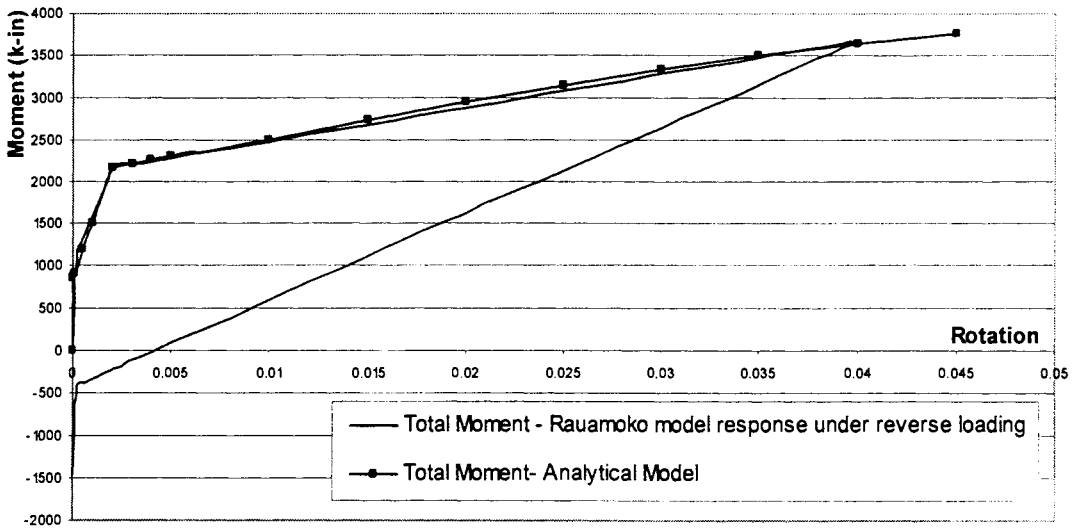

Figure 4.5 Rauamoko model that represents total moment-rotation response at the connection level

4.2.2 Hybrid Frame Systems

In a building system based on hybrid framing concept, moments and shear due to lateral forces are expected to resist by hybrid frame system while a separate mechanism, such as wall, may exist to resist gravity loads. This subsection describes a suitable finite element model of the hybrid building system described in section 4.2.1.

As explained in Section 1.3, beam and column members jointed by hybrid framing concept are expected to remain elastic; therefore these beam and column members can be modeled using standard elastic FRAME elements of RAUAMOKO. In a typical hybrid framing system, beams and columns are post-tensioned reinforced concrete members with high axial compression. When modeling for dynamic analysis, these members are not

expected to retain their gross section properties as large moments develop at their ends. In reality, their sectional properties will vary depending on the moment demand at the critical section. Generally, finite element programs, including RAUAMOKO, do not allow use of variable elastic properties for the structural elements. Therefore, it was decided to use 50% of the gross section properties for all beam members, 60% of the gross section properties for the first floor columns and 100% of the gross properties for the rest of the column members. The rationale behind using a larger proportion of gross sectional properties for column elements is that they are generally subjected to axial loads due to gravity and that the selected values are consistent with the test observation reported for the PRESSS building by Priestley et al. [50].

Further more, RAUAMOKO differentiates the seismic mass of the structure from the gravity mass for the purpose of calculating inertia effects. For the building analysis, seismic mass, most of which is at the floor level, was assumed to be concentrated separately in a gravity column and linked to the hybrid frame using flexible springs.

A layout of the finite element model developed for the hybrid frame with a gravity column is illustrated in Figure 4.6. In this model, the frame is also connected to base using hybrid connections, while gravity column is connected to the base using a pin connection. Seismic masses are connected to hybrid frames using axial spring elements, which have pinned hinges at both ends. Double spring elements, as explained in Section 4.2.1, were used for the hybrid connection at the ends of each beam and at the column base.

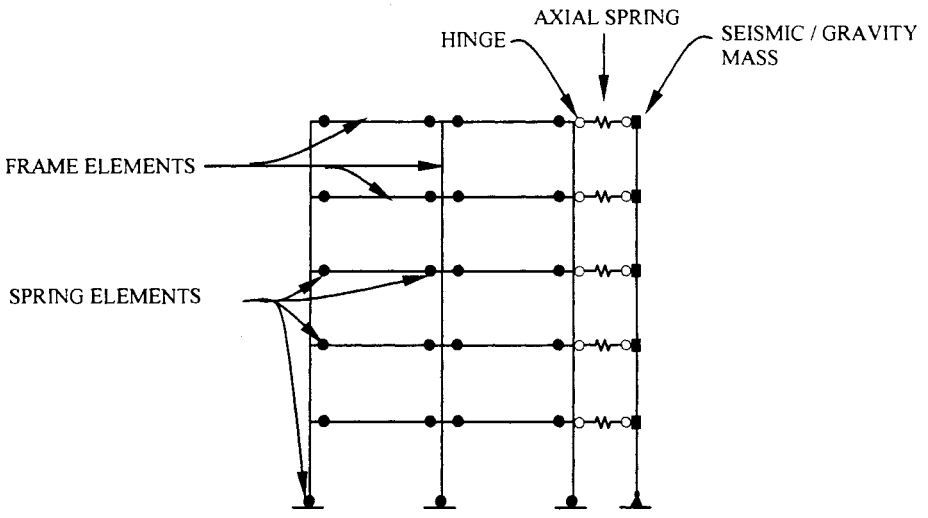

Figure 4.6 Finite element model of the five-story hybrid frame.

4.3 Building Response

4.3.1 Overview

Pushover and dynamic analyses were carried out on the finite element model of the five-story hybrid building to examine moment-rotation behavior predicted by the analytical model described in Section 3.4 and the modeling concept described in Section 4.2. The finite element model of the building had dimensions similar to that of the five-story hybrid building and properties of elements of the model were calculated based on the five-story hybrid building sectional and connection details [50]. Although the building had a 60% scaled down dimensions of the prototype building, test building dimensions were used for analysis model so that the test data from the PRESSS building could be used to validate the analysis model.

It should be noted that the PRESSS test building had two moment resisting frames in one direction and a wall system in the orthogonal direction. One of the two moment resisting frames had hybrid connections for the first three floors. Beams and columns in the top two floors in that frame were connected using pretentioned connections [49]. However, in the analysis, all of the beam-to-column connections in the building were assumed to be framed using the hybrid concept.

4.3.2 Pushover Analysis

Analysis of the building model subjected to monotonically increasing inverse-triangular load was carried out as the first step in the validation process. The goal of this analysis was to perform validation of the model using the test results. Because hybrid connections were used at all five floors of the analytical model, as described in Section 4.3.1, the experimental results obtained at the first three levels as a function of base-moment were appropriate for comparison with the analysis results. Figure 4.7 shows the variation of base moment with third floor displacement obtained from the PRESSS test building and the pushover analysis.

The predicted response envelope satisfactorily captures the experimental hysteretic behavior obtained from the PRESSS test building and this confirms the validity of the model in terms of strength and stiffness. The failure of the analytical curve to capture experimental behavior at larger displacement level was expected, as some damage occurred at large later displacement of testing in the PRESSS building [49].

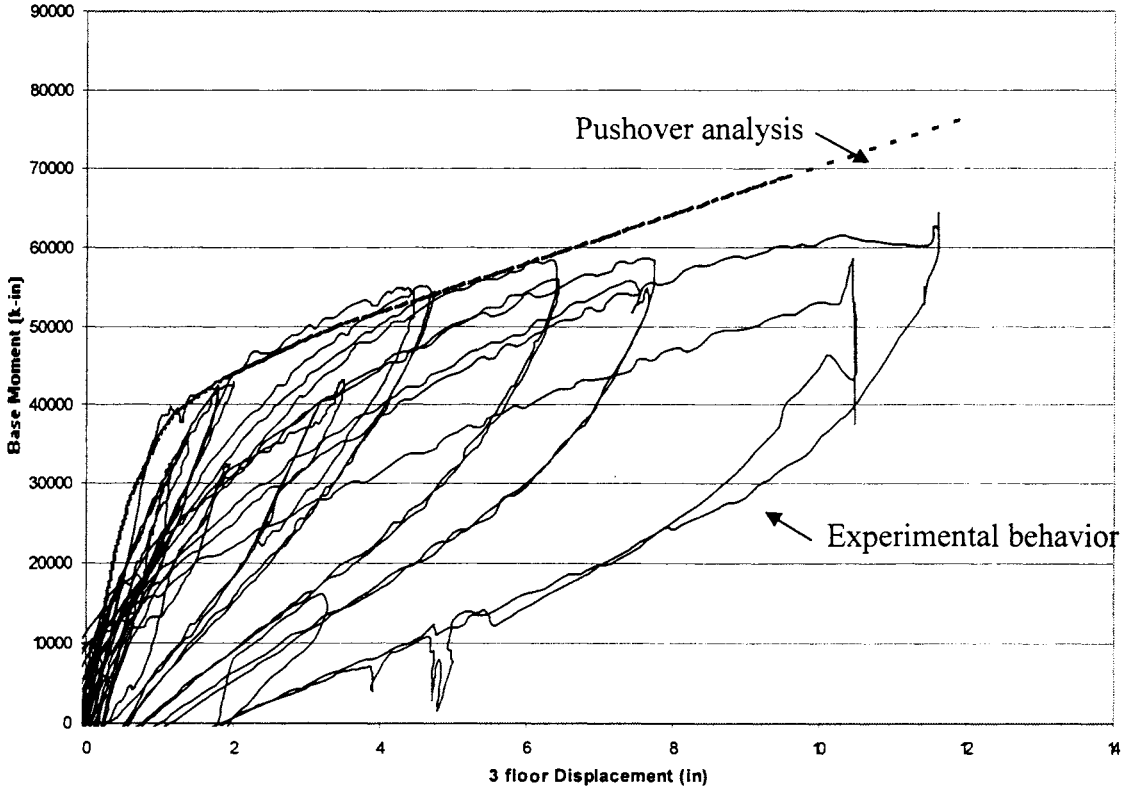

Figure 4.7 Comparison of experimental and calculated responses

4.3.3 Dynamic Analyses

Dynamic analyses were carried out using input excitations that were used for the PRESSS test building. These records included four levels input motions established based on four levels of earthquakes represented with appropriate acceleration response spectra. These were range from EQ-I to EQ-IV and derivation of these input motions was presented in reference [50]. These four levels of earthquake motions are considered to correspond to performance levels of service, damage control, design and survival limit states [60].

In the PRESSS test, it was realized that the original input motions of EQ-III and EQ-IV established for the tests demanded force and displacements beyond the capacities of

hydraulic actuators used in the tests. Therefore, the original input motions were modified by reducing high frequency content in the input motions [50]. Figure 4.8 and Figure 4.9 show these original and modified input motions, respectively. In order to use the dynamic analysis results for validation of the analysis model with the test data, the modified input motions were used in the analysis. However, the unmodified EQ-III was used for the analysis reported in Section 4.4.

In addition to the four levels of modified input motions, 0.5EQ-I was also included as used in the PRESSS test. These records were input in tandem and in the order of increasing intensity to reflect the same strength and stiffness degradations experienced by the test building as analyzed by Pampanin at el. [43].

Displacement and base moment time histories are generally very good representatives of building response under earthquake loads. Figure 4.10 shows time histories of 3rd floor displacement obtained from the dynamic analysis. Experimental time histories of 3rd floor displacement are also included in this Figure 4.10 and they are shown by solid lines. Similarly, base moment time histories are compared in Figure 4.11.

It is observed from the comparison shown in Figure 4.10 that the peak displacements and the fundamental period reflected in the dynamic analysis results are slightly higher than experimental values during 0.5EQ-I and EQ-I. However, the analytical results almost exactly match the experimental values for EQ-II and EQ-III, indicating that the stiffness values used for beams and columns in the building model closely matched the conditions of the test building during testing to EQ-II and EQ-III. At lower level of excitation, the PRESSS

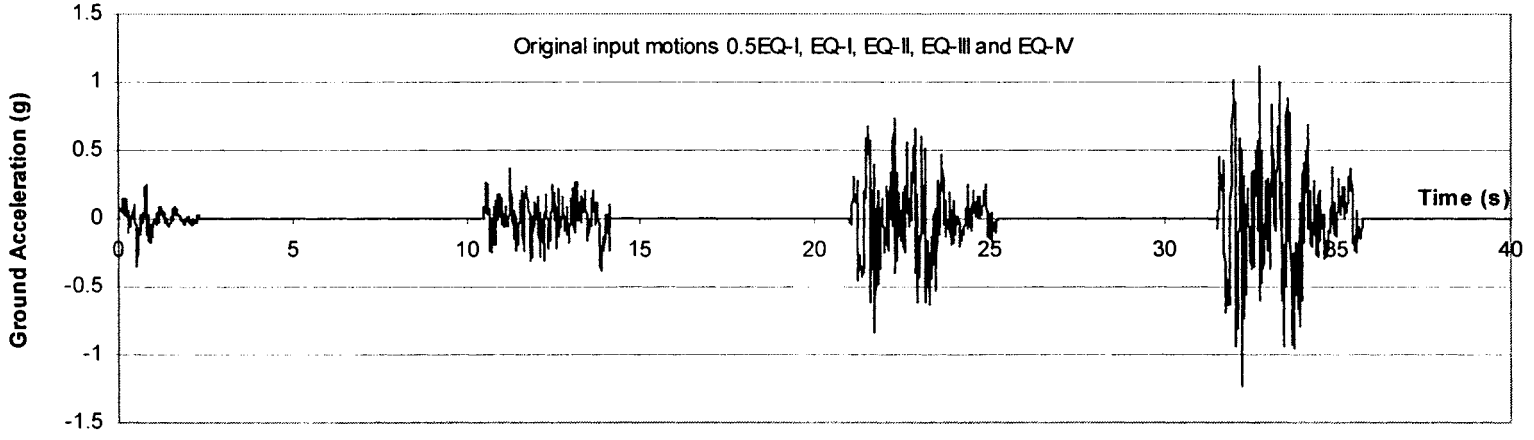

Figure 4.8 Acceleration time histories of the original input motion [50].

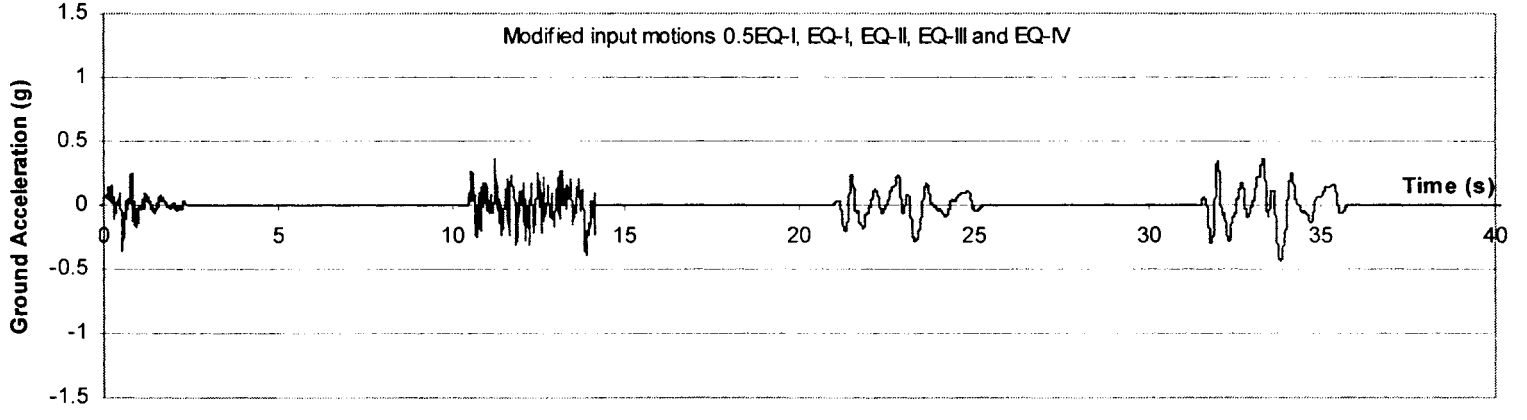

Figure 4.9 Acceleration time histories of the modified input motion [50].

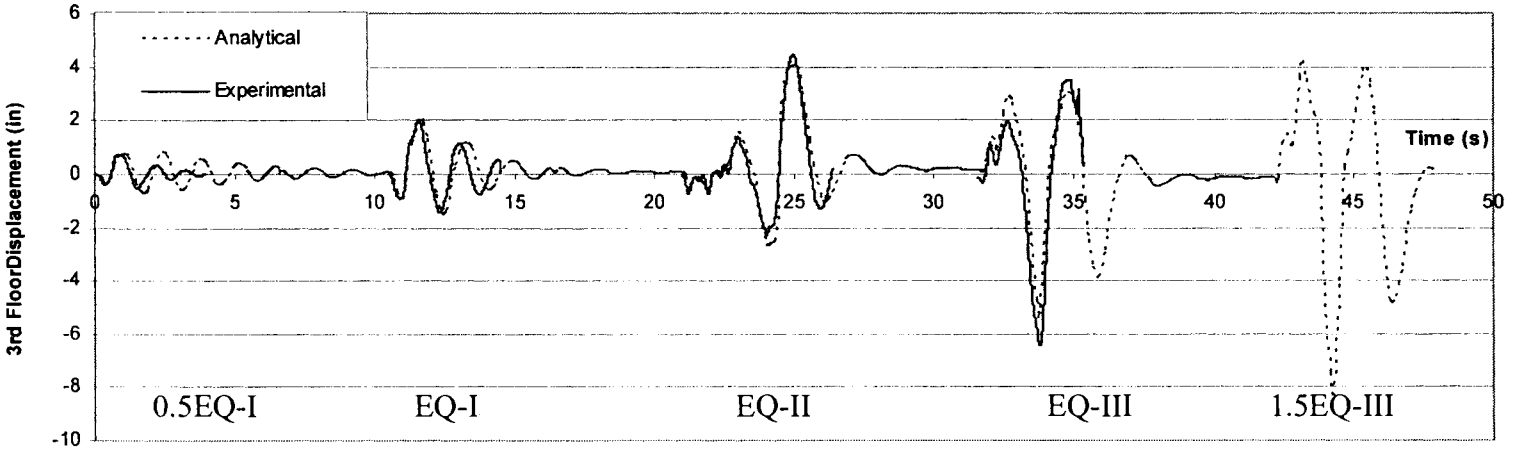

Figure 4.10 Third floor lateral displacement time histories obtained for modified input ground motions.

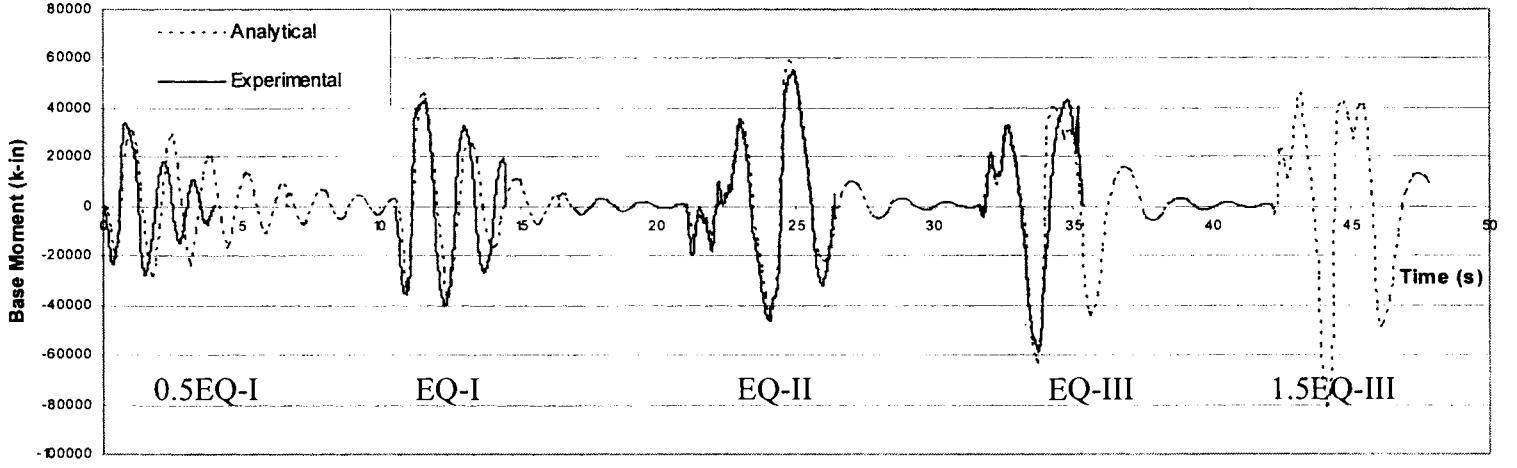

Figure 4.11 Base moment time histories obtained for modified input ground motions.

building would have been stiffer than the model due to the beams and columns having higher stiffness values than those assumed in the building model.

The behavior of the PRESSS building was predicted in a previous study by Pampanin et al. [43]. Their study differed from the current investigation that they modeled the four jointed connection types used in the PRESSS building and the moment-rotation behavior of the connection was based on the expressions developed by them using the monolithic beam analogy. In the current study, the building is assumed to have only hybrid connections and the connection analysis was based on the modified expressions derived from the monolithic beam analogy, as described Section 3.3. Therefore, it is of interest to compare the results obtained from the current study with that predicted by Pampanin at el. Figure 4.12 compares the two analysis results with the test data. It is seen that the response prediction obtained from the building modeled shown in Figure 4.6 more closely matches the observed response than the prediction by Pampanin et al [43].

Table 4.1 compares the peak displacement values extracted from the plot shown in Figure 4.12. The table also shows the percent difference between the predicted and experimental values, which also confirm that the modeling of the five-story hybrid frame building selected for further investigation is satisfactory.

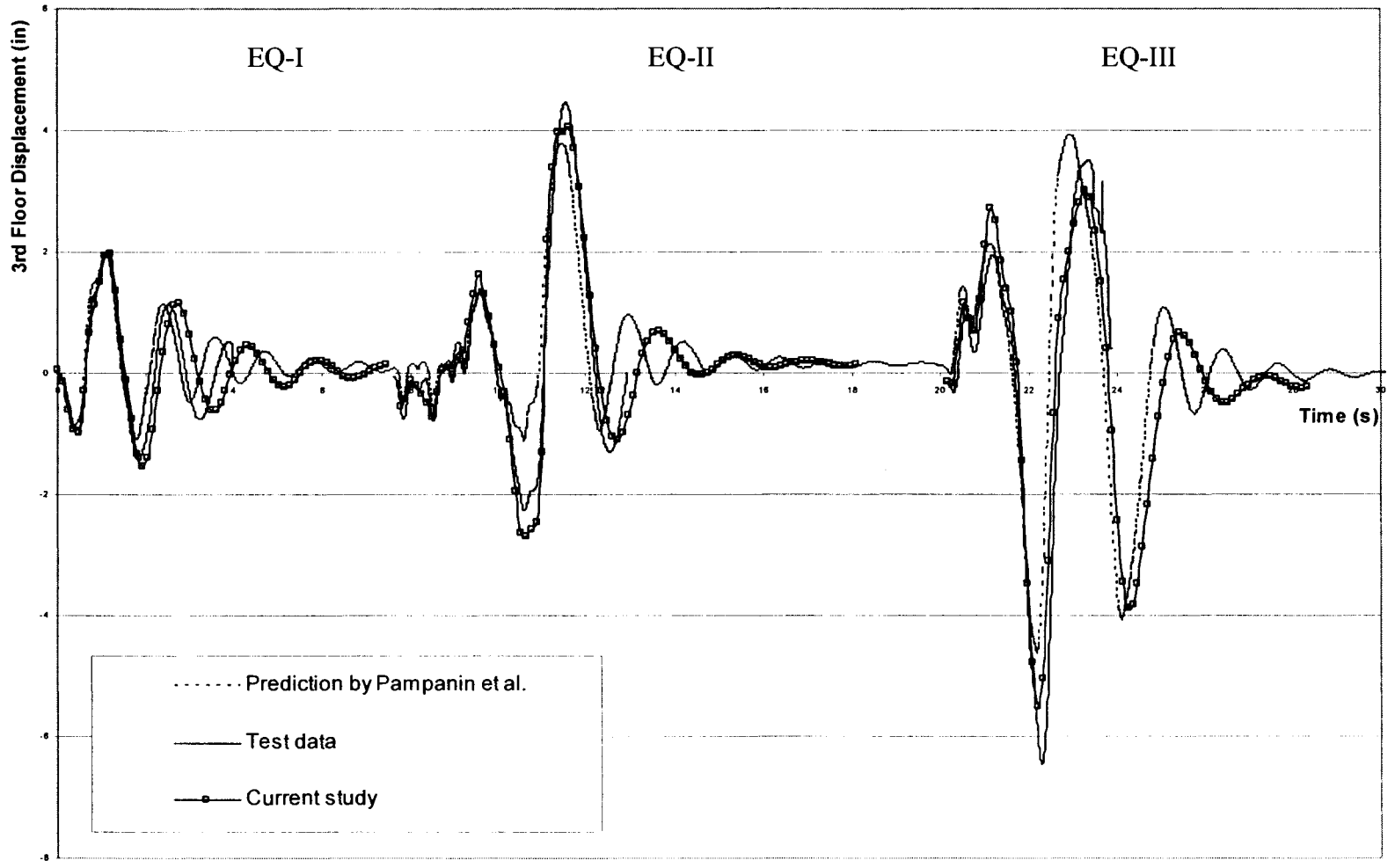

Figure 4.12 Third floor displacement time histories obtained for modified input motions

Table 4.1: Comparison of peak lateral displacement obtained at the third floor of the building

Description		EQ-I		EQ-II		EQ-III	
		Positive	Negative	Positive	Negative	Positive	Negative
3rd Floor Displacement - Test Data (in)		1.97	1.42	4.46	2.27	6.45	3.50
3rd Floor Displacement Prediction (in)	By Pampanin at el. [43]	1.87	1.11	3.75	1.12	4.64	3.92
	Current study	1.96	1.54	4.07	2.70	5.51	3.02
Percentage different	By Pampanin at el. [43]	5	22	16	51	28	- 12
	Current study	1	- 8	9	- 19	15	14

4.4 Performance Based Seismic Analysis

Performance based seismic engineering is generally regarded as the future direction of earthquake-resistant design, which has been addressed in the latest recommended design practice by the Structural Engineers Association of California (SEAOC). This concept requires multiple performance levels to be met in the design such that the structural response will be satisfactory when subjected to earthquake ground motions with different intensities. In accordance with this concept, four different levels of acceleration time histories were developed and used in the PRESSS experimental study involving the five-story test building [49]. As described in Section 4.3.3, these records referred to them as EQ-I, EQ-II, EQ-III and 1.5EQ-III, were used in the actual test except for 1.5EQ-III. Also, the EQ-III motion was modified to control the actuator forces and displacements during testing of the PRESSS

buildings. For a performance-based analysis of the five-story hybrid building, the original EQ-I, EQ-II, EQ-III and 1.5EQ-III are used without any modification.

Further more, seismic mass at each floor was adjusted to match the appropriate value suggested by Priestley et. al. [50]. Accordingly, the analysis was performed using seismic mass of 35 kip/in/s^2 per floor which is required as appropriate to reflect the seismic response of the prototype building used in the PRESSS test.

The goal of performance based seismic analysis is to examine various demand levels computed for structural elements and compare the results against a specific set of acceptance criteria established for those demand levels. As lateral displacement response of a building is a useful performance measure of damage under earthquake loading, peak inter-story drift values were computed and compared with the recommended inter-story drifts for performance based seismic assessment of special concrete moment frames. A five-story hybrid precast building with dimensions identical to that of PRESSS test building was selected for this study.

Table 4.2 summarizes the peak inter-story drifts obtained at different floor levels from the dynamic analysis of the five-story hybrid frame building when subjected to the four levels of earthquake input motions. Also included in this table is the SEAOC recommended permissible drifts for the four intensities of ground motions. The performance of the hybrid building was remarkably good, producing drift demands about 63-73 percent of the recommended values at damage control level (EQ-II), design level (EQ-III) and survival limit level (EQ-IV) of earthquakes. At service level, the drift demand in the building exceeded by 20% at the first floor level while satisfying the recommended values at all other floor levels. The reason for the inter-story drift at the first floor to exceed the recommended

value may be due to the use of cracked sectional properties in the dynamic analysis for service loading condition.

The inter-story drift of 1.8% calculated for the design level earthquake appears to be satisfactory since the hybrid building details were determined from the displacement-based design using a target drift of 2% [50]

Table 4.2 Peak inter-story drifts obtained for different levels of earthquake motions

Level of earthquake motion	Peak inter-story drift %					
	Story level (Analytical values)					SEAOC recommended values
	1	2	3	4	5	
EQI	0.6	0.5	0.5	0.4	0.3	0.5
EQII	1.1	1.0	0.8	0.6	0.4	1.5
EQIII	1.8	1.7	1.5	1.3	0.9	2.5
EQIV	2.4	2.3	2.3	2.1	1.8	3.8

4.5 Influence of Flexible Floor Links

For the dynamic analyses performed for the results presented in Section 4.4, floor mass was assumed to be connected by flexible links of axial SPRINGS. The properties of the axial springs were calculated using the cross sectional detail of "X" bars used in the PRESSS test building. Dynamic analyses were performed on five-story hybrid frame building with flexible and rigid links between the seismic frames and floors. These analyses were motivated investigate the effects using flexible floor connections on the overall seismic response of the

hybrid building. It is noted that such floor connections were used in the PRESSS test building.

Table 4.3 summarizes the peak top floor displacements and base moments obtained using flexible and rigid floor links in the dynamic analysis. The percent difference of these values for flexible and rigid floor links, also shown in this table, reveals that using rigid link instead of using actual flexible link would result in larger floor displacements and base moments by about 10%.

Table 4.3: Comparison of peak top floor displacements and base moments obtained from analysis with flexible and rigid floor links

Description	EQ-I		EQ-II		EQ-III		EQ-IV	
	Peak displacement	Max. base moment	Peak displacement	Max. base moment	Peak displacement	Max. base moment	Peak displacement	Max. base moment
Flexible Link	2.02	41400	3.49	48309	6.54	53200	9.83	62135
Rigid Link	2.39	44769	3.86	43609	7.53	46659	10.6	52070
% Difference	18	-8	11	10	15	12	8	16

4.6 Response Modification Factor

The response modification (R) factor is used in forced-based design to determine design base shear and design moments for structures expected to behave nonlinearly under the design-level earthquake. The R-factor enables design forces to be determined using elastic response spectra. The SEAOC Seismology Committee established in 1993 recommended that the R-factor consists of three parts, namely, R_d that accounts for the global ductility capacity of lateral force resisting systems; R_o that relates to the over-strength inherent in the system; and R_ρ that relates to redundancy of the system. Ignoring the effect of R_ρ, the R-factor in the UBC 1997 was introduced as $R_d \times R_o$ [51]. A detail description of these components of R-factor can be found in the SEAOC Blue Book [60].

Hybrid frames, as described in Section 1.2.2, are considered as non-emulative structural systems, for which R-factors are not provided in design codes [5, 13, 60]. Therefore, it is interest to examine a suitable R-factor using the hybrid frame building investigated in this study. Figure 4.13 shows the variation of base shear plotted against top floor displacement obtained by performing a pushover analysis on the finite element model of the hybrid building described in Section 4.3. Also included in this figure is the linear elastic response of the model, which was obtained by modifying the finite element model to experience elastic response at all hybrid connections including at the column bases. Using these plots, the following procedure is adopted to determine a suitable R factor that may be recommended for forced-based design of precast hybrid buildings.

According to the SEAOC Blue Book[60],

$$R_d = \frac{V_E}{V_M} \qquad 4.1$$

and $$R_o = \frac{V_M}{V_S} \qquad 4.2$$

where, V_E is the elastic response base shear; V_M is the probable maximum base shear capacity of a lateral load resisting system; and V_S is the base shear that is expected when the structure is subjected to the design seismic forces.

The SEAOC Blue Book specifies V_E as the value of the fundamental period ordinate of the elastic acceleration spectra, corresponding to a seismic zone and soil condition, times the seismic weight of the structure. The five-story hybrid building used in this analysis was designed for Zone 4 with soil condition of SE category and the fundamental period of the building was found to be 0.97 s by performing modal analysis on the building model using the computer program RAUAMOKO. Based on these parameters, V_E for the building was quantified as 0.578W, where W is the seismic weight of the building and was equal to 2106 kips [60]. Therefore,

$$V_E = 0.578 \text{ x } 2106 \text{ kips.} = 1217 \text{ kips.}$$

Sritharan et al. [59] reported that the design team of the five-story hybrid frame building estimated a value of 132.0 kips per hybrid frame as the design base shear, V_S, using the displacement-based design approach. The building had two hybrid frames, therefore, total V_S may be estimated as:

$$V_S = 2 \text{ x } 132 \text{ kips.} = 264 \text{ kips.}$$

Using these values, V_E, V_S and their corresponding elastic response displacements Δ_E and Δ_S are located in the plot shown in Figure 4.13.

The SEAOC Blue Book defines the displacement, Δ_M, corresponding to V_M as the maximum inelastic response when the structure is subjected to the design ground motion. Therefore, considering EQ-III as design ground motion, Δ_M was determined from the value of peak top-floor displacement by performing dynamic analysis on the building model using EQ-III as the input motion (See Section 4.4). The dynamic analysis revealed that Δ_M was equal to 6.99 in. V_M was then quantified as Δ_M ordinate of the base shear-displacement envelope, as shown in Figure 4.13, obtained from the inelastic pushover analysis on the building model. The value of V_M was 331.0 kips. From Eq. 4.1 and 4.2, the components of R factor can be calculated as,

$$R_d = (1217)/(331) = 3.68$$

$$R_o = (331)/(264) = 1.25$$

Therefore, the response modification factor that may be recommended for forced-based design of precast hybrid frame buildings can be calculated as:

$$R = R_d \times R_o = (3.68)/(1.25) = 4.6$$

The above recommended value was uniquely determined and reliable, because of three reasons. First, the five-story building was originally designed using the displacement-based approach, which is considered to be superior to the forced-based design approach, therefore the back-calculated R factor would be dependable. Second, the building was seismically experimented, analyzed and found to be adequate for high seismic regions from a performance-based earthquake engineering view point. Third, the R factor is calculated specifically to a unique building system.

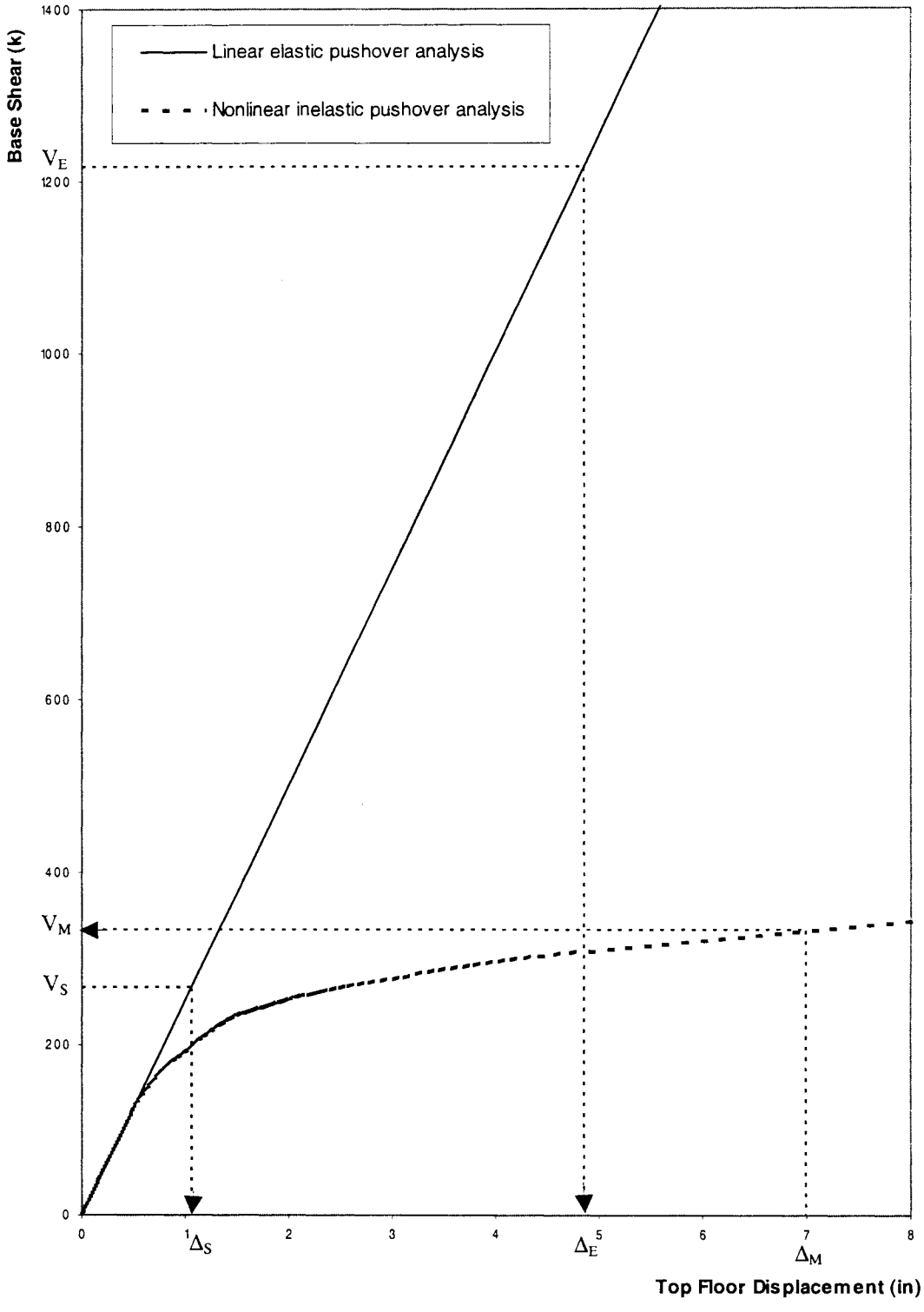

Figure 4.13 Linear and non-linear base moment response vs. top floor displacement.

CHAPTER 5

CONCLUSIONS AND RECOMMENDATIONS

5.1 Overview

This thesis presents the results of an analytical investigation on precast hybrid frame buildings. First, a comprehensive literature review addressing the performance of precast buildings in earthquakes, experimental investigation of various precast framing concepts, analytical investigation of hybrid systems and design methods for hybrid frame systems was completed. Next, an improved set of equations was established in accordance with the "monolithic beam analogy" to perform connection level analysis for the hybrid frame systems. A user-friendly computer tool was then developed incorporating the improved set of equations, which enabled the investigation of hybrid systems at the member and system levels. The connection level analysis results were compared with available experimental results to validate adequacy of the improved analysis results. Assisted by the computer program, dynamic response of a five-story hybrid frame building was investigated under different levels of earthquake input motions. Using the PRESSS test building results, the analysis model of the hybrid building was verified. Using this building model, the effects of using flexible floor links in precast buildings were investigated. This was also demonstrated through the dynamic analysis a performance based seismic assessment of precast buildings and determination of suitable R-factors for force-based design. Conclusions drawn from the studying and recommendation for future research are presented below.

5.2 Literature Review

Conclusions drawn from the literature review conducted as part of the study are listed below under four different topics.

5.2.1 Performance of precast concrete building systems during the past earthquakes

1. Limited information on the performance of lateral-load resisting moment systems incorporating only precast concrete members was generally found in earthquake reconnaissance reports [12-21]. The little information available in literature may be due to limited application of precast technology in seismic regions.
2. Contrary to the popular belief, many precast buildings with and without other types of structural members performed satisfactorily during past earthquakes [16].
3. Although some of the buildings that incorporated precast structural members and other types of structural members in the gravity and/or lateral load resisting systems experienced severe earthquakes damage, the cause of damage was were not generally attributed to the use of precast structural members [12, 16].
4. The followings were found to be the common reasons for failure of structural systems in buildings that incorporated precast structural elements.
    a) Under-estimation of design parameters [14, 15, 16].
    b) Poorly detailed connections between different precast structural members [14, 18, 19, 22].

c) Use of improper transfer mechanisms for the gravity and seismic forces within and between gravity and lateral-load resisting systems [18, 19].

d) Brittle behavior of structural members, mainly due to the use of improper transfer mechanism in design [14, 18, 19, 21].

e) Failure of floor panels due to unseating [19, 22].

f) Use of inferior quality of materials, and lack of supervision and use of quality control measures during construction [14, 15].

5.2.2 **Experimental investigation**

Various framing concepts were studied to introduce precast buildings in seismic regions. These studies included the emulative concept and jointed systems which took advantages of precast technology.

1. Several different precast framing concepts have been proposed by researchers with emulative connections. Generally, these emulative systems provided performance comparable to equivalent monolithic frame systems in terms of strength, ductility and energy dissipation systems. However, some of the systems investigated did not provide comparable behavior, and required further research
2. The jointed precast systems which include the hybrid frame system have been introduced successfully as an alternative to the emulative concept [39, 49]. An extensive research has been conducted on the hybrid frame systems which shows that this will provide superior performance to the monolithic counterparts by providing ductile response with reduced residual displacements [37, 38, 48].

5.2.3 Analytical investigation of hybrid systems

1. The strain incompatibility that exists between concrete and steel at hybrid connections forced researchers to develop analytical models based on several simplified assumptions [42, 10, 43].
2. The monolithic beam analogy introduced by Pampanin at el. [43] provided an alternative connection level analysis which enables a continuous moment-rotation envelope to be determined with sufficient accuracy. However, the accuracy of predicted results was not adequately investigated by corresponding theoretical strains and neutral axis depth obtained at the section level with experimental results.

5.2.4 Design Methods for Hybrid Frame Systems

Due to the same reason stated above in III (1), existing design provisions were developed using several simplified assumptions [10]. These assumptions include the followings:

- Equivalent rectangular compression stress block is used to represent approximate confined concrete stress distribution.
- Compression steel contribution is neglected.
- A constant value of additional length is added to account for the growth in unbonded length of mild steel reinforcing due to cyclic strain.

5.3 Connection Level Analysis of Hybrid Systems

Using the equivalent monolithic beam analogy suggested by Pampanin et al [43], an improved set of equations were developed in this study to quantify the strains at the connection of a hybrid system. The modified equations incorporate the following changes:

1. Considering the effect of the strain penetration and elastic component of strain hardening of the tension steel in evaluating beam end displacement of precast beam with the hybrid connection;
2. Including the compression force contribution of the mild steel reinforcement in evaluating bending moment at the hybrid connection; and
3. Using Mattock's model to represent the stress-strain relation of the tendon.

A user-friendly computer program was developed using the improved equations developed for the monolithic beam analogy. The following conclusions were drawn from the connection level analysis and some of these results of which were compared with available test results.

1. The connection level analysis revealed that moment-rotation behavior was not sensitive to the estimate of extreme fiber concrete strain, which was consistent with a finding by Pampanin et al. [43]. However, predictions of other parameters at the hybrid connection such as the neutral axis depth, the strain in the post-tensioned steel and mild steel strains were found to be sensitive to the concrete strain.
2. The moment-drift response obtained using the modified the set of equations provided good envelopes satisfactorily matching the experimental hysteresis response.
3. The calculated neutral axis depth plotted against rotation showed good correlation to experimental values extracted from test data.

5.4 Dynamic Analysis a Five-story of Hybrid Frame Building

Using the enhanced analytical model, a suitable combination of elements and their properties were determined in creating a nonlinear finite element model to represent hybrid moment resisting frames. The finite element model represented the PRESSS test building and, therefore was verified with the experimental data by performing a series of pushover and dynamic analyses. The results and conclusions are summarized below:

1. The pushover analysis, performed on the building model provided base moment-lateral displacement envelope that satisfactorily matched the experimental response deduced from the PRESSS building. Starting from a drift of 2.2% the experimental result showed somewhat lower base moments which was attributed to system degradation experienced in the PRESSS building.
2. Dynamic response of the hybrid building was examined under input motion representing four levels of earthquakes ranging from EQI through 1.5EQ-III. Good correlations were found between experimental and analytical time histories of base moment and displacement, confirming satisfactory modeling of the hybrid building.
3. Peak displacements predicted by Pampanin et al. and those predicted using the improved set of equations were compared. The percent difference between the predicted values and the experimental data was found to be reduced by more than 50% when using the improved set of equations. This demonstrated the importance of accurately modeling various parameters that influence the connection level behavior.
4. A performance based seismic analysis was conducted on the hybrid frame building using four levels of earthquake input motion. For this analysis, the floors were assumed to be connected through flexible links and the mass was revised to reflect a more realistic

building in the field. The peak inter-story drifts determined from these analysis were compared with the values recommended by SEAOC [60]. It was found that the hybrid building satisfied various permissible drift levels , except for the first floor under EQ-I loading.

5. Modeling the links that connects floor mass to the hybrid moment resisting frame as rigid links instead of flexible links resulted in larger values of displacements by about 10 percent and lower values of base moment by about 10 percent.
6. Based on a performance-based assessment of a five-story precast hybrid building, a suitable response modification (R) factor of 4.6 was recommended for force-based design of precast hybrid buildings.

5.5 Recommendations

1. Previous experimental studies on hybrid frame systems did not provide an adequate set of experimental data for validation of results at the connection level. Availability of such data set would have provided an opportunity to thoroughly verify the adequacy of the theoretical strains and neutral axis depth. An experimental program on hybrid systems with an emphasis of obtaining the relevant data at the connection level would enhance the understanding of hybrid frame behavior.
2. Although dynamic analysis show a good correlation with experimental results, the use of the modified Takeda model for the moment contribution of the reinforcement steel somewhat approximates the hysteresis behavior. In this approach, the unbonded post-tensioning system was assumed not to provide hysteresis energy dissipation which is not

consistent with experimental results. An investigation focusing on more appropriate hysteresis rules for the elements contributing to the moment resistance is recommended.

REFFERENCES

[1] Fintel, M. (1995) Performance of Buildings with Shear Walls in Earthquakes of the Last Thirty Years. *PCI Journal.* 40(3): pp 62-80.

[2] Cheok, G. S., and Lew, H. S. (1991) Performance of Precast Concrete Beam-to-Column Connections Subject to Cyclic Loading. *PCI Journal*, 36(3): pp 56-67.

[3] Park, R. (1995) A Perspective on the Seismic Design of Precast Concrete Structures in New Zealand. *PCI Journal*, 40(3): pp 40-60.

[4] Paulay, T. and Priestley, M. J. N. (1992) Seismic Design of Reinforced Concrete and Masonry Buildings, *John Wiley & Son, New York*, pp 38-46.

[5] Priestley, M. J. N. (1998) Displacement Based Approaches to Rational Limit States Design of New Structures, Keynote Lecture, Eleventh European Conference on Earthquake Engineering, Paris.

[6] Ghosh, S. K. (2001) Seismic Design Provisions for Precast Concrete Structures in ACI 318. *PCI Journal, 2002,* 46(1): pp28-32.

[7] Priestley, M. J. N. (1991) Overview of PRESSS Research Program. *PCI Journal.* 2(2): 50-57.

[8] Ghosh, S. K. (2002) Seismic Design Provisions in U.S. Codes and Standards: A Look Back and Ahead. *PCI Journal,* 47(1): pp 94-99.

[9] ACI Innovative Task Group 1 and Collaborators, Special Hybrid Moment Frames Composed of Discretely Jointed Precast and Post-Tensioned Memebrs (ACI T1.2-XX) and Commentary (T1.2R-XX). *ACI Journal,* 98-S75: pp 771-784.

[10] Cheok, G. S., Stone, W. C., and Nakaki, S. D. (1996) Simplified Design Precedure for Hybrid Precast Concrete Connections. *National Institute of Standards and Technology, SCTR 5765.*

[11] Stanton, J. F., and Nakaki, S. D. (2001) Design Guidelines for Precast Seismic Structural Systems. *Department of Civil Engineering, University of Washington, Seattle, WA, Report No. SM 01-02.*

[12] Sritharan, S. and S. D. Nakaki, "Construction Details and Material Properties", PRESSS Phase 3: The Five-Story Precast Test Building (V-2), Department of Civil and Construction Engineering, Iowa State University, Ames, (in preparation).

[13] Bhatt, P., and Kirk, D. W., "Tests on an Improved Beam Column Connection for Precast Concrete," *ACI Journal*, V.82, No. 6, November-December 1985, pp. 834-843.

[14] Kunze, W. E., Sbarounis, J. A., and Amrhein, J. E. (1965) Behavior of Prestressed Concrete Structures During the Alaskan Earthquake. *PCI Journal,* 10(2) : pp 80-91.

[15] Fintel, M. (1977) Performance of Precast Concrete Structures During Rumanian Earthquake of March 4, 1977. *PCI Journal,* 22(2): pp 10-15.

[16] Fintel, M., (1986) Performance of Precast and Prestressed Concrete in Mexico Earthquake. *PCI Journal,* 31(1): pp 18-42.

[17] Iverson, J. K., (1989) First Impression of Earthquake Damage in San Francisco Area. *PCI Journal,* 34(6): pp 108-124.

[18] Iverson, J. K., and Hawkins, N. M., (1994) Performance if Precast/Prestressed Concrete Building Structures During Northridge Earthquake. *PCI Journal,* 39(6): pp 38-55.

[19] Ghosh, S. K. (1995) Observations on the Performance of Structures in the Kobe Earthquake of January 17, 1995. *PCI Journal.* 40(2): 14-22.

[20] Paulay, T and Priestley, M. J. N. (1992) Seismic Design of Reinforced Concrete and Masonry Buildings, John Wiley and Sons, Inc., New York.

[21] http://www.johnmartin.com/earthquakes/eqshow/index.htm.
(Note: Accessed on September 20, 2002)

[22] Ghosh, S. K. (1995) Observations From the Bhuj Earthquake of January 26, 2001. *PCI Journal.* 46(2): 34-42.

[23] Uniform Building Code, International Conference of Building Officials, Whittier, CA, 1977

[24] American Concrete Institute. (1983) Building Code Requirements for Structural Concrete (ACI 318-99) and Commentary (ACI 318R-99), ACI: Michigan.

[25] American Concrete Institute. (1983) Building Code Requirements for Structural Concrete (ACI 318-83) and Commentary (ACI 318R-83), ACI: Michigan.

[26] Stover CW, Coffman IL. 1993. Seismicity of the United States, 1568-1989 (revised). US Geol. Surv. Prof Pap. pp. 1527-418

[27] Blakeley, R. W. G., and Park, R. (1971) Seismic Resistance of Prestressed Concrete Beam-to-Column Assemblies. *ACI Journal, Sep 1971*: pp 677-692

[28] Pillai, S. U., and Kirk, D. W. (1981) Ductile Beam-to –Column Connection in Precast Concrete. *ACI, N-D 1981*: pp 480-487.

[29] French, C. W., Hafner, M., and Jeyashankar, V., (1989) Connections between Precast Elements – Failure within Connection Region. *ACSE 12/89*: pp 3171-3192.

[30] Seckin, M., and Fu, H. C. (1990) Beam-to-Column Connections in Precast Reinforced Concrete Construction. *ACI Structural Engineering Journal*. May-June 1990: pp 252-261.

[31] Restrepo, J. I., Park, R., and Buchanan, A. H. (1995) Tests on Connections of Earthquake Resisting Precast Reinforced Concrete Perimeter Frames of Buildings. *PCI Journal*, 40(4): pp 44-61.

[32] Alcocer at el. (2002) Seismic Tests on Beam-to-Column Connections in a Precast Concrete Frame in Seismic Regions. *PCI Journal.* 47(3): pp 70-89.

[33] French, C. W., Amu, O., and Tazikhan, C., (1989) Connections between Precast Elements – Failure outside Connection Region. *ACSE 7/89*: pp 316-340.

[34] Nakaki, S. D., Englekirk, R. E., and Plaehn, J. L. (1994) Ductile Connectors for Precast Concrete Frame. *PCI Journal.* 39(5): pp 46-59.

[35] Ersoy, U., and Tankut, T. (1993) Precast Concrete Members with Welded Plate Connections under Reversed Cyclic Loading. *PCI Journal.* 38(4): pp 94-100.

[36] Ochs, J. E. and Ehasani, M. (1993) Moment Resisting Connections in Precast Connection Frames for Seismic Regions. *PCI Journal.* 39(5): pp 46-59.

[37] Cheok, G. S., and Lew, H. S., (1991) Performance of Precast Concrete Beam-to-Column Connections Subject to Cyclic Loading. *PCI Journal*, 36(3), pp. 56-67.

[38] Cheok, G. S., and Lew, H. S., (1993) Model Precast Concrete Beam-to-Column Connections Subject to Cyclic Loading. *PCI Journal*, 38(3), pp. 80-92.

[39] Stone, W. C., Cheok, G. S., and Stanton, J. F., (1995) Performance of Hybrid Moment-Resisting Precast Beam-Column Concrete Connections Subjected to Cyclic Loading. *ACI Structural Journal*, 92(2): pp 229-249.

[40] Priestley, M. J. N., and MacRae, G. A. , (1996) Seismic Tests of Precast Beam-to-Column Joint Subassemblages With Unbonded Tendons. *PCI Journal*, 41(1): pp 64-81.

[41] EngleKirk, E. E., (1989) An Analytical Approach to Establishing the Seismic Resistance Available il;p/n Precast Concrete Frame Structures. *PCI Journal*, 34(1): pp 92-101.

[42] Priestley, M. J. N., and Tao, J. T., (1993) Seismic Response of Precast Prestressed Concrete Frames with Partially Debonded Tendons. *PCI Journal*, 38(1): pp 58-69.

[43] Pampanin, S., Priestley, M. J. N., and Sritharan, S. 2001. Analytical Modeling of Seismic Behavior of Precast Concrete ductile Frame Connection, Journal of Earthquake Engineering, 5(3): pp 329-367.

[44] Sritharan S., [1999] "Analysis of Concrete Bridge Joint Subjected to Seismic Actions", PhD. Dissertation, University of California, San Diego, CA.

[45] Mander, J. B., Priestley, M. J. N., and Park, R., (1988) Theoretical Stress-Strain Model for confined concrete. *ASCE Journal of the Structural Engineering*, 114(8), pp 1804-1826.

[46] Restrepo, J. I., (1993) "Seismic Behavior of Connections Between Precast Concrete Element", Ph.D. Dissertation, Department of Civil Engineering, University of Canterbury, Christchurch, New Zealand.

[47] Mattock, Alan H., (1979) Flexural Strength of Prestressed Concrete Sections by Programmable Calculator, *PCI Journal,* 24(1): pp 32-54

[48] Stanton, J., Stone, W. C., and Cheok, G. S., (1997) A Hybrid Reinforced Precast Frame for Seismic Regions. *PCI Journal*, 42(2): pp 20-32.

[49] Nakaki, S. D., Stanton, J. F., and Sritharan, S, (1999) An Overview of the PRESSS Five-Story Precast Concrete Test Building. *PCI Journal,* 44(2): pp 26-37.

[50] Priestley, M. J. N. (Editor), Report on the Third U. S. PRESSS coordinating meeting, Report No. PRESSS 92/02, Department of Applied Mechanics and Engineering Sciences, University of California at San Diego, La Jolla, CA, August 1992, pp.12-16.

[51] Uniform Building Code, International Conference of Building Officials, Whittier, CA, 1994

[52] Uniform Building Code, International Conference of Building Officials, Whittier, CA, 1997

[53] Collins, M. P. and Mittchal, D. (1997) Prestressed Concrete Structures. Canada, Response Publications.

[54] Sritharan, S., Performance of Four Jointed Precast Frame Systems under Simulated Seismic Loading, Proceeding of the Seventh U. S. National Conference on Earthquake Engineering, Paper No. 480, Boston, Massachusetts, July 2002.

[55] Sritharan, S., and S. Vernu, Analysis and Design of Precast Hybrid Frames, Proceedings of 2003 Pacific Conference on Earthquake Engineering.

[56] Pampanin, S., Priestley, M. J. N., and Sritharan, S. Frame direction Response, PRESSS Phase 3: The Five-Story Precast Test Building (V3-4), Report No. SSRP – 2000/08, Department of Structural Engineering, University of California at San Diego, California, November 2000.

[57] Sritharan, S., Igarashi, A., Priestley, M. J. N., and Seible, F., "Test Design of the PRESS Five-Story Precast Concrete Building," *Proceedings of the 68th SEAOC Annual Convention,* Structural Engineers Association of California, Santa Barbara, 1999, pp. 255-261.

[58] Carr, A. J., RAUAMOKO – Inelastic Dynamic Analysis Program, University of Canterbury, 2000.

[59] Sritharan, S., S. Pampanin, J. Conley, Final Report on Design, Verification, Instrumentation & Test Procedures latest PRESSS: PRESSS Phase 3: The Five-Story Precast Test Building (V-2), Department of Civil and Construction Engineering, Iowa State University, Ames, 2002.

[60] PBE, Ad-Hoc Committee of Structural Engineering Association of California, APPENDIX I – Tentative Guidelines for Performance Based Seismic Engineering Guidelines, SEAOC Blue Book, 1999.